NTNU
Norwegian University of
Science and Technology

Corrosion properties of AA5083 and AA6082 in seawater - effect of temperature, pH and potential

Ove Nese

Subsea Technology
Submission date: June 2016
Supervisor: Roy Johnsen, IPM

Norwegian University of Science and Technology
Department of Engineering Design and Materials

NTNU - NORGES TEKNISK-
NATURVITENSKAPELIGE UNIVERSITET
INSTITUTT FOR PRODUKTUTVIKLING
OG MATERIALER

MASTEROPPGAVE VÅR 2016
FOR
STUD.TECHN. OVE NESE

Korrosjonsegenskaper til AA5083 og AA6082 i sjøvann – effekt av temperatur, pH og potensial

Corrosion properties of AA5083 og AA6082 in seawater – effect of temperature, pH and potential

Bakgrunn:

Bruk av aluminium under vann (subsea) får stadig økende interesse i industrien. Dette skyldes både egenvekt og korrosjonsegenskapene til enkelte aluminiumslegeringer i sjøvann. Aluminium har vært i utstrakt bruk som konstruksjonsmateriale for skip i mange år. I tillegg benyttes aluminium i utvalgte komponenter og utstyr for bruk under vann. Til tross for akseptable korrosjonsegenskaper, blir ofte komponenter som er eksponert i sjøvann katodisk beskyttet ved kopling mot offeranoder eller et påtrykte spenningsanlegg. En viktig årsak til dette er at aluminium ofte er koplet mot karbonstål og denne koplingen av metaller må beskyttes for å unngå korrosjon.

I litteraturen finnes det begrenset informasjon om katodisk beskyttelse av aluminium i sjøvann. En viktig referanse er et Pourbaix diagram utviklet for AA5086 i sjøvann. Dette diagrammet viser sammenhengen mellom elektrokjemisk potensial, pH og ulike tilstander for legeringen. AA5083 og AA6082 er to aluminiumslegeringer som er godkjent for bruk i sjøvann ifølge NORSOK M-121. Det er usikkert om det publiserte Pourbaix diagrammet er gyldig for disse legeringene. Dette vil bli undersøkt i denne masteroppgaven. I tillegg vil beskyttelsesstrøm bli fastlagt.

Målsetting:

For AA5083 og AA6082 i sjøvann:

1. Dokumentere effekt av temperatur, elektrokjemisk potensial og pH på korrosjonsegenskapene.
2. Fastlegge sammenhengen mellom korrosjonspotensial og strøm.

Aktiviteter:

Eksperimentelt arbeid vil være hovedaktiviteten innenfor masteroppgaven. Følgende aktiviteter inngår:

1. Detaljplanlegging av eksperimentelt arbeid. Følgende elementer skal inngå:
    - Miljø – i) Naturlig sjøvann, ii) Kunstig sjøvann m/justert pH
    - Temperatur – i) Innløpstemperatur Sealab (10^{0}C), ii) Romtemperatur, iii) 30^{0}C
    - pH – i) 3, ii) 8.2, iii) 10
    - Potensial – i) -1500, ii) -1050, iii) OCP, iv) -700 mV vs. Ag/AgCl
    - Eksponerings tid – opp til 1000 timer
2. Gjennomføre eksperimentelt arbeid
3. Karakterisering av overflater etter eksperimentelt arbeid (lysmikroskop, SEM)
4. Utarbeide master thesis rapport med konklusjoner og anbefalinger.

Oppgaven gjennomføres i samarbeid med Hydro.

Formelle krav:

Senest 3 uker etter oppgavestart skal et A3 ark som illustrerer arbeidet leveres inn. En mal for dette arket finnes på instituttets hjemmeside under menyen masteroppgave (https://www.ntnu.no/web/ipm/masteroppgave-ved-ipm). Arket skal også oppdateres en uke før innlevering av masteroppgaven.

Risikovurdering av forsøksvirksomhet skal alltid gjennomføres. Eksperimentelt arbeid definert i problemstilling skal planlegges og risikovurderes innen 3 uker etter utlevering av oppgavetekst. Konkrete forsøksvirksomhet som ikke omfattes av generell risikovurdering skal spesielt vurderes før eksperimentelt arbeid utføres. Risikovurderinger skal signeres av veileder og kopier skal inngå som vedlegg til oppgaven.

Besvarelsen skal ha med signert oppgavetekst, og redigeres mest mulig som en forskningsrapport med et sammendrag på norsk og engelsk, konklusjon, litteraturliste, innholdsfortegnelse, etc. Ved utarbeidelse av teksten skal kandidaten legge vekt på å gjøre teksten oversiktlig og velskrevet. Med henblikk på lesning av besvarelsen er det viktig at de nødvendige henvisninger for korresponderende steder i tekst, tabeller og figurer anføres på begge steder. Ved bedømmelse legges det stor vekt på at resultater er grundig bearbeidet, at de oppstilles tabellarisk og/eller grafisk på en oversiktlig måte og diskuteres utførlig.

Besvarelsen skal leveres i elektronisk format via DAIM, NTNUs system for Digital arkivering og innlevering av masteroppgaver.

Kontaktperson: Trond Furu, Hydro

Torgeir Welo
Instituttleder

Roy Johnsen
Faglærer

NTNU
Norges teknisk-naturvitenskapelige universitet
Institutt for produktutvikling og materialer

Preface

This master's thesis is submitted to the Norwegian University of Science and Technology (NTNU) as a part of the master's degree program Subsea Technology at the Department of Engineering Design and Materials. The project has been a collaboration between NTNU and Hydro, with Professor Roy Johnsen as the main supervisor.

Acknowledgement

First of all, I would like to thank my supervisor Professor Roy Johnsen for all help and guidance during the project period. His engagement, helpfulness and availability have been highly appreciated. I would also like to thank my co-supervisor Dr. Trond Furu.

I would also like to give a special thanks to Cristian Torres.

Trondheim, June 10, 2016

Ove Nese

Ove Nese

Abstract

Aluminium is an interesting material for use in subsea structures due to its low weight. So called corrosion resistant aluminium alloys from the Al-Mg (5xxx)- and Al-Mg-Si (6xxx) series have been used for many years in ship hulls, and the experiences are good. However, corrosion failures have been observed. Used for subsea structures, aluminium will in most cases be in metallic contact with carbon steel or more noble metals, hence galvanic corrosion becomes a threat. Carbon steel is always connected to a cathodic protection (CP) system in seawater, this means that the aluminium alloy also will be connected to the CP.

In this study the aluminium alloys accepted in NORSOK for use subsea, AA5083 and AA6082, have been investigated. AA5083 and AA6082 were tested in natural seawater with temperature of 10 ± 2 ^{o}C and 32 ± 2 ^{o}C, and in synthetic seawater (SSW) with adjusted pH at room temperature. The adjusted pH was 3 and 10. Samples were freely exposed, anodic polarized to −700 mV vs Ag/AgCl, cathodic polarized to −1500 mV vs Ag/AgCl and coupled to a sacrificial anode. Recording of potentiodynamic polarization curves, open circuit potentials (OCP) and current demand was performed during exposure. Surface examination in a scanning electron microscope (SEM) was also performed.

The results from this study indicate that the temperature affects the corrosion behavior for both AA5083 and AA6082. Increased temperature increases the severity and rate of corrosion, the overall effect of temperature tended to be the same for both alloys. The electrochemical potential had a significant effect on the corrosion behavior. Freely exposed samples and samples coupled to sacrificial anodes exhibits good resistance to corrosion in seawater, both at 10 ^{o}C and 32 ^{o}C. Anodic polarization to −700 mV vs Ag/AgCl and cathodic polarization to −1500 mV vs Ag/AgCl will cause severe corrosion on AA5083 and AA6082. Different pH also affects the corrosion behavior of AA5083 and AA6082. Both alloys are sensitive to changes in pH, but the results in this study indicate that AA6082 tended to be less sensitive to low pH than AA5083. The experimental potential – pH diagram for AA5086, Figure 3, is a good guideline for AA5083 and AA6082 at seawater conditions (pH 8,2). The diagram can also be used as a rough guideline for AA5083 and AA6082 at pH 3, but the results showed that it is not valid for AA5083 and AA6082 at pH 10. After 800 hours of exposure the required cathodic current density for CP in nearly stagnant natural seawater at 10 ^{o}C for AA5083 and AA6082 were −1,8 and −2,3 $\mu A/cm^2$, respectively. Required cathodic current density for CP in nearly stagnant natural seawater at 32 ^{o}C for AA5083 and AA6082 were −0,75 and −1,7 $\mu A/cm^2$, respectively.

Sammendrag

På grunn av dets lave vekt er aluminium et interessant materiale for bruk i subseastrukturer. Såkalte korrosjonsbestandige aluminiumslegeringer fra 5xxx (Al-Mg)- og 6xxx (Al-Mg-Si) seriene har blitt brukt i skipsskrog i mange år, og erfaringene med det er gode. Likevel, svikt og feil som følge av korrosjon har blitt observert. Brukt i subseastrukturer vil aluminium i de fleste tilfeller være metallisk koblet til karbonstål eller enda edlere metaller, og da blir galvanisk korrosjon en trussel for aluminium. I sjøvann vil karbonstål alltid være koblet til et katodisk beskyttelsessystem, det betyr at også aluminium vil være tilkoblet det katodiske beskyttelsessystemet.

I denne studien har aluminiumslegeringene, AA5083 og AA6082, som er akseptert i NORSOK for subseabruk blitt undersøkt. AA5083 og AA6082 ble testet i naturlig sjøvann ved temperaturene 10 ± 2 °C og 32 ± 2 °C, og i syntetisk sjøvann med justert pH ved romtemperatur. Den justerte pH var 3 og 10. Prøvene ble fritt eksponert, anodisk polarisert til −700 mV vs Ag/AgCl, katodisk polarisert til −1500 mV vs Ag/AgCl og koblet mot offeranode. Gjennom eksponeringstiden ble det tatt opp potensiodynamiske polarisasjonskurver, samt strømbehovet og åpen krets potensial (OCP) ble logget. De eksponerte overflatene ble også undersøkt i et skanning elektronmikroskop (SEM).

Resultatene fra denne studien indikerer at temperaturen påvirker korrosjonsoppførselen til både AA5083 og AA6082. Økt temperatur øker alvorligheten og raten av korrosjonen. Den generelle effekten av temperatur er den samme for begge legeringene. Det elektrokjemiske potensialet hadde en markant effekt på korrosjonsoppførselen. Fritt eksponerte prøver og prøver koblet mot offeranode utøver god korrosjonsbestandighet i sjøvann, både ved 10 og 32 °C. Anodisk polarisasjon til −700 mV vs Ag/AgCl og katodisk polarisasjon til −1500 mV vs Ag/AgCl fører til alvorlig korrosjon på AA5083 og AA6082. Forskjellig pH har også en påvirkning på korrosjonsoppførselen til AA5083 og AA6082. Begge legeringene er sensitive til endringer i pH, men resultatene indikerer at AA6082 er mindre sensitiv for lav pH enn AA5083. Det eksperimentelle potensial – pH diagrammet for AA5086, Figure 3, gir en god retningslinje for AA5083 og AA6082 ved sjøvannsbetingelser (pH 8,2). Diagrammet kan også brukes som en grov retningslinje for AA5083 og AA6082 ved pH 3, men resultatene viser at det ikke er gyldig for AA5083 og AA6082 ved pH 10. Etter 800 timers eksponering er den katodiske strømtettheten som kreves for katodisk beskyttelse i nær stillestående sjøvann ved 10 °C for AA5083 og AA6082 henholdsvis −1,8 og −2,3 µA/cm^2. Katodisk strømtetthet som kreves for katodisk beskyttelse i nær stillestående sjøvann ved 32 °C for AA5083 og AA6082 er henholdsvis −0,75 og −1,7 µA/cm^2.

Content

Preface ... i

  Acknowledgement ... i

Abstract ... iii

Sammendrag ... v

Content ... vii

List of Abbreviations ... xi

List of Figures ... xiii

List of Tables ... xvii

1 Introduction ... 1

  1.1 Background ... 1

  1.2 Aim of this work ... 1

2 Theory ... 3

  2.1 Aluminium and aluminium alloys ... 3

    2.1.1 Al-Mg (5xxx) alloys ... 5

    2.1.2 Al-Mg-Si (6xxx) alloys ... 5

  2.2 Corrosion of aluminium ... 6

    2.2.1 Concepts for corrosion of aluminium in seawater ... 6

    2.2.2 Uniform corrosion and pitting corrosion on aluminium ... 9

    2.2.3 Crevice corrosion on aluminium ... 10

    2.2.4 Galvanic corrosion on aluminium ... 11

    2.2.5 Effect of temperature ... 12

    2.2.6 Effect of microstructure and alloying elements ... 14

  2.3 Cathodic protection of aluminium ... 16

  2.4 Calcareous deposit ... 18

    2.4.1 Formation of calcareous deposit ... 18

    2.4.2 Microstructure of calcareous deposit ... 19

3 Literature Review ... 21

4 Experimental procedure ... 23

4.1 Materials 23

4.2 Test samples 23

4.3 The different conditions and setups 25

4.3.1 SEALAB 25

4.3.2 Corrosion Laboratory Perleporten 27

4.4 Measurements 29

4.4.1 SEALAB 29

4.4.2 Corrosion Laboratory Perleporten 29

4.5 Surface examination 30

5 Results 31

5.1 SEALAB 31

5.1.1 Open Circuit Potential 31

5.1.2 Current density curves 32

5.1.3 Potentiodynamic polarization curves 35

5.1.4 SEM images and EDS analyses 40

5.2 Corrosion Laboratory Perleporten 54

5.2.1 Open Circuit Potential 54

5.2.2 Current density curves 56

5.2.3 Potentiodynamic polarization curves 59

5.2.4 SEM images 63

6 Discussion 65

6.1 Effect of temperature 65

6.1.1 OCP and pitting potential 65

6.1.2 Current density 66

6.1.3 Surface examinations 68

6.2 Effect of electrochemical potential 69

6.3 Effect of pH 71

6.3.1 OCP and pitting potential 71

6.3.2 Current density 72

6.3.3 Surface examination 73

6.4 Effect of exposure time 74
6.5 Current density required for protection 75
6.6 AA5083 vs AA6082 77
7 Conclusion 79
8 Suggestions for further work 81
References 83
Appendix A 87
Hydrogen in aluminium alloys 87
Appendix B 89
Photos of samples after exposure in SEALAB 89
Appendix C 93
Potential from sacrificial anode and current density for carbon steel coupled to sacrificial anode 93
Appendix D 95
Complete polarization curves for AA6082 exposed at 10 ^{o}C and 32 ^{o}C 95
Appendix E 97
SEM images of samples prior to exposure 97
Appendix F 99
EDS analysis of corrosion products on samples polarized to −1500 mV vs Ag/AgCl 99
Appendix G 101
OCP and current density for samples exposed in SSW with pH 8,2 101
Appendix H 103
Potentiodynamic polarization curves for pH 3 and 10 103
Appendix I 107
Risk assessment 107

List of Abbreviations

AA	Aluminium Association standard
β	Equilibrium phase in Al-Mg (5xxx) alloys
CP	Cathodic protection
CS	Carbon steel (used in figures and tables)
DNV	Det Norske Veritas
E	Potential
E_{corr}	Corrosion potential
E_{OCP}	Open Circuit Potential
E_{pit}	Pitting potential
EDS	Energy-Dispersive Spectroscopy
EN AW	European standard
FCC	Face-Centered Cubic
FSW	Friction Stir Welding
HAZ	Heat Affected Zone
HISC	Hydrogen Induced Stress Cracking
i	Current density
i_{pass}	Passive current density
IGC	Intergranular corrosion
MIG	Metal Inert Gas
NTNU	Norwegian University of Science and Technology
OCP	Open Circuit Potential
R_m	Tensile strength
$R_{p0,2}$	Yield strength
SCC	Stress Corrosion Cracking
SCE	Saturated Calomel Reference Electrode
SEM	Scanning Electron Microscope
SiC	Silicon Carbide
SSW	Synthetic Seawater
SWAAT	Cyclic Acidified Synthetic Seawater (Fog) Testing
T	Temperature
wt%	Weight percent
ΔE	Potential drop
$\Delta E_{\mathrm{pit\text{-}OCP}}$	Difference between pitting potential and OCP

List of Figures

Figure 1: Wrought aluminium alloys correlated to their main alloying elements and strengthening categories [10]. 3

Figure 2: Pourbaix diagram for aluminium. Modified from [12]. 7

Figure 3: Experimental potential - pH diagram for alloy 5086 in chloride solution [12]. 8

Figure 4: Typical pits on aluminium alloys. a) AA6061, b) AA5456 [18]. 8

Figure 5: Schematic illustration of localized corrosion on aluminium alloys [12]. 10

Figure 6: Simple sketch of crevice corrosion [23]. 11

Figure 7: The effect of temperature on the passivity of aluminium [24]. 12

Figure 8: Temperature effect on the critical pitting potential [26]. 13

Figure 9: Temperature effect on pitting potential in chloride containing solutions [27]. 13

Figure 10: Cathodic polarization curves of freshly exposed aluminium and steel samples at a flow rate of 8 cm/s [34]. 17

Figure 11: Schematic representation of typical current – time behavior of an aluminium alloy during cathodic polarization at a constant potential [34]. 17

Figure 12: Detachment and isolation of an intermetallic particle during CP [12]. 18

Figure 13: $CaCO_3$ microstructures, aragonite (left) and calcite (right) [41]. 19

Figure 14: SEM photograph of $Mg(OH)_2$ deposit [42]. 19

Figure 15: Painted and grinded sample. 24

Figure 16: Sample ready for exposure. 25

Figure 17: Easy-to-understand illustration of the experimental setup. 26

Figure 18: Overview photo SEALAB. 27

Figure 19: Experimental setup in the corrosion laboratory. 28

Figure 20: Cross-section polished to mirror quality. 30

Figure 21: Development in OCP for freely exposed AA5083 and AA6082 in natural seawater. 31

Figure 22: Current density for samples anodic polarized to −700 mV vs Ag/AgCl. 33

Figure 23: Current density for the samples coupled to sacrificial anode (potential of approximately −1050 mV vs Ag/AgCl) 34

Figure 24: Current density for samples cathodic polarized to −1500 mV vs Ag/AgCl. 35

Figure 25: Recorded anodic- and cathodic polarization curves for the freely exposed AA5083 sample at 10 °C, the complete polarization curve recorded at the end of the exposure time is also included. AD and CD means anodic direction and cathodic direction, respectively. CC means the complete polarization curve. All the curves were recorded on the same sample. 36

Figure 26: Recorded anodic- and cathodic polarization curves for the freely exposed AA5083 sample at 32 °C, the complete polarization curve recorded at the end of the exposure time is also included. AD and CD means anodic direction and cathodic direction, respectively. CC means the complete polarization curve. All the curves were recorded on the same sample. 37

Figure 27: Recorded anodic- and cathodic polarization curves for the freely exposed AA6082 sample at 10 °C, the complete polarization curve recorded at the end of the exposure time is also included. AD and CD means anodic direction and cathodic direction, respectively. CC means the complete polarization curve. A new sample, that only had been freely exposed for 1000 hours, was used for recording the complete polarization curves. 38

Figure 28: Recorded anodic- and cathodic polarization curves for the freely exposed AA6082 sample at 32 °C, the complete polarization curve recorded at the end of the exposure time is also included. AD and CD means anodic direction and cathodic direction, respectively. CC means the complete polarization curve. A new sample, that only had been freely exposed for 1000 hours, was used for recording the complete polarization curves. ... 39
Figure 29: SEM image of an AA5083 sample freely exposed in natural seawater at 10 °C. An EDS analysis is performed for the pit inside the marked area. ... 41
Figure 30: EDS spectra for the marked area in Figure 29. ... 41
Figure 31: SEM images and EDS spectra of freely exposed AA5083 in natural seawater at 32 °C. ... 42
Figure 32: SEM images and EDS spectra for freely exposed AA6082 in natural seawater at 10 °C. ... 43
Figure 33: SEM image and EDS spectra for AA6082 freely exposed in natural seawater at 32 °C. ... 44
Figure 34: SEM images of cross-sections of the freely exposed samples in SEALAB, a) AA5083 at 10 °C, b) AA5083 at 32 °C, c) AA6082 at 10 °C and d) AA6082 at 32 °C. Note that the magnification is not the same for all the images. Image a) is from another SEM. ... 45
Figure 35: SEM images of AA5083 anodic polarized to −700 mV vs Ag/AgCl in natural seawater in SEALAB. a) and b) at 10 °C, and c) and d) at 32 °C. ... 46
Figure 36: SEM images and EDS of AA6082 anodic polarized to −700 mV vs Ag/AgCl in natural seawater in SEALAB. Image a) and b) for 10 °C and c), d) and e) for 32 °C. ... 47
Figure 37: Crevice formed beneath the coating. ... 48
Figure 38: SEM image of crystallographic pitting on the cross-section of AA6082 anodic polarized to −700 mV vs Ag/AgCl at 32 °C. ... 48
Figure 39: SEM images of AA5083 coupled to sacrificial anode in natural seawater, a) at 10 °C and b) at 32 °C. ... 49
Figure 40: SEM images and EDS spectra for AA6082 coupled to a sacrificial anode in natural seawater, a) and c) at 10 °C, and b) and d) at 32 °C. ... 50
Figure 41: SEM images of the cross-sections for the samples coupled to a sacrificial anode; a) AA5083 at 32 °C, b) AA6082 at 10 °C and c) AA6082 at 32 °C. ... 51
Figure 42: SEM images of the samples cathodic polarized to −1500 mV vs Ag/AgCl in natural seawater, a) AA5083 at 10 °C, b) AA5083 at 32 °C and c) AA6082 at 32 °C. ... 52
Figure 43: SEM images of the cross-sections of the samples cathodic polarized to −1500 mV vs Ag/AgCl; a) AA5083 at 10 °C, b) AA5083 at 32 °C and c) AA6082 at 32 °C. ... 53
Figure 44: OCP for freely exposed AA5083 and AA6082 in SSW with pH 3 at room temperature. ... 54
Figure 45: OCP for freely exposed AA5083 and AA6082 in SSW with pH 10 at room temperature. . 55
Figure 46: Current density for samples anodic polarized to −700 mV vs Ag/AgCl in SSW with pH 3. ... 56
Figure 47: Current density for samples anodic polarized to −700 mV vs Ag/AgCl in SSW with pH 10. ... 56
Figure 48: Current density for the samples cathodic polarized to −1050 mV vs Ag/AgCl in SSW with pH 3. ... 57
Figure 49: Current density for the samples cathodic polarized to −1050 mV vs Ag/AgCl in SSW with pH 10. ... 57

Figure 50: Current density for the samples cathodic polarized to −1500 mV vs Ag/AgCl in SSW with pH 3. 58
Figure 51: Current density for the samples cathodic polarized to −1500 mV vs Ag/AgCl in SSW with pH 10. 58
Figure 52: Complete polarization curves recorded for AA5083 after 24 hours exposure in SSW at room temperature. 59
Figure 53: Complete polarization curves recorded for AA5083 after 168 hours exposure in SSW at room temperature. 60
Figure 54: Complete polarization curves recorded for AA6082 after 24 hours exposure in SSW at room temperature. 61
Figure 55: Complete polarization curves recorded for AA6082 after 168 hours exposure in SSW at room temperature. 62
Figure 56: SEM images of AA5083 freely exposed in SSW with different pH-values, a) pH 3, b) pH 8,2 and c) pH 10. 63
Figure 57: SEM images of AA6082 freely exposed in SSW with different pH-values, a) pH 3, b) pH 8,2 and c) pH 10. 64
Figure 58: The three important factors for hydrogen embrittlement/HISC [53]. 87
Figure 59: Freely exposed samples in natural seawater at 10 ^{o}C in SEALAB; a) AA5083 and b) AA6082. 89
Figure 60: Samples anodic polarized to −700 mV vs Ag/AgCl in natural seawater at 10 ^{o}C in SEALAB; a) AA5083 and b) AA6082. 89
Figure 61: Samples polarized coupled to a sacrificial anode (approximately −1050 mV vs Ag/AgCl) in natural seawater at 10 ^{o}C in SEALAB; a) AA5083 and b) AA6082. 89
Figure 62: Samples cathodic polarized to −1500 mV vs Ag/AgCl in natural seawater at 10 ^{o}C in SEALAB; a) AA5083 and b) AA6082. 90
Figure 63: Freely exposed samples in natural seawater at 32 ^{o}C in SEALAB; a) AA5083 and b) AA6082. 90
Figure 64: Samples anodic polarized to −700 mV vs Ag/AgCl in natural seawater at 32 ^{o}C in SEALAB; a) AA5083 and b) AA6082. 90
Figure 65: Samples polarized coupled to a sacrificial anode (approximately −1050 mV vs Ag/AgCl) in natural seawater at 10 ^{o}C in SEALAB; a) AA5083 and b) AA6082. 91
Figure 66: Samples cathodic polarized to −1580 mV vs Ag/AgCl in natural seawater at 32 ^{o}C in SEALAB; a) AA5083 and b) AA6082. 91
Figure 67: Potential from the sacrificial anode used in the experiments performed in SEALAB. 93
Figure 68: Current density for carbon steel coupled to sacrificial anode in SEALAB. 93
Figure 69: Complete polarization curves for AA6082 exposed at 10 ^{o}C and 32 ^{o}C in natural seawater. 95
Figure 70: AA5083 sample prior to exposure. 97
Figure 71: AA6082 sample prior to exposure. 97
Figure 72: EDS analysis of corrosion products on AA5083 polarized to −1500 mV vs Ag/AgCl at 10 ^{o}C. Image a) is a SEM image of an area on the surface, b) indicates the composition of the same area. 99

Figure 73: EDS analysis of corrosion products on AA5083 polarized to −1500 mV vs Ag/AgCl at 32 °C. Image a) is a SEM image of an area on the surface, b) indicates the composition of the same area. 100
Figure 74: EDS analysis of corrosion products on AA6082 polarized to −1500 mV vs Ag/AgCl at 32 °C. Image a) is a SEM image of an area on the surface, b) indicates the composition of the same area. 100
Figure 75: OCP for freely exposed AA5083 and AA6082 in SSW with pH 8,2 at room temperature. 101
Figure 76: Current density for AA5083 and AA6082 polarized to −700 mV vs Ag/AgCl in SSW with pH 8,2. 101
Figure 77: Current density for AA5083 and AA6082 coupled to a sacrificial anode (ca −1050 mV vs Ag/AgCl) in SSW with pH 8,2. 102
Figure 78: Current density for AA5083 and AA6082 polarized to −1500 mV vs Ag/AgCl in SSW with pH 8,2. 102
Figure 79: Potentiodynamic polarization curves for AA5083 in SSW with pH 3 after 24 hours and 168 hours of exposure. 103
Figure 80: Potentiodynamic polarization curves for AA6082 in SSW with pH 3 after 24 hours and 168 hours of exposure. 104
Figure 81: Potentiodynamic polarization curves for AA5083 in SSW with pH 10 after 24 hours and 168 hours of exposure. 104
Figure 82: Potentiodynamic polarization curves for AA6082 in SSW with pH 10 after 24 hours and 168 hours of exposure. 105

List of Tables

Table 1: The basic temper groupings [11]. 4

Table 2: Important T-tempers for heat-treatable alloys [7]. 4

Table 3: Overview of strain-hardened tempers [11]. 4

Table 4: Selected mechanical properties for the Al-Mg (5xxx) alloys [7]. 5

Table 5: Selected mechanical properties for Al-Mg-Si (6xxx) alloys [7]. 5

Table 6: Overview of corrosion potential (OCP), E_{corr}, for intermetallic particles common to aluminium alloys in chloride containing solutions [28]. 14

Table 7: Chemical composition (wt%) of the alloys in this study. 23

Table 8: Characteristic values for AA5083 during anodic- and cathodic polarization after 168 hours (one week) and 1000 hours (six weeks) of exposure. 40

Table 9: Characteristic values for AA6082 during anodic- and cathodic polarization after 168 hours (one week) and 1000 hours (six weeks) of exposure. 40

Table 10: EDS analysis of the marked area in Figure 29. 41

Table 11: EDS analysis of the freely exposed AA5083 in Figure 31. 42

Table 12: EDS analysis for the indicated pit in image b) in Figure 32. 43

Table 13: Results of EDS of the indicated pits in image a) in Figure 33. 44

Table 14: Results from EDS of marked areas in Figure 39. 49

Table 15: Characteristic values for AA5083 during anodic- and cathodic polarization after 1 day (24 hours) and 1 week (168 hours) of exposure. 62

Table 16: Characteristic values for AA6082 during anodic- and cathodic polarization after 1 day (24 hours) and 1 week (168 hours) of exposure. 62

Table 17: Current density values, i [$\mu A/cm^2$], for the samples coupled to a sacrificial anode in natural seawater. 76

1 Introduction

1.1 Background

Due to today's low oil price there is a demand for cost effective solutions in the offshore oil and gas industry. This makes aluminium an interesting material, and due to its low weight the interest for using aluminium in subsea structures has increased during the last years. The density of aluminium is approximately 1/3 compared to steel; this allows for considerable weight savings.

So called corrosion resistant aluminium alloys from the Al-Mg (5xxx)- and Al-Mg-Si (6xxx) series have been used for many years in ship hulls, and the experiences are good. However, corrosion failures have been observed [1, 2]. The main problem is connection to more noble metals e.g. carbon steel, stainless steel and copper alloys, that will cause galvanic corrosion on aluminium [3]. Used for subsea structures, aluminium will in most cases be in metallic contact with carbon steel (and even with more noble metals). Carbon steel is always connected to a cathodic protection (CP) system in seawater [4], which means that the aluminium alloy also will be connected to the CP system.

AA5083 and AA6082 are the most frequently used aluminium alloys for seawater applications, and also the recommended ones according to NORSOK [5]. In the literature, limited detailed information is published about the behavior of AA5083 and AA6082 under CP in seawater. It is known that both temperature, electrochemical potential and pH affects the corrosion behavior of these alloys.

1.2 Aim of this work

The aim of this study is to examine the behavior of the aluminium alloys AA5083 and AA6082 under different conditions in natural seawater. Samples will be exposed to natural seawater at two different temperatures ($10 \pm 2\ ^{o}C$ and $32 \pm 2\ ^{o}C$) under different conditions (freely exposed and at different fixed electrochemical potentials). In addition, to study the effect of pH will samples under the same conditions be exposed to synthetic seawater (SSW) with pH-values: 3, 8,2 and 10. Recording of potentiodynamic polarization curves, current requirements and open circuit potentials (OCP), in addition to surface examinations will be included in an effort to examine the corrosion behavior.

2 Theory

2.1 Aluminium and aluminium alloys

Aluminium is a silvery-white, soft, non-magnetic and ductile metal. Aluminium has a face-centered cubic (FCC) crystal structure [6]. Aluminium and its alloys have an excellent combination of properties such as low weight, good corrosion resistance, high ductility, formability, electrical and thermal conductivity [7]. The strength and hardness of pure aluminium are relatively low. Thus, aluminium is seldom used in its pure form. Aluminium is usually alloyed with elements to increase physical properties such as strength and hardness. The modulus of elasticity for aluminium is 69 GPa [8].

Age hardening and strain hardening (work hardening) can increase the strength and hardness of the aluminium alloys. The age hardenable alloys achieve strength through controlled precipitation during heat treatment and/or through solution heat treatment. Non-heat treatable alloys normally obtain strength from work hardening, the strength is increased because of movement of dislocations and generation of new dislocations within the crystal structure of the metal [9]. Figure 1 shows the different wrought aluminium alloys related to the main alloying element and strengthening category.

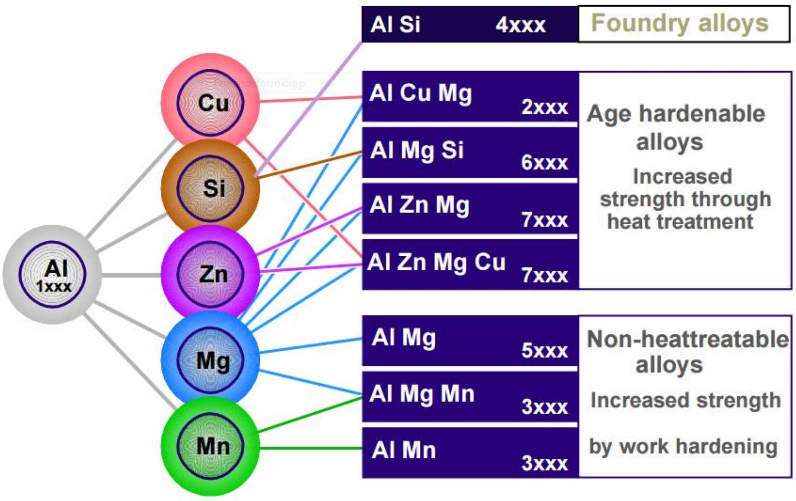
Al Si 4xxx
Foundry alloys
Al Cu Mg 2xxx
Al Mg Si 6xxx
Al Zn Mg 7xxx
Al Zn Mg Cu 7xxx
Age hardenable alloys
Increased strength through heat treatment
Al Mg 5xxx
Al Mg Mn 3xxx
Al Mn 3xxx
Non-heattreatable alloys
Increased strength by work hardening
Al 1xxx
Cu
Si
Zn
Mg
Mn

Figure 1: Wrought aluminium alloys correlated to their main alloying elements and strengthening categories [10].

The different wrought aluminium alloys are classified according to the international alloy designation system each with a four-digit number based on composition, alloy additions and level of impurities. The first digit tells to which series it belongs. The series are ranging from 1xxx-series to 8xxx-series. A prefix is used to designate the standard AA of the Aluminium Association or EN AW for the European Standard [7].

The mechanical properties of one and the same alloy, in terms of composition, can vary drastically depending on the heat treatment- and work hardening processing. It is therefore important to specify the temper of an aluminium alloy, how strength is provided to the alloy [7]. To specify the temper designation a further nomenclature extends the alloy numbering system with letters and digits. Table 1 gives an overview of the basic temper designations.

Table 1: The basic temper groupings [11].

Letter	Meaning
F	As fabricated – Applies to products of a forming process in which no special control over thermal or strain hardening conditions is employed
O	Annealed – Applies to products which has been heated to produce the lowest strength condition to improve ductility and dimensional stability
T	Thermally Treated – To produce stable tempers other than F, O or H. Applies to products, which have been heat-treated, sometimes with supplementary strain-hardening, to produce a stable temper. The “T” is always followed by one or more digits
H	Strain Hardened – Applies to products, which are strengthened through cold-working. The strain hardening may be followed by supplementary thermal treatment, which produces some reduction in strength. The “H” is always followed by two or more digits

There are nine different T-tempers. The digits expresses which heat treatment process that has applied for the alloy. The three most important T-tempers are described in Table 2.

Table 2: Important T-tempers for heat-treatable alloys [7].

Temper	Description
T3	Solution heat treated – Cold worked – Naturally aged
T6	Solution heat treated – Artificially aged
T7	Solution heat treated – Overaged (i.e. beyond maximum strength)

At least two additional digits describe the strain-hardened tempers (H). The first digit expresses the basic operations applied on the alloy, and the second digit indicates the degree of strain hardening. Table 3 shows the different basic operations and the levels of strain hardening.

Table 3: Overview of strain-hardened tempers [11].

Basic operations	Degree of strain hardening
1: Strain Hardened Only	2: Quarter hard
2: Strain Hardened and Partially Annealed	4: Half hard
3: Strain Hardened and Stabilized	6: Three quarter hard
4: Strain Hardened and Lacquered or Painted	8: Hard
	9: Extra hard

A brief introduction to the aluminium alloy series relevant for this study will be given in the following.

2.1.1 Al-Mg (5xxx) alloys

The alloys in this series are the so-called seawater-resistant alloys [12]. Alloys of this series are moderate in strength. These alloys are non-heat treatable, thus the strength is normally obtained through work hardening. Alloys of this series have good resistance to corrosion in aggressive environments and seawater. However, they become susceptible to intergranular corrosion (IGC) if the Mg content exceeds 4,5% [12], some literature say 3,5% [3], this is further discussed in Section 2.2.7. Mg is the main alloying element and the Mg additions are ranging from 0,2 – 6,2% [11], elements like Si, Fe, Mn, Cr, Cu and Zn are also included [13].

The good formability and weldability, combined with medium strength and good corrosion resistance makes these alloys suitable for outdoor exposure applications, which typical include shipbuilding, vehicle bodies, and pressure vessels. According to NORSOK M-121 the alloy EN AW 5083 should be the prime alloy selection for plates used in offshore applications, and for structures submerged in seawater EN AW 5083 and/or 6082 should be used [5]. Some selected mechanical properties for the Al-Mg (5xxx) alloys are given in Table 4.

Table 4: Selected mechanical properties for the Al-Mg (5xxx) alloys [7].

Yield strength, $R_{p0.2}$ [MPa]	Tensile strength, R_m [MPa]	Elongation [%]
185 – 345	200 – 415	6 – 15

2.1.2 Al-Mg-Si (6xxx) alloys

The Al-Mg-Si (6xxx) alloys are characterized by medium strength, good weldability, excellent extrudibility and good corrosion resistance [14]. Typical applications for these alloys include bridges, car frames and cranes. Due to its extrudability these alloys are often preferred for architectural and structural applications where unusual or particular strength- or stiffness-criticality is important [14]. The main alloying elements are Mg and Si, with additions of 0,3 – 1,5% [7]. Elements like Fe, Cu, Mn, Cr, Zn and Ti are often added in small amounts [15]. These alloys are age hardenable, which means strength is achieved through heat treatment, alloying atoms trapped between the aluminium atoms increases the strength [3, 16].

The Al-Mg-Si (6xxx) alloys are suitable for applications in marine environments. According to NORSOK M-121 the alloy EN AW 6082 should be the prime alloy selection for profiles used in offshore applications [5]. Some selected mechanical properties for these alloys are given in Table 5.

Table 5: Selected mechanical properties for Al-Mg-Si (6xxx) alloys [7].

Yield strength, $R_{p0.2}$ [MPa]	Tensile strength, R_m [MPa]	Elongation [%]
130 – 235	210 – 345	12 – 26

As mentioned, both the Al-Mg (5xxx) - and the Al-Mg-Si (6xxx) alloys have good weldability. The welding process will affect the properties of the base material in an area near the deposited metal (filler alloy) due to the heating that occurs during welding. This area is called the heat-affected zone (HAZ), and heat-treated and work hardened aluminium alloys, e.g. 5xxx- and 6xxx series, will develop a weakness in the HAZ. This subject will not be further discussed in this report.

2.2 Corrosion of aluminium

Corrosion may be a problem for materials, especially in marine environments and seawater. In general, aluminium is known to be resistant to corrosion in most environments due to its protective oxide, but the corrosion properties will vary according to alloy, environmental parameters, protective actions, etc.

2.2.1 Concepts for corrosion of aluminium in seawater

If aluminium is scratched in water, the bare surface oxidizes immediately according to the reaction sequence in Equation 2.1 and 2.2 [17].

$$\mathrm{Al} \rightarrow \mathrm{Al}^{3+} + 3\mathrm{e}^{-} \tag{2.1}$$

$$2\mathrm{Al}^{3+} + 3\mathrm{H_2O} \rightarrow \mathrm{Al_2O_3} \tag{2.2}$$

The electrons released by the first reaction are consumed by a reduction reaction of the type in Equation 2.3 or 2.4 [17].

$$\mathrm{O_2} + 2\mathrm{H_2O} + 4\mathrm{e}^{-} \rightarrow 4\mathrm{OH}^{-} \tag{2.3}$$

$$2\mathrm{H}^{+} + 2\mathrm{e}^{-} \rightarrow \mathrm{H_2} \tag{2.4}$$

This protective layer can be broken down in environments with high or low pH, or in environments with aggressive ions. Chloride is an aggressive ion and seawater contains large quantities of it. Seawater is therefore an environment where so-called local corrosion may be initiated [3]. This can also be seen if we look at it from a thermodynamic point of view and look at the Pourbaix diagram for aluminium. The Pourbaix diagram is shown in Figure 2 and the red line indicates seawater conditions with pH 8,2. This Pourbaix diagram is based on thermodynamic calculations, and the diagram shows that aluminium does not look suitable for applications in seawater. The reason is that the metal is not in the passive region at pH 8,2 according to the diagram.

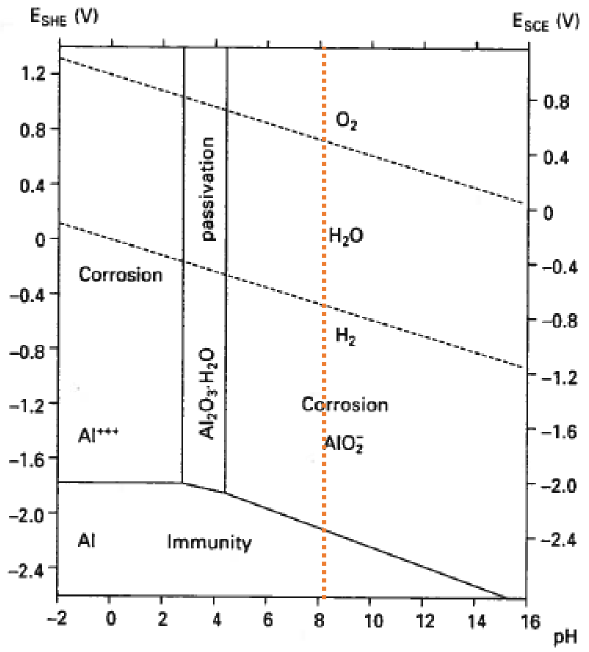

Figure 2: Pourbaix diagram for aluminium. Modified from [12].

Therefore, the passivity of aluminium in slightly alkaline environments like seawater is ensured by use of alloying elements, such as Mg and Mn [12]. Figure 3, which is a practical Pourbaix diagram for the alloy AA5086 produced from experimental corrosion data obtained in chloride solutions [12], proves this point. Figure 3 shows that passivity is possible for this alloy at pH 8,2, and this is due to the presence of the passivating alloying elements Mg and Mn. The oxide of these alloying elements becomes increasingly passive with increasing pH, and this effect contributes to a larger range of passivating oxide on the aluminium alloy than the thermodynamic calculations for aluminium according to Figure 2 indicates. These solid-solution alloying elements becomes enriched in the oxide in exposure to seawater because of selective dissolution of the more active aluminium component and, thus, render the oxide more passive against seawater [12].

Localized corrosion of aluminium is primarily determined by the properties, size and distribution of the intermetallic compound. If copper is not present, the properties of the solid-solution matrix alloys is also a contributing factor [12]. The corrosion on aluminium alloys starts in weak points in the oxide, often in contact with or around the intermetallic particles [3, 12]. The weak points are generally due to the presence of a flaw in the particle-matrix interface. The stable aluminium oxide is an insulator against electrical conduction because it is ceramic, and the reduction reaction required for corrosion can only occur on the type of intermetallic particles that are more electrochemically noble than the matrix [12], this is further discussed in Section 2.2.2. In Figure 4 scanning electron microscope (SEM) images of typical pits for the aluminium alloys AA6061 and AA5456 can be seen [18].

2.2 Corrosion of aluminium

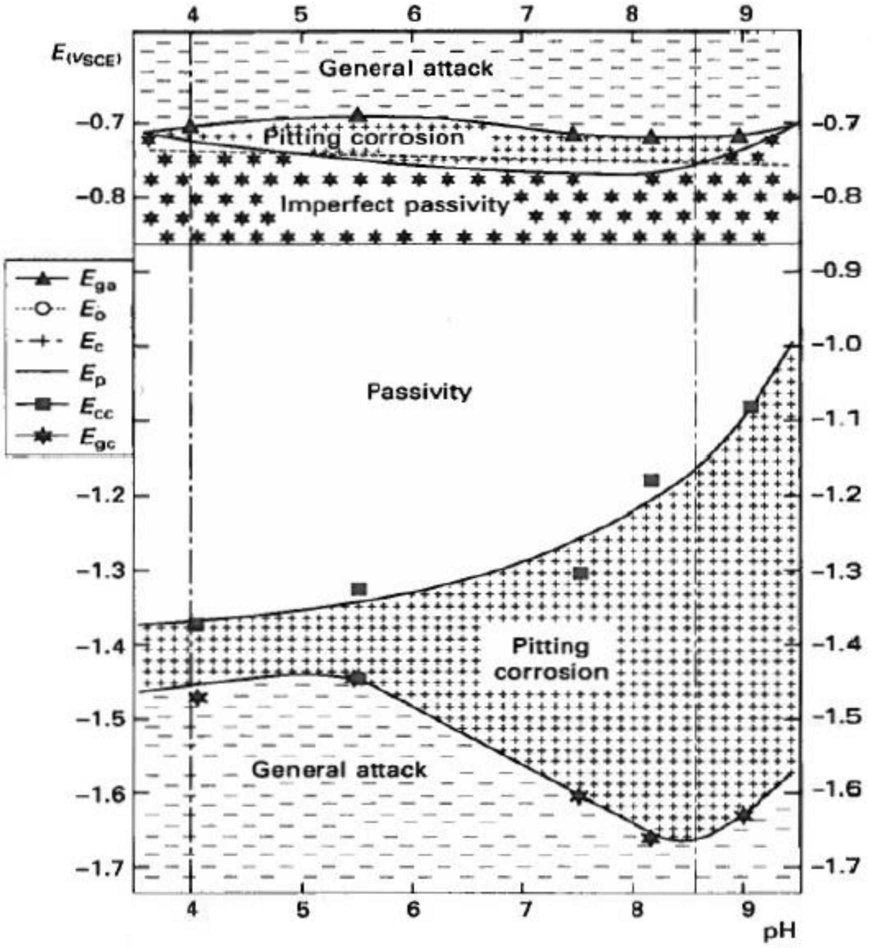

Figure 3: Experimental potential - pH diagram for alloy 5086 in chloride solution [12].

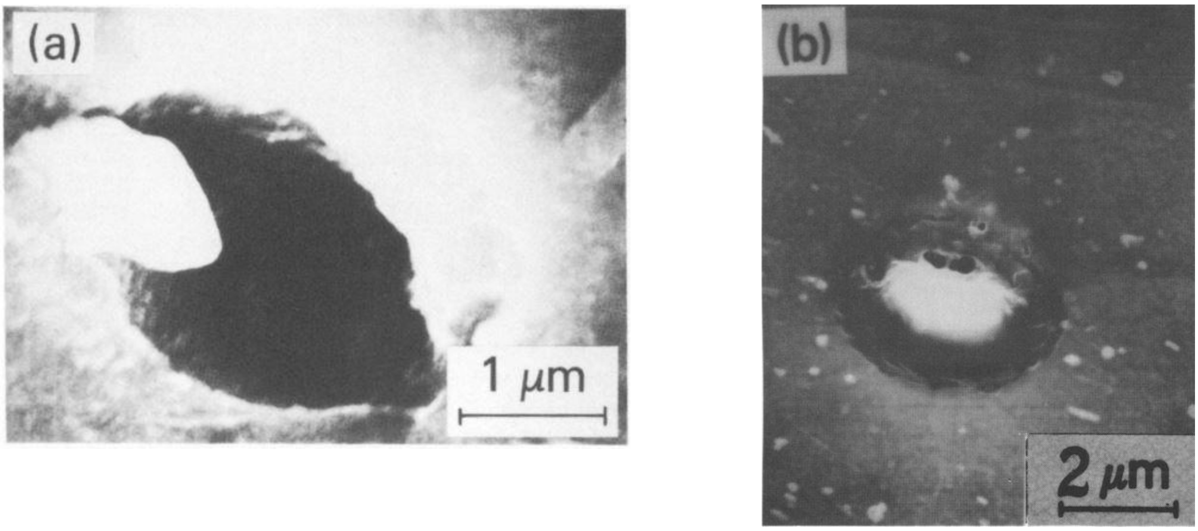

Figure 4: Typical pits on aluminium alloys. a) AA6061, b) AA5456 [18].

2.2.2 Uniform corrosion and pitting corrosion on aluminium

Uniform corrosion will cause a uniform degradation of the exposed surface. As the protective oxide is stable, this is seldom a problem for aluminium. Under stagnant and low flow-rate conditions, the uniform corrosion rate of the seawater resistant alloys in seawater lies below 1 µm/year [12].

As explained in the previous section corrosion of aluminium is primarily in form of localized attacks. Pitting corrosion is the most common type of corrosion on aluminium, and as explained earlier the corrosion starts from weak points (normally around intermetallics) in the oxide. The events that occur during a stable localized attack like pitting corrosion are summarized in Figure 5. It illustrates the development of a localized environment in the pit (acid) and adjacent to the cathodic site (alkaline), resulting from the metal hydrolysis and reduction processes. High pH developing adjacent to the cathodic site leads to destabilization of the amphoteric aluminium oxide which again leads to etching of the aluminium matrix around the intermetallic particle that act as the cathode. At the same time, this local alkalization alters the chemistry and structure of the intermetallics on aluminium. The more noble particles becomes essentially enriched at the surface because of the selective dissolution of the aluminium component. The enriched particles can also be active or passive, hence the enrichment of particles at the surface may be beneficial for the corrosion process, or it can be restraining for the corrosion process. Figure 5 also shows how corrosion products, Fe^{2+}, from iron-rich intermetallics in the pit can redeposit in or at the immediate vicinity of the pit and increase the cathodic area, thereby fueling the corrosion process [12]. However, in pitting corrosion the corrosion rate generally decreases over time, because the surface is often enriched by more active and passive components. The alloying elements Mg and Mn are known to have a positive effect against pitting corrosion, and Cu and Fe to have a negative effect [3, 19], this is described more detailed in Section 2.2.6.

The type of pit illustrated in Figure 5 can propagate autocatalytically and cause material damage, but it does not initiate unless the metal surface can be polarized temporarily more positive than the critical pitting potential, which is about −0,75 V_{SCE}[1] in seawater (and about −0,73 to −0,76 V_{SCE} in 3% NaCl) [12, 20, 21]. However, once such pits are initiated they can propagate at potentials more negative than the pitting potential because of the acidic environment in the pit [12]. The critical pitting potential is temperature dependent; this is discussed in Section 2.2.5.

---

[1] The potential against a saturated calomel reference electrode (SCE) can be converted to potential against a silver chloride reference electrode (Ag/AgCl) by adding +44 mV.

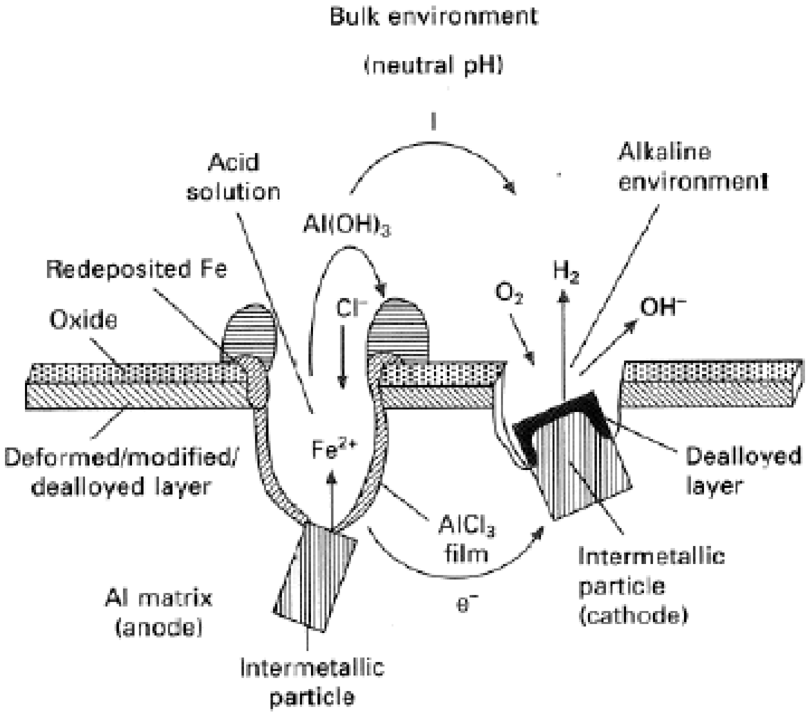
Bulk environment
(neutral pH)
I
Acid solution
Alkaline environment
Al(OH)$_3$
Redeposited Fe
Cl$^-$
O$_2$
H$_2$
OH$^-$
Oxide
Deformed/modified/ dealloyed layer
Fe^{2+}
Dealloyed layer
AlCl$_3$ film
Intermetallic particle (cathode)
Al matrix (anode)
e$^-$
Intermetallic particle

Figure 5: Schematic illustration of localized corrosion on aluminium alloys [12].

2.2.3 Crevice corrosion on aluminium

Crevice corrosion is local corrosion concentrated in crevices. The crevice need to be sufficient open such that the liquid can enter, and at the same time sufficient narrow such that the liquid stays in the crevice. Crevice corrosion can occur in narrow crevices between metal-to-metal connections and between metal-to-non-metal connections. Crevices can also form beneath coating or under fouling. The most pronounced crevice corrosion occurs on metals that are passive or easily can be passivated, such as aluminium and stainless steel. The passivity will be broken down locally [22].

Aggressive ions needs to be present in the liquid for crevice corrosion to occur, for example chlorides in seawater. As the liquid is trapped in the crevice an environment different from the surroundings is developed. The oxygen will be consumed in the crevice due to the corrosion reactions. When the oxygen is consumed, the anodic metal dissolution reaction will continue in the crevice and be maintained by the cathodic reduction reaction outside the crevice. Due to migration of Cl$^-$-ions into the crevice, the pH will drop, such that the conditions inside the crevice will become more aggressive over time. The protective oxide will be dissolved due to the low pH and active corrosion will start in the crevice [3].

The severity of the corrosion will to a certain extent depend on whether the crevice is above the seawater or submerged in the seawater. For a crevice submerged in seawater the process is explained above. If the crevice is above the waterline, both the anode and cathode reactions will take place in the crevice and the pH will not drop. Thus, the principle effect will be that the aluminium surface stays wet for a longer period [3]. Figure 6 shows a simple illustration of crevice corrosion for a component submerged in a corrosive electrolyte.

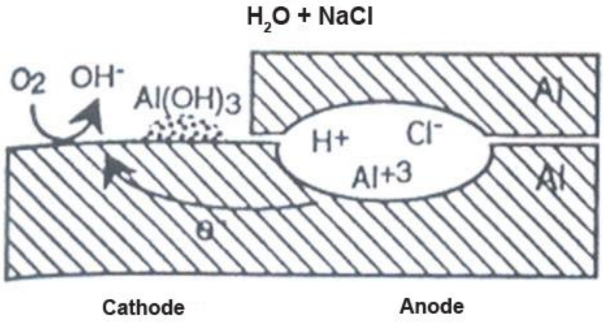

Figure 6: Simple sketch of crevice corrosion [23].

From Figure 6 the crevice corrosion process can be understood as follows; the metal ions reacts to the water molecules (hydrolysis) causing an acid environment, according to Equation 2.5, inside the crevice.

$$M^{n+} + H_2O \rightarrow MOH + H^+ \tag{2.5}$$

To balance the positive charged ions in the crevice, chloride ions starts to migrate into the crevice. This results in metal-hydroxide and formation of hydrochloric acid in the crevice, Equation 2.6.

$$M^+Cl^- + H_2O \rightarrow MOH + HCl \tag{2.6}$$

The low pH inside the crevice results in a very aggressive environment, and the migration of chloride ions increases as the corrosion rate increases, the corrosion process is autocatalytic [22].

2.2.4 Galvanic corrosion on aluminium

Galvanic corrosion may be a problem for aluminium submerged in seawater. Galvanic corrosion occurs when two dissimilar metals are coupled, and exposed to a corrosive and electrical conducting fluid (seawater). The least noble metal will then act as a sacrificial anode and protect the noble metal, this is due to the same principle as for sacrificial anodes in CP systems [22]. Aluminium is less noble than most of the construction metals and galvanic corrosion must always be considered when using aluminium, otherwise it can be a serious problem. Galvanic corrosion on aluminium will in most cases occur as pitting.

2.2.5 Effect of temperature

The temperature has an effect on the corrosion behavior of aluminium. The passive zone in the Pourbaix diagram is supposed to shift towards lower pH with increasing temperatures, this is shown in Figure 7 [24, 25]. This diagram is based on thermodynamic calculations at temperatures of 25 °C (298 °K), 100 °C (373 °K) and 159 °C (432 °K). Based on these purely thermodynamic considerations in Figure 7 the corrosion resistance of aluminium in acidic environments is expected to increase, while the corrosion resistance in neutral and alkaline environments is expected to decrease with increasing temperatures.

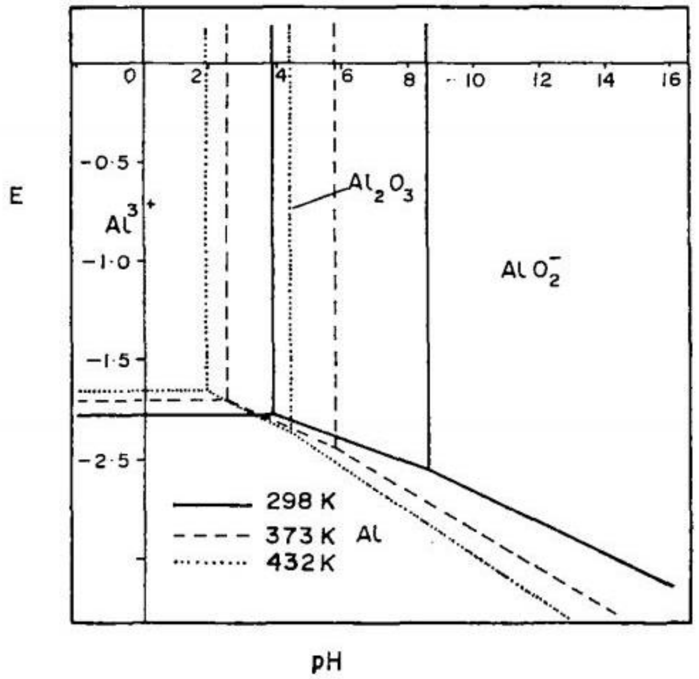

Figure 7: The effect of temperature on the passivity of aluminium [24].

As discussed in Section 2.2.1 and 2.2.2 uniform corrosion is only possible in highly acidic and alkaline environments. At near neutral pH the corrosion is highly localized and dependent on the critical pitting potential to initiate. If the potential is raised above the critical pitting potential in the presence of chloride ions, the aluminium oxide layer becomes unstable and pitting corrosion can initiate. The critical pitting potential of aluminium in chloride solutions tends to be independent of temperature up to approximately 30 °C. This temperature is seen as a transition point, above 30 °C the critical pitting potential starts to decrease significantly more, and above 40 °C, the pitting potential decreases drastically with increasing temperature [26, 27]. The effect of temperature on the critical pitting potential for aluminium in chloride solutions can be seen in Figure 8 and Figure 9, the transition point at approximately 30 °C (303 °K) can be seen in both the diagram from 1975 and the newer one from 2011.

J. Soltis, et al. [27], suggested that the drastic decrease in pitting potential at increased temperatures above 40 °C may be related to the surface films formed on aluminium when exposed to water. Films formed below 40 °C consist exclusively of bayerite, while those formed at higher temperatures (up to 100 °C) have an inner layer of pseudo-boehmite and an outer layer of bayerite crystals [27].

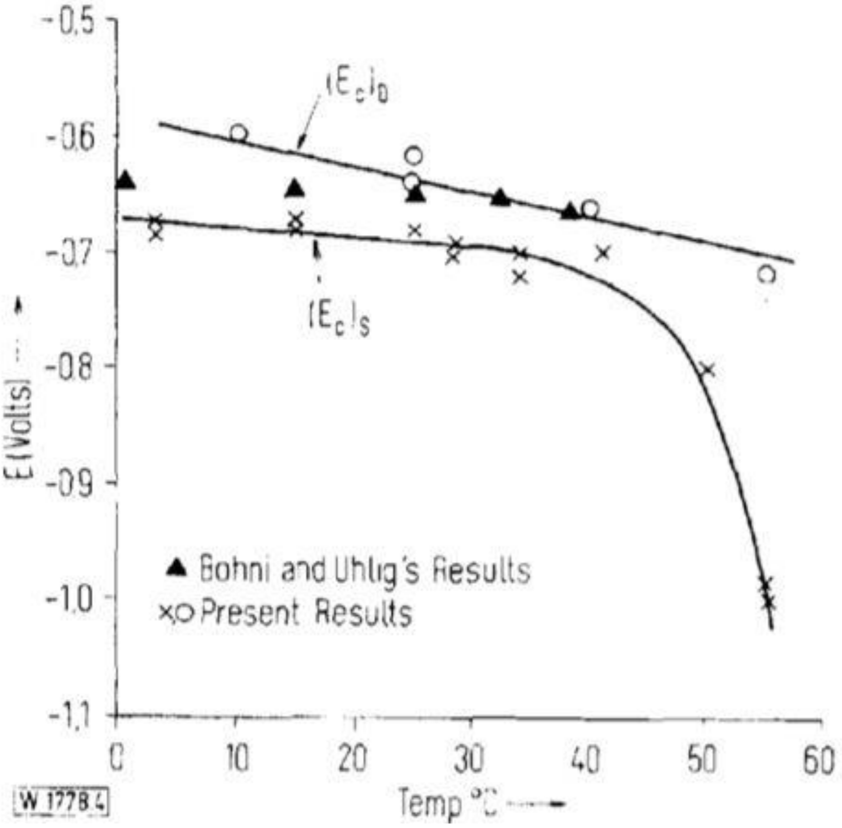

Figure 8: Temperature effect on the critical pitting potential [26].

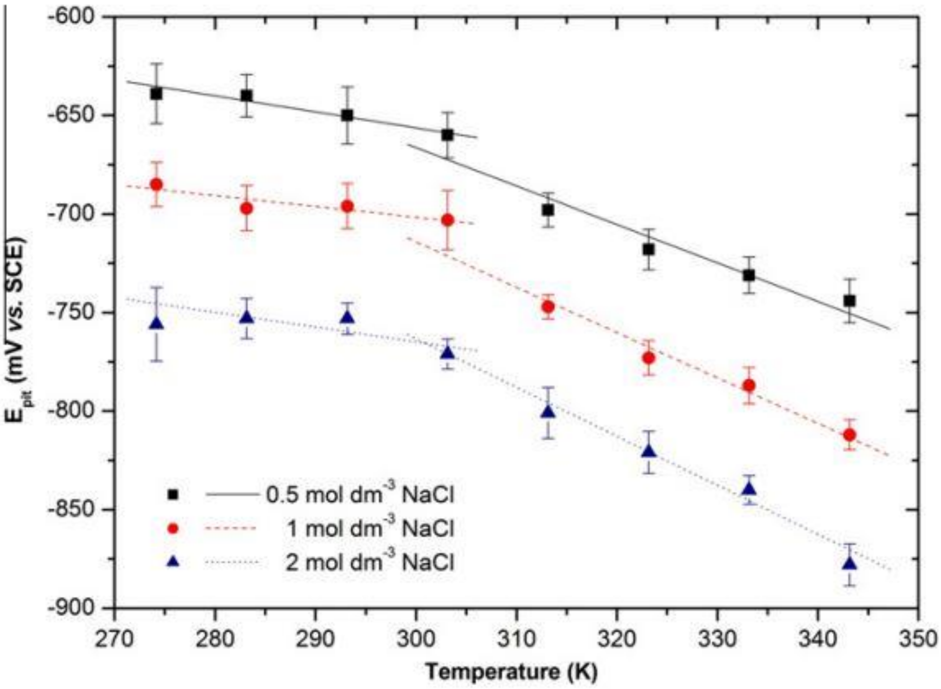

Figure 9: Temperature effect on pitting potential in chloride containing solutions [27].

2.2.6 Effect of microstructure and alloying elements

The different aluminium alloy microstructures are developed as a result of alloy composition and thermomechanical treatment, as discussed in Section 2.1. From a corrosion point of view, the important features of alloy microstructure are grain structure and distribution of secondary phase (intermetallic) particles as constituent particles, dispersoids or precipitates. The electrochemical characteristics of such particles differ from the behavior of the surrounding alloy matrix, making alloys susceptible to localized forms of corrosion attack (microgalvanic corrosion) [28], this has also been discussed in Section 2.2.1 and 2.2.2.

The critical pitting potential of aluminium depends on the alloying elements as long as these are in solid solution with the aluminium. Noble alloying elements raise the pitting potential in the positive direction, and active elements decrease the pitting potential in the negative direction [25]. Table 6 shows an overview of corrosion potential (OCP), E_{corr}, for intermetallic particles common to aluminium alloys in chloride containing solutions.

Table 6: Overview of corrosion potential (OCP), E_{corr}, for intermetallic particles common to aluminium alloys in chloride containing solutions [28].

Phase	E_{corr} [mV$_{\mathrm{SCE}}$] in 0,1 M NaCl
Al_3Fe	−539
Al_2Cu	−665
Al_6Mn	−779
Al_3Ti	−603
$Al_{32}Zn_{49}$	−1004
Mg_2Al_3	−1013
$MgZn_2$	−1029
Mg_2Si	−1538
Al_7Cu_2Fe	−551
Al_2CuMg	−883
$Al_{20}Cu_2Mn_3$	−565
$Al_{12}Mn_3Si$	−810
Al – 2%Cu	−672
Al – 4%Cu	−602

Fe containing intermetallic particles, like Al_3Fe and Al_6Fe, are electrochemically more noble than the surrounding aluminium matrix, and will act as sites for the reduction reactions in Equations 2.3 and 2.4. The rate of the reduction reaction is dependent on the ratio of the area of exposed intermetallic particles relative to area of the matrix alloy. If the reduction reaction rate is high enough these cathodes are capable of increasing the potential of the surrounding aluminium matrix in the positive direction. Depending on the corrosivity of the environment, the oxide layer may break down in weak spots and a microgalvanic cell (pitting) may be established, similar to the illustration in Figure 5 [17]. The addition of Mn and Si increases the resistance of pitting [29]. Mn prevents the formation of Al_3Fe-particles. In addition, enrichment of Mn on the aluminium surface contribute to passivity, both the oxidation and reduction reaction rates will be decreased [17, 30].

The alloying elements with a certain solubility in aluminium also contribute to the corrosion behavior, depending on whether these elements are more noble or more active than aluminium [31]. Cu, which is more noble than aluminium, will increase the corrosion rate of the active aluminium matrix, this is called selective dissolution. The surface will be enriched with the more noble component, Cu, and will then behave more according to the electrochemical properties of Cu [31]. Enrichment of the surface with Cu is known to have a negative effect on initiation of pitting, while the active alloying element Mg is known to have the opposite effect [12].

For alloying elements which are more active (less noble) than aluminium, Mg is the only element that is commercially used today. The Al-Mg (5xxx) alloys usually contain between 1 – 5% Mg [31]. If the concentration of Mg is above 4,5% [12] the unwanted β-phase Mg_5Al_8 may precipitate on the grain boundaries. This will lead to brittleness and stress corrosion cracking (SCC) [32]. During precipitation the Mg-rich β-phase Al_3Mg_2 may also form, Al_3Mg_2 grows heterogeneous along the grain boundaries. This β-phase will lead to SCC, because it is anodic relative to the matrix. Al_3Mg_2 can grow as a continuous film along the grain boundaries [32, 33], so-called IGC.

In the right amounts, Mg is beneficial, as mentioned in Section 2.2.1 since it makes the oxide less soluble in alkaline environments. In addition, it corrodes faster than aluminium, causing the surface to be purer in aluminium, which is more resistant to corrosion than an Al – Mg alloy. The dissolved Mg will act as sacrificial anodes for the aluminium surface [17].

Silicon increases the corrosion resistance of aluminium in alkaline environment, this is because the silicon particles are resistant to both most acids and salts. The Si containing particles will be cathodic to the aluminium matrix [30, 31].

What kind of compounds the alloying elements form depends on the amount of the different alloying elements and working procedure. According to Mondolfo [30] the following intermetallic compounds are possible for the alloys in this study with the composition described in Table 7.

- AA5083: Mg_5Al_8, $(FeMn)Al_6$, $FeAl_3$ and $(CrFe)Al_7$.
- AA6082: Mg_2Si, $FeSiAl_5$, $(FeMn)_3Si_2Al_{15}$ or $(CrFe)_4Si_4Al_{13}$ and $FeSiAl_8$.

2.3 Cathodic protection of aluminium

CP is a method to protect aluminium and other metals from corrosion when submerged in seawater, or other conducting corrosive electrolytes. In CP, an external current is applied to the structure to be protected to lower the potential into the immune region of the Pourbaix diagram. This can be done either by sacrificial anodes or by an impressed current system.

In terms of CP, two important issues distinguish aluminium alloys from steel. Firstly, for aluminium protection is achieved by moving the potential into the passive region of the Pourbaix diagram. This is because the protective oxide is amphoteric, and becomes unstable in acid environments and alkaline environments. Seawater is a slightly alkaline environment, and if the rate of the cathodic reaction is too high, the metal surface becomes more alkaline and hence the protective oxide becomes destabilized. This can happen if the potential of aluminium is lowered in an attempt to move it into the immune region of Figure 2, and can lead to higher corrosion rate rather than reduced corrosion rate. The transition between passivity and cathodic pitting in Figure 3 can be used as a rough guideline for the negative limit of the potential applied during CP to avoid too high rate of the cathodic reaction, although the limit actually depends on the flow rate. The protection is therefore achieved by maintaining the passivity of the surface rather than by bringing the potential close to or into the range of immunity, as is the case for steel. Thus, in principle, for aluminium we are talking about anodic protection rather than cathodic protection [12, 34].

The other thing is that the current required for protection is low compared to CP of steel. This is because the cathodic process is mainly restricted to the cathodic intermetallic sites and this is just a small fraction of the area that is exposed. For steel, all of the exposed area needs CP, not only weak spots. The cathodic current density on steel is given by the limiting current for the oxygen reduction on a uniformly accessible surface, and it does not vary significantly with changes in applied potential in the potential range −800 to −1000 mV_{SCE}, see Figure 10. The current density on aluminium is about a magnitude smaller than steel, and it does vary with change in applied potential. The current level is also dependent on the type of alloy [12, 34].

Figure 10 shows cathodic polarization curves of freshly exposed aluminium alloys and steel samples in natural seawater at a flow rate of 8 cm/s. As it can be seen, the current density requirement for steel is significantly higher than for aluminium at potentials more positive than −1400 mV_{SCE} according to this article [34].

The current requirement for CP of aluminium in seawater is reduced over time. This can be seen in Figure 11 which is a schematic representation of typical current – time behavior for aluminium alloys during cathodic polarization at constant potentials [34]. At the beginning of the exposure, the current density is increasing due to dissolution of the protective oxide and resulting corrosion around the intermetallic particles. After reaching a maximum value, the current exhibit an exponential reduction. Calcareous deposits covering the cathodic particles and detachment of cathodic intermetallic particles from the surface causes this reduction. This detachment of the particles is a result of the cathodic etching phenomenon. This phenomenon is described in the Section 2.2.2 as the part of what happens in the alkaline environments that develops adjacent to the pit. A summary of what happens is illustrated in Figure 12.

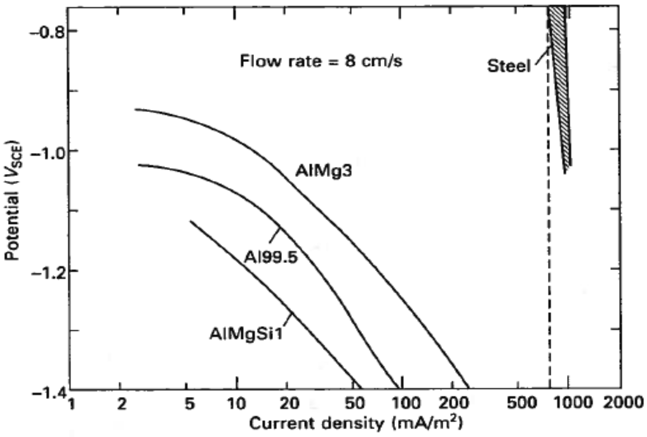

Figure 10: Cathodic polarization curves of freshly exposed aluminium and steel samples at a flow rate of 8 cm/s [34].

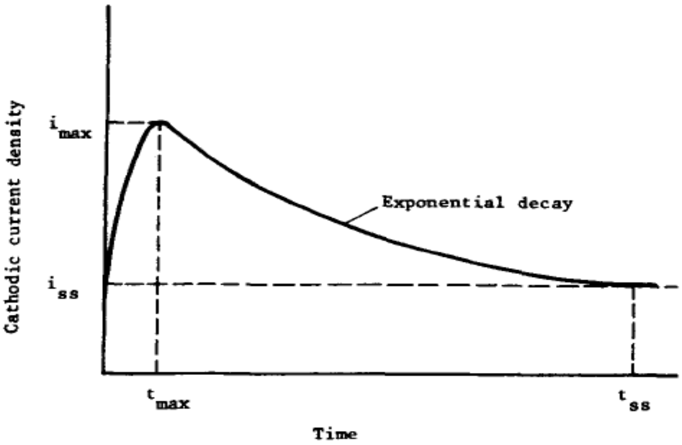

Figure 11: Schematic representation of typical current – time behavior of an aluminium alloy during cathodic polarization at a constant potential [34].

Figure 12 shows from a) to c) how an alkaline environment is developed and etching the aluminium matrix around the cathodic particle. At the end, the cathodic particle is detached and does not require current for CP anymore. The small area of cathodic sites (intermetallic particles), together with the isolation of cathodic sites over time leads to low current demand. The current requirement may in fact become a few mA/m^2 positive [12]. It is therefore very beneficial to protect aluminium with sacrificial anodes, because the consumption of these will be low. What is explained in this section applies for stagnant and low flow rate conditions.

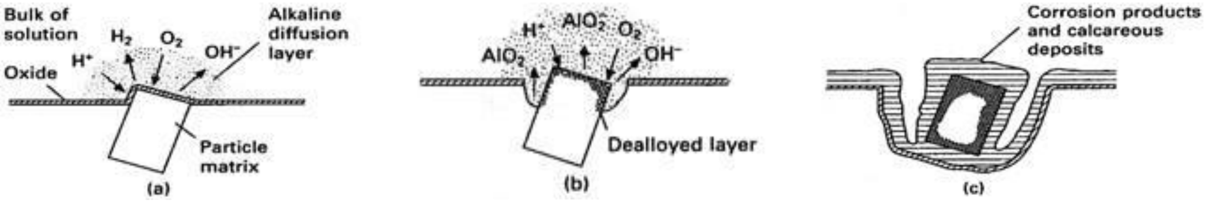

Figure 12: Detachment and isolation of an intermetallic particle during CP [12].

When the flow rate increases, the pitting will at some point change to uniform corrosion of the aluminium surface. Under such conditions, CP becomes ineffective, and in some cases, it may increase the corrosion rate rather than reducing it. This is because the corrosion rate is controlled by the chemical dissolution rather than by an electrochemical process. The dissolved oxide is replaced by anodic formation of new oxide at the metal-oxide interface, hence the corrosion rate is increased. In such situations a good surface treatment will provide better corrosion protection [12].

CP is also a source of hydrogen, a brief overview of the effect of hydrogen in aluminium can be found in Appendix A.

2.4 Calcareous deposit

The calcareous deposits formed on immersed metals is mostly a consequence of CP [35]. The term calcareous deposit describes Mg and Ca containing compounds [36]. The calcareous deposit acts as a barrier for oxygen diffusion to the metal surface [35], and hence this will contribute to reduce the current density required for CP. However, for aluminium alloys the calcareous deposits are thought to play a less important role for determining the current requirement for CP [34].

2.4.1 Formation of calcareous deposit

An important factor for the formation of calcareous deposit is the ability the applied current for the CP system have of changing the pH at the metal surface [37]. The oxygen reduction on the metallic surface produces hydroxyl ions, OH^-, and this results in local pH increase near the metal/seawater interface [35]. Calcareous deposits mainly precipitate at pH between 8 and 10, the interfacial pH is therefore of vital importance for the calcareous deposits [38, 39]. The calcareous deposit is essentially made of calcium carbonate, $CaCO_3$, and magnesium hydroxide, $Mg(OH)_2$ and some magnesium carbonate, $MgCO_3$ [35, 40]. The reactions for precipitation of $CaCO_3$, $Mg(OH)_2$ and $MgCO_3$ can be seen in Equations 2.7, 2.8 and 2.9:

$$Ca^{2+} + HCO_3^- + OH^- = H_2O + CaCO_3 \tag{2.7}$$

$$Mg^{2+} + 2OH^- = Mg(OH)_2 \tag{2.8}$$

$$Mg^{2+} + HCO_3^- + OH^- = H_2O + MgCO_3 \tag{2.9}$$

2.4.2 Microstructure of calcareous deposit

The different types of calcareous deposits have different microstructures. $CaCO_3$ mainly exists in two forms, calcite and aragonite [36, 41]. Calcite has a rhombohedral shape with a certain space between each crystal, while aragonite spreads out like a flower and cover more of the surface, this makes aragonite more protective to the substrate material [31, 41]. The calcite- and aragonite microstructures can be seen in Figure 13.

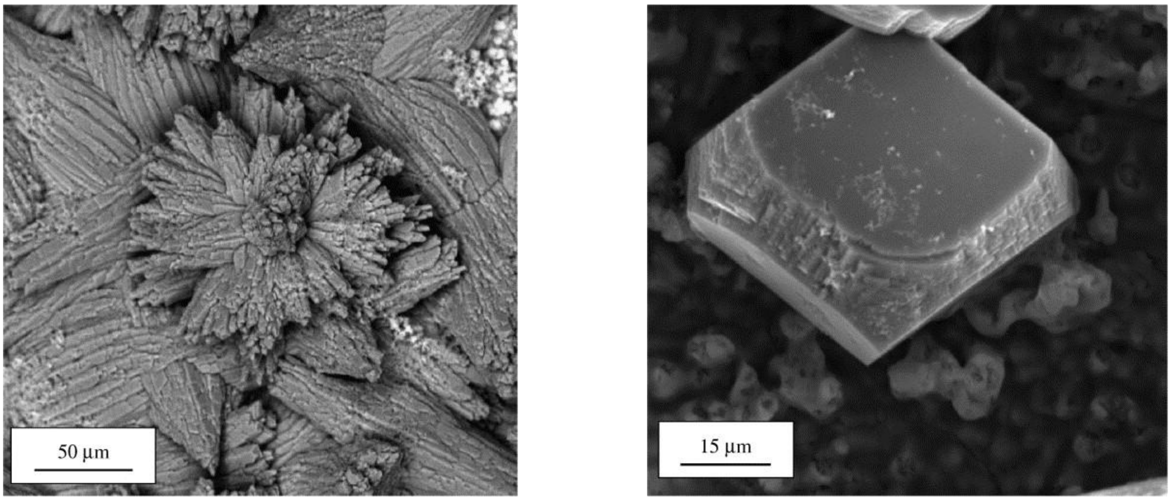

Figure 13: $CaCO_3$ microstructures, aragonite (left) and calcite (right) [41].

The Mg rich deposit is often referred to as brucite, it is easily recognizable as hexagonal platelets [31, 35, 42]. The structure of $Mg(OH)_2$ is a thin film in the range of micrometers [42]. The film is not significantly protective, and it has a lower electrically insulating capability than $CaCO_3$ [31]. Mg^{2+} has an inhibiting effect on the nucleation and growth of calcite and the nucleation of aragonite. When aragonite is formed Mg will not affect further growth. Aragonite is the phase which is most likely to precipitate when magnesium ions are present. $CaCO_3$ will be found as particles in a thin layer of $Mg(OH)_2$ [31, 40, 42]. In Figure 14 a SEM image of $Mg(OH)_2$ deposit can be seen.

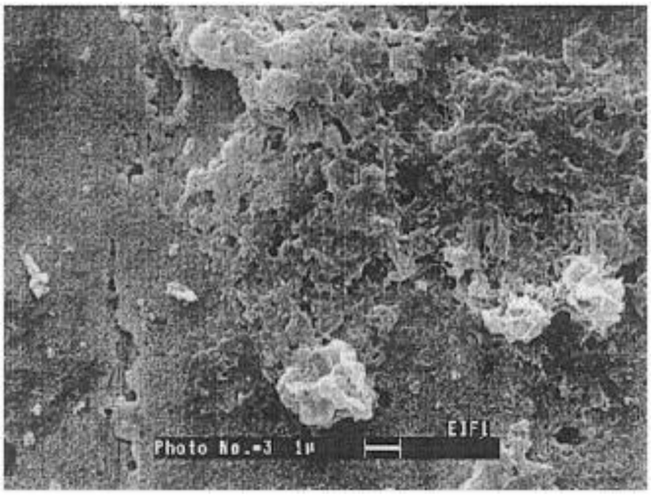

Figure 14: SEM photograph of $Mg(OH)_2$ deposit [42].

3 Literature Review

In the literature, several articles about the corrosion process for aluminium can be found. However, these articles are mainly related to freely exposed aluminium. Limited detailed information is published about the behavior of AA5083 and AA6082 under CP, and under different temperatures and pH-values in seawater. In the following, a brief summary of relevant available published literature is given.

In 2001 A. Aballe, et al. [43] published an article about localized corrosion of AA5083 in neutral 3,5% NaCl solution. AA5083 samples were exposed in aerated 3,5% NaCl with pH 5,5. The exposure time varied from 1 to 30 days. It was concluded that when AA5083 corrodes freely in a solution of NaCl at 3,5%, the samples undergo a process of corrosion localized to the area surrounding the precipitates of Al(Mn,Fe,Cr), which results in hemispherical pits. For the formation of crystallographic pitting to be produced, it is necessary to polarize the alloy at the nucleation potential of pitting or to apply a constant anodic current at a density above a critical level.

K. A. Yasakau, et al. [44] published an article about the role of intermetallic phases in localized corrosion of AA5083 in 2007. Experimental work where polished AA5083 samples were immersed in 0,5 M and 0,005 M NaCl solutions was performed. The localized corrosion activity of different intermetallics was investigated by use of advanced microscopic and local electrochemical techniques [2]. The results indicated that the different types of intermetallics plays an important role in the localized corrosion attack. The following was concluded; the Mg_2Si intermetallics have an anodic behavior and demonstrate partial dissolution with distinct dealloying due to selective leaching of magnesium. The formation of hydroxide deposits and the enrichment of the intermetallics in silicon stop further propagation of defects preventing formation of deep pits. The Fe-rich intermetallics work as local cathodes promoting fast anodic dissolution of aluminium and formation of pits.

A study on the corrosion behavior of aluminium alloys in seawater was performed by H. Ezuber, et al. in 2008 [45]. In this study, AA5083 and AA1100 were tested in seawater at 23 and 60 ^{o}C. The study concluded that both AA1100 and AA5083 suffered from pitting corrosion attack in seawater at room temperature as well as 60 ^{o}C, with better corrosion resistance for AA1100. The intensity of the pitting attack increases with increasing test temperature from 23 to 60 ^{o}C. Hemispherical pits were found on AA5083, while for AA1100 a higher number of shallow pits was found. The results also showed that the type of intermetallic particles in aluminium alloys plays a major role in passivity breakdown and pit morphology of aluminium alloys in seawater.

---

[2] Scanning Kelvin probe force microscopy in addition to SEM and EDS.

Less literature is available for AA6082. A study from 2011 performed by M. Händel, et al. [46] investigated the effect of different grain sizes and textures on the corrosion behavior of AA6082. Commercially extruded AA6082 was potentiodynamic polarized in 0,1 M NaCl to investigate the susceptibility to selective corrosion. The results indicated that there is a possibility that pitting starts earlier in the finer-grained part of the sample, but proceeds more slowly than in the coarser-grained part.

In 2013 a study of the corrosion development in welded AA6082 alloys was carried out by K. Blommedal [47]. Four variants of AA6082 with Cu additions ranging from 0,001 to 0,60 wt% were subjected to an IGC test, in addition to Cyclic Acidified Synthetic Sea Water (Fog) Testing (SWAAT). The results from the study revealed significant pitting corrosion on most variants, and the severity was found to increase with increasing Cu content and ageing time. Also, attacks from pitting corrosion was occasionally observed to be accompanied with IGC attacks along sub grains. Weld seams formed during friction stir welding (FSW) proved to be more susceptible to pitting corrosion attacks than weld seams formed during MIG welding.

4 Experimental procedure

In this study, the aluminium alloys AA5083 and AA6082 were tested under different conditions to examine the corrosion behavior. A total of four different conditions were tested, this will be further explained in this section. The experiments were carried out at NTNU/Sintef SEALAB Brattøra in Trondheim and in the Corrosion Laboratory at Perleporten/NTNU at Gløshaugen.

4.1 Materials

The samples used in the experiments were made out of plates of the alloys EN AW 5083 H321 and EN AW 6082 T6. For AA6082 the material certificate was not available, however it was confirmed that the material used was EN AW 6082 T6. The information for AA6082 in this chapter is therefore based on information from [15] because the material used was some extra material from that study.

The chemical composition of the materials in this study is given in Table 7.

Table 7: Chemical composition (wt%) of the alloys in this study.

	Si	Fe	Cu	Mn	Mg	Cr	Zn	Ti	Al
AA5083	0,11	0,31	0,06	0,52	4,71	0,07	0,12	0,02	Rest.
AA6082	0,93	0,18	0,008	0,55	0,60	0,011	0,002	0,011	Rest.

4.2 Test samples

The AA5083 samples were cut out of plates with thickness 8 mm and the AA6082 samples were cut out of plates with thickness 10 mm. Due to lack of test material the samples for the experiments in the Corrosion laboratory were made smaller than the samples for the experiments in SEALAB. The dimension of the samples were as following:

$$length \times width \times thickness$$

Corrosion lab: $20\,mm \times 20\,mm \times 8$ or $10\,mm$
SEALAB: $50\,mm \times 50\,mm \times 8$ or $10\,mm$

The sample sizes were made with an accuracy of ± 0,5 mm, this was done to secure that equal surface areas were exposed.

Further, the samples were painted with Jotun Jotamastic 87 std 038 [48], which is a two component polyamine cured epoxy mastic coating. The samples were painted such that only a specified surface area was exposed during the experiments, the exposed surface areas were as following:

Corrosion lab: $Area = 4\,cm^2 \pm 0,0025\,cm^2$
SEALAB: $Area = 25\,cm^2 \pm 0,0025\,cm^2$

4.2 Test samples

The non-painted surfaces of the samples were grinded with gradually finer SiC paper, ended with P220, to remove surface containments and to achieve uniform surfaces. An image of a painted and grinded sample can be seen in Figure 15.

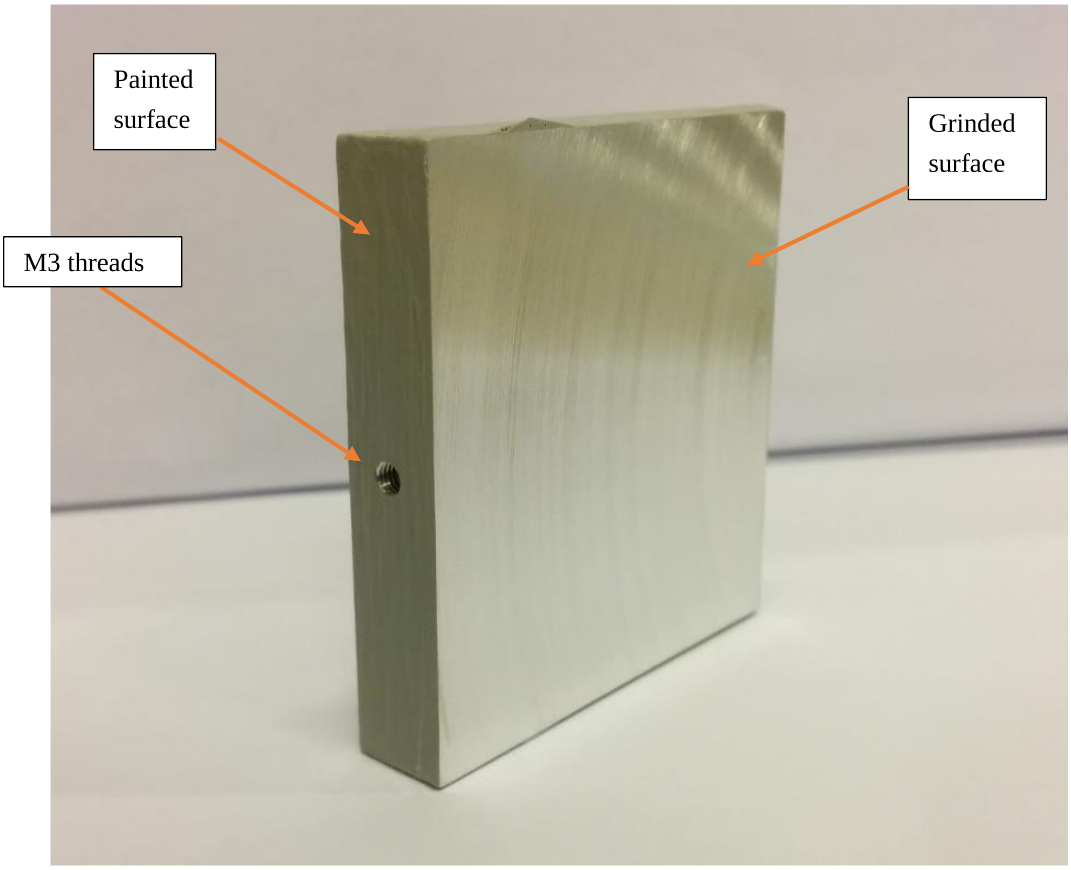

Figure 15: Painted and grinded sample.

M3 threads were made in the samples, such that a 3 mm threaded rod could be fixed into the samples to obtain proper electrical connection. The threaded rods were sealed with heat-shrinkable tubing and silicon to avoid exposure to the electrolyte. Figure 16 shows an image of a sample ready for exposure, as it can be seen the threaded rod is fixed into the sample and sealed.

Before exposure the samples were degreased in acetone, rinsed in ethanol and dried in air.

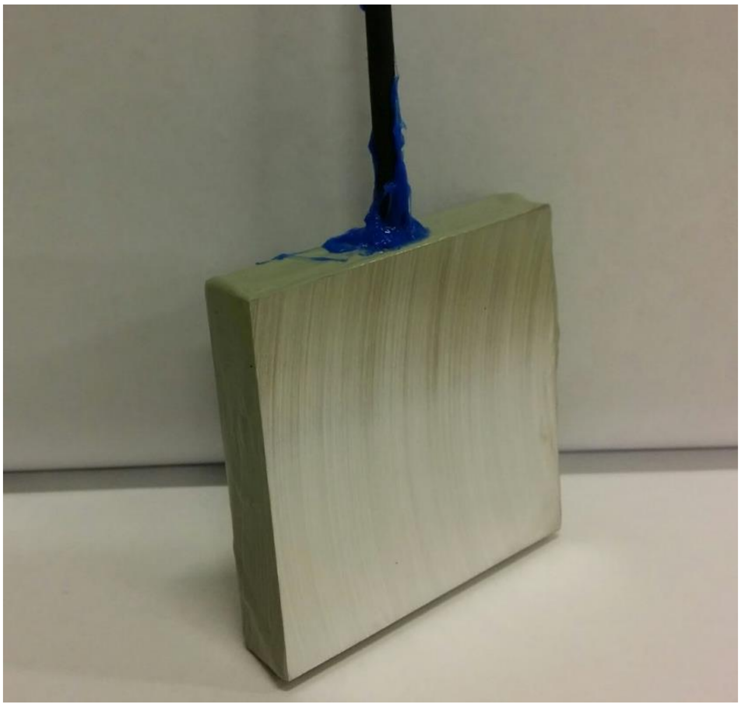

Figure 16: Sample ready for exposure.

4.3 The different conditions and setups

4.3.1 SEALAB

In the SEALAB laboratory at Brattøra in Trondheim the test samples were exposed to natural seawater. The seawater was taken from 80 m depth in the Trondheimsfjord, and pumped into the containers with test samples. Fresh seawater entered the container with a rate of 0,1 l/min. The circulation of the seawater was so slow such that the conditions can be described as nearly stagnant. The experiments were performed with two different temperatures, 10 ± 2 ^{o}C (natural inlet temperature) and 32 ± 2 ^{o}C.

First, the AA5083 samples were exposed for 1000 hours (6 weeks), and then the AA6082 samples were exposed for 1000 hours. Due to lack of test material, fewer AA6082 samples were exposed in SEALAB.

For both temperatures, the setup of AA5083 was as following:

- Two samples anodic polarized to −700 mV vs Ag/AgCl.
- Three samples freely exposed, one used for recording potentiodynamic polarization curves.
- Two samples coupled to a conventional sacrificial anode, electrochemical potential of approximately −1050 mV vs Ag/AgCl.
- Two samples cathodic polarized to −1500 mV vs Ag/AgCl (the samples exposed at 32 ^{o}C had a potential of approximately −1580 mV vs Ag/AgCl).

4.3 The different conditions and setups

For both temperatures, the setup of AA6082 was as following:

- One sample anodic polarized to −700 mV vs Ag/AgCl.
- Two samples freely exposed, one used for recording potentiodynamic polarization curves.
- One sample coupled to a conventional sacrificial anode, electrochemical potential of approximately −1050 mV vs Ag/AgCl.
- One sample cathodic polarized to −1500 mV vs Ag/AgCl (the sample exposed at 32 °C had a potential of approximately −1580 mV vs Ag/AgCl).

In Figure 17 the experimental setup is illustrated in an easy-to-understand way. Note that for AA6082 it was one sample less at the different conditions. The reference electrodes used were Ag/AgCl Saturated KCl, and the counter electrodes were platinum.

Two carbon steel St 52 samples were also coupled to the sacrificial anode, one at each temperature. The purpose of this was to compare the results for the aluminium samples coupled to the sacrificial anode to the results for the carbon steel samples.

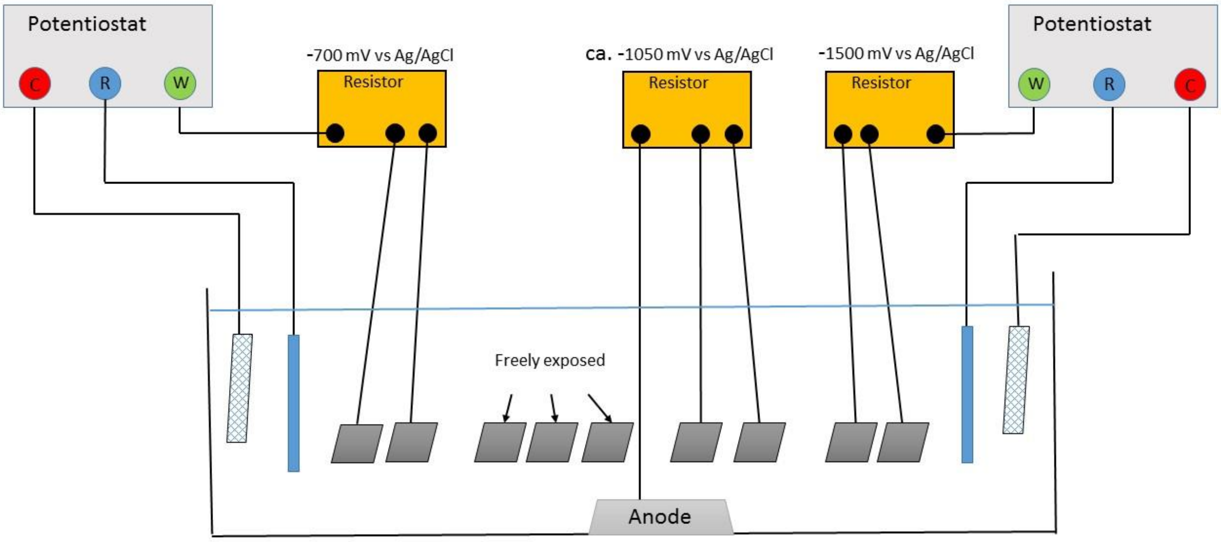
Potentiostat
C
R
W
-700 mV vs Ag/AgCl
Resistor
ca. -1050 mV vs Ag/AgCl
Resistor
-1500 mV vs Ag/AgCl
Resistor
Potentiostat
W
R
C
Freely exposed
Anode

Figure 17: Easy-to-understand illustration of the experimental setup.

Figure 18 shows an overview photo of the two containers used for the experiments. The container to the left had a temperature of 10 °C and the one to the right 32 °C.

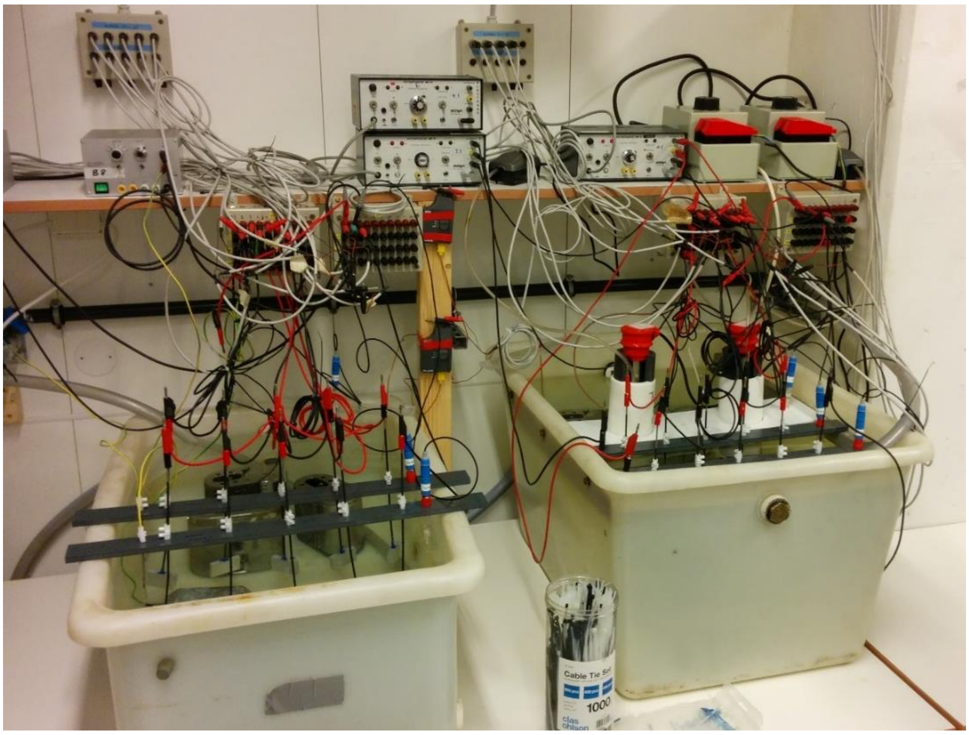

Figure 18: Overview photo SEALAB.

4.3.2 Corrosion Laboratory Perleporten

In the Corrosion Laboratory at Perleporten/NTNU at Gløshaugen the test samples were exposed to synthetic seawater (SSW), made in accordance to ASTM D 1141 [49], with three different pH-values: 3, 8,2 and 10. The samples were exposed for 168 hours (1 week) in room temperature (21 ± 2 ^{o}C) for each of the three different pH values.

For both AA5083 and AA6082 the setup was as following:

- Two samples anodic polarized to −700 mV vs Ag/AgCl.
- Three samples freely exposed, one used for recording potentiodynamic polarization curves after 24 hours and one used for recording potentiodynamic polarization curves after 168 hours.
- Two samples coupled to a conventional sacrificial anode, electrochemical potential of approximately −1050 mV vs Ag/AgCl.
- Two samples cathodic polarized to −1500 mV vs Ag/AgCl.

This means that at each pH a total number of 18 test samples were exposed at the same time, nine of each alloy. For each of the alloys the experimental setup is the same as illustrated in Figure 17. Figure 19 shows an overview photo of the experimental setup in the corrosion laboratory.

4.3 The different conditions and setups

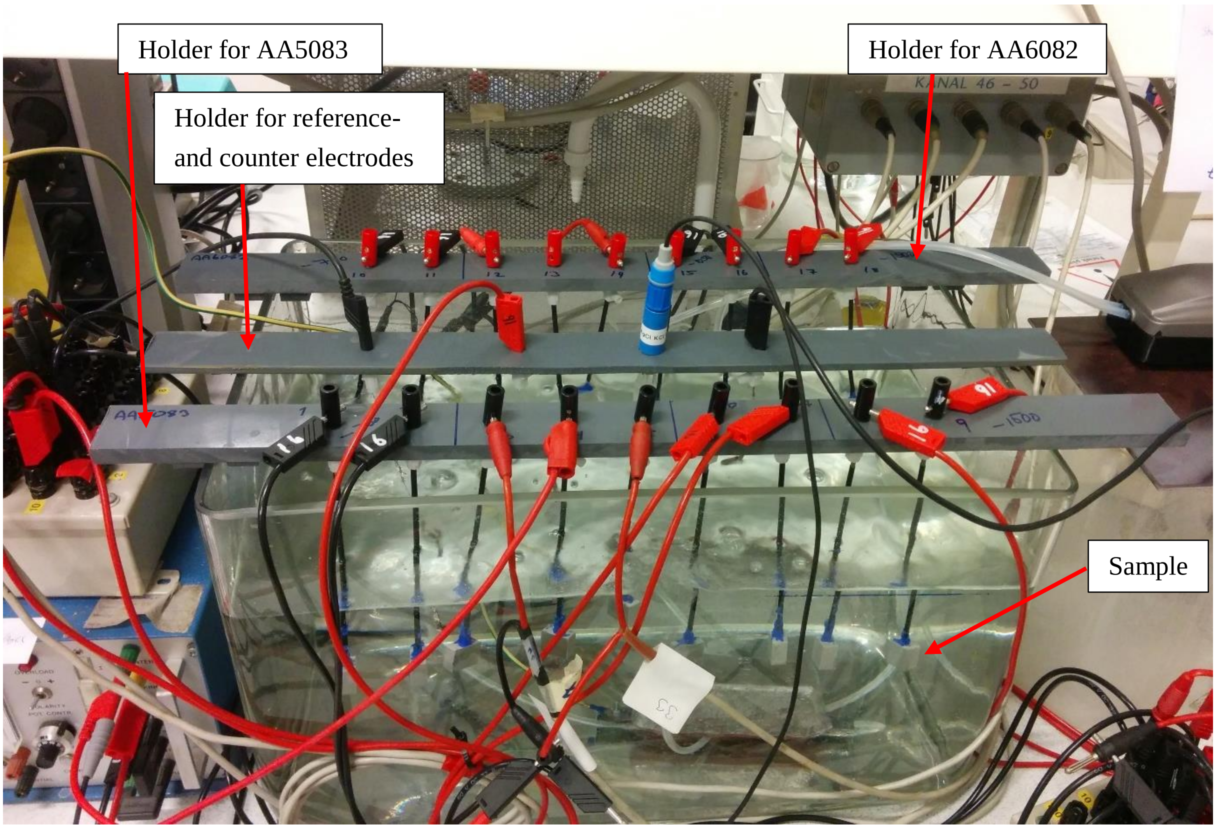
Holder for AA5083
Holder for reference- and counter electrodes
Holder for AA6082
KANAL 46 – 50
Sample

Figure 19: Experimental setup in the corrosion laboratory.

The reference electrode used was Ag/AgCl Saturated KCl, and the counter electrodes used were platinum. An aquarium pump was used to achieve circulation in the electrolyte.

The following were done to adjust the pH of the SSW: To obtain pH 3 small amounts of 37% HCl were added to the SSW. To obtain pH 10 small amounts of 20% NaOH were added to the SSW. The pH was measured several times per day and adjusted when necessary.

For the different conditions, the pH varied as following:

- For pH 3: 2,72 – 3,40
- For pH 8,2: 8,03 – 8,17
- For pH 10: 9,35 – 11,50

4.4 Measurements

4.4.1 SEALAB

During exposure the following were recorded:

- Potential drop, ΔE, across a fixed resistor (see Figure 17), for all the polarized samples. It was emphasized to obtain $\Delta E = 1$ mV. The potential drop was used to calculate the anodic- and cathodic current requirement for the samples by the use of Ohm's law.
- The OCP for the freely exposed samples.

The recordings were done every fifth minute by the computer program Corrosion Lab Datalogger. It was possible to follow the current- and potential development in situ during the whole exposure period.

For one of the freely exposed samples (at both temperatures) cathodic- and anodic polarization curves (potentiodynamic polarization curves) were recorded. The polarization curves were recorded after one day of exposure, and then once a week. First, the cathodic polarization curves were recorded from OCP and down to −1600 mV vs Ag/AgCl with a sweep rate of 600 mV/h. Applied potential was then turned off and OCP was stabilizing for minimum one hour. The anodic polarization curves were recorded from OCP and 400 mV in anodic direction, by use of the same sweep rate; 600 mV/h.

At the end of the exposure time, complete polarization curves were recorded. The complete polarization curves were recorded with the same limits and the same sweep rate as for the cathodic- and anodic polarization curves. Both the complete polarization curves, and the cathodic- and anodic polarization curves were recorded manually.

For AA5083 all polarization curves including the complete polarization curve were recorded on the same sample. For AA6082 the complete polarization curves were recorded on samples that had only been freely exposed for six weeks, and not experienced the previous anodic- and cathodic polarizations. The other polarization curves for AA6082 were recorded on the same sample.

4.4.2 Corrosion Laboratory Perleporten

During exposure, several recordings were done, and the following were recorded:

- Potential drop, ΔE, across a fixed resistor, for all the polarized samples. It was emphasized to obtain $\Delta E = 1$ mV. The potential drop was used to calculate the anodic- and cathodic current requirement for the samples by the use of Ohm's law.
- The OCP for the freely exposed samples.

The same recordings were performed for each of the tests with different pH values. The recordings were done every fifth minute by the computer program Corrosion Lab Datalogger.

It was possible to follow the current- and potential development in situ during the whole exposure period.

Two of the freely exposed samples (for both alloys) were used to record complete polarization curves. For one of the samples the complete polarization curve was recorded after one day (24 hours) of exposure. For the other sample, the complete polarization curve was recorded at the end of the exposure time (168 hours). The complete polarization curves were recorded automatically by use of a Gamry^{TM} potentiostat. The limits and sweep rate were the same as for the polarization curves recorded manually in SEALAB. Sweep rate of 600 mV/h from OCP and down to −1600 mV vs Ag/AgCl. Then a reverse sweep rate of 600 mV/h and up to 400 mV above the original OCP.

4.5 Surface examination

The samples were rinsed in distilled water and acetone immediately after exposure. Subsequently the samples exposed in SEALAB were examined by the use of SEM, a Hitachi S-3200N SEM and a FEI Quanta FEG 650 Environmental SEM were used in this study. The samples were cut in smaller pieces to fit into the SEM. In an attempt to remove corrosion products before examination in SEM, the samples were rinsed for three minutes in 65% HNO_3 at room temperature and washed with distilled water.

It was emphasized on studying pits and intermetallic particles. The composition of the intermetallic particles and the surface in and adjacent to the pits were determined using EDS (Energy Dispersive Spectroscopy).

In an attempt to determine the pitting depths the cross-section of the samples was also examined in SEM. Prior to this, the cross-sections were mechanically fine grinded with SiC ended with P2400 and polished to mirror quality using Struers MDDac plates with diamond grain sizes from 3 µm to 1 µm. A polished cross-section ready for inspection in SEM can be seen in Figure 20. Before examination in SEM the samples were also rinsed in ethanol.

Originally, no surface examination was planned for the samples exposed in the Corrosion laboratory, but it was found interesting to examine the freely exposed samples at each pH-value. These samples were also rinsed in 65% HNO_3 with the same procedure as described above.

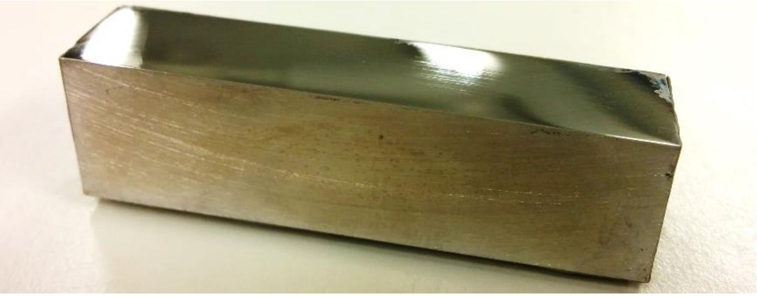

Figure 20: Cross-section polished to mirror quality.

5 Results

5.1 SEALAB

The results from the experimental work in SEALAB are presented in this section. Photos of the samples after exposure in SEALAB can be seen in Appendix B.

5.1.1 Open Circuit Potential

Figure 21 shows the development in OCP for freely exposed AA5083 and AA6082 in natural seawater at 10 °C and 32 °C in SEALAB.

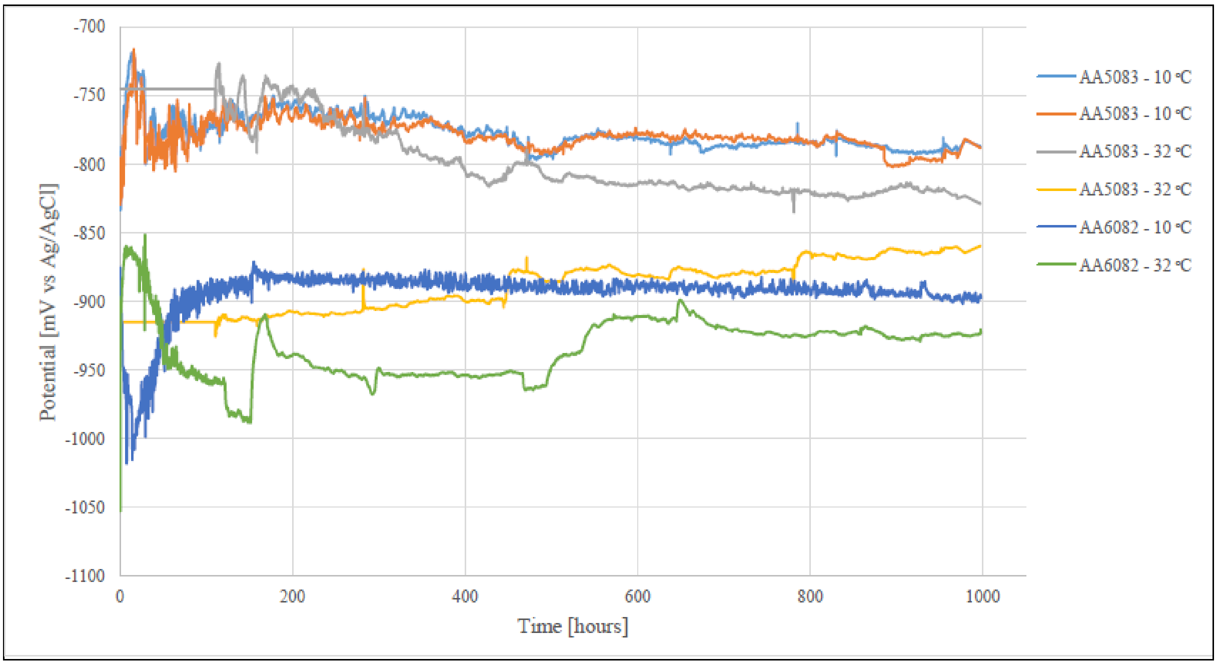

Figure 21: Development in OCP for freely exposed AA5083 and AA6082 in natural seawater.

The OCP for AA5083 exposed at 10 °C started at −830 mV vs Ag/AgCl, but showed a fluctuating behavior the first 80 hours of exposure. After this the OCP stabilized, but with a little variating behavior. The OCP was in the range −750 to −800 mV vs Ag/AgCl for the rest of the exposure period. After 1000 hours, the OCP was −785 mV vs Ag/AgCl.

The OCP-curves for AA5083 exposed at 32 °C were in two different potential ranges, −745 to −800 mV vs Ag/AgCl and −900 to −915 mV vs Ag/AgCl. The grey curve showed a fluctuating behavior the first 200 hours, while the yellow curve had a stable behavior the whole exposure period. After 200 hours of exposure, the grey curve decreased and the yellow curve increased. The two curves were relatively stable, but the grey curve decreased faster than the yellow curve increased. The curves tended to unify in the range −840 to −850 mV vs Ag/AgCl.

The OCP for AA6082 exposed at 10 °C started at −950 mV vs Ag/AgCl, and experienced a fluctuating behavior the first 80 hours of exposure. First, it decreased to −1020 mV vs Ag/AgCl and then increased to −870 mV vs Ag/AgCl. After this, the OCP exhibited a more stable behavior, and was in the range of −880 to −900 mV vs Ag/AgCl for the rest of the exposure period. After 1000 hours of the exposure, the OCP was −900 mV vs Ag/AgCl.

The OCP for AA6082 exposed at 32 °C started at −1050 mV vs Ag/AgCl, but increased rapidly to −860 mV vs Ag/AgCl. Then, the OCP decreased a little slower down to −990 mV vs Ag/AgCl before it increased rapidly to −910 mV vs Ag/AgCl, after this the OCP started to exhibit a more stable behavior. The first 170 hours of exposure the OCP was very fluctuating, after this the OCP was in the range of −900 to −960 mV vs Ag/AgCl for the rest of the exposure period. After 1000 hours, the OCP was −925 mV vs Ag/AgCl.

5.1.2 Current density curves

The specified potentials in this study were as following: −700 mV vs Ag/AgCl, −1050 mV vs Ag/AgCl (coupled to sacrificial anode) and −1500 mV vs Ag/AgCl, as earlier mentioned the samples exposed at 32 °C had a potential of approximately −1580 mV vs Ag/AgCl.

The current densities are plotted as positive and negative values according to the following rule:

- Cathodic current is defined as negative current, which means the current goes from the potentiostat through the counter electrode to the polarized sample.
- Anodic current is positive, which means that current goes from the sample to the potentiostat through the counter electrode.

−700 mV vs Ag/AgCl

Figure 22 shows the current density for the samples polarized to −700 mV vs Ag/AgCl.

At 10 °C the anodic current density for both alloys, AA5083 and AA6082, was relatively stable at values between 3 to 5 µA/cm^2. The current densities for the AA5083 samples exposed at 32 °C were much larger than for the samples exposed at 10 °C. The current densities experienced a drop in the beginning and then they increased for the rest of the exposure period, reaching values as high as 110 µA/cm^2. The current density for the AA6082 sample exposed at 32 °C was relative stable between 3 and 5 µA/cm^2 for the first 570 hours of exposure. At this point, the current density increased for the rest of the exposure time, and reached values of 25 to 30 µA/cm^2.

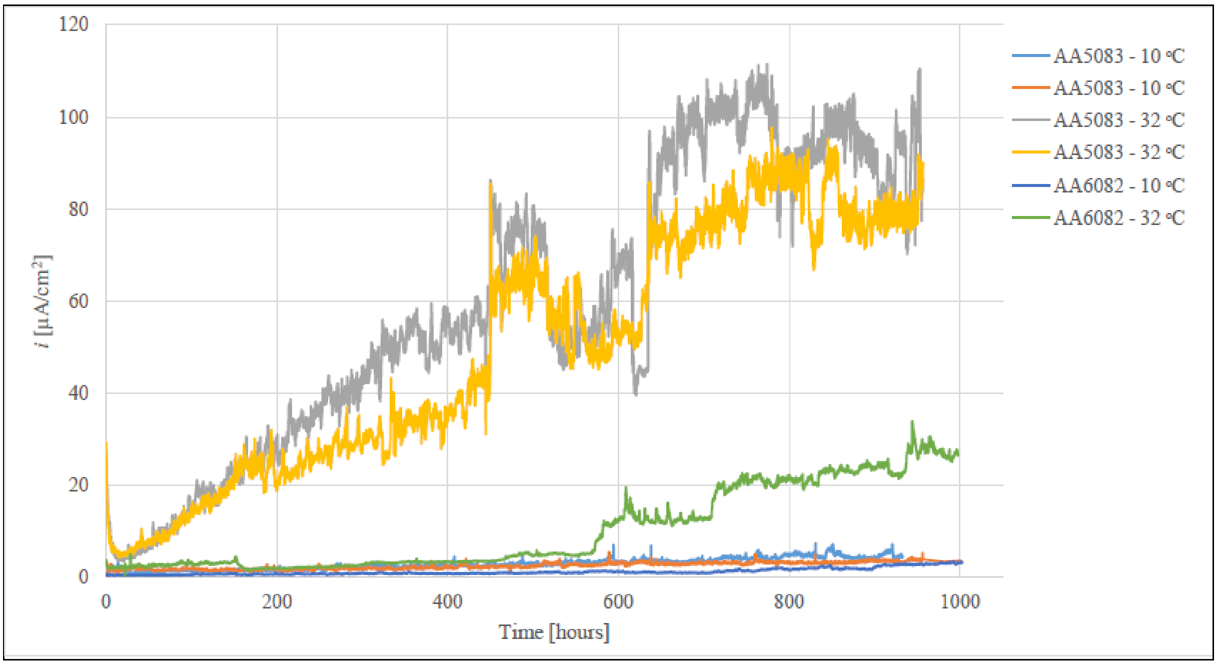

Figure 22: Current density for samples anodic polarized to −700 mV vs Ag/AgCl.

−1050 mV vs Ag/AgCl (samples coupled to sacrificial anode)

In Figure 23 the cathodic current density for the samples polarized to −1050 mV vs Ag/AgCl can be seen. The samples were coupled to a sacrificial anode, and the potential was therefore not constant at −1050 mV vs Ag/AgCl. The potential from the sacrificial anode at 10 °C varied between −1070 and −1080 mV vs Ag/AgCl, and the potential from the sacrificial anode at 32 °C varied between −1025 and −1045 mV vs Ag/AgCl. Plots of the potential from the sacrificial anode can be seen in Appendix C.

The AA5083 samples exposed at 10 °C experienced an increase in the current density in the beginning, after 150 hours of exposure the current density reached −5 µA/cm^2. Then it decreased, and tended to stabilize at −1,8 µA/cm^2. The AA5083 samples exposed at 32 °C experienced a rapid increase in current density in the beginning, reaching −11 µA/cm^2. Then the current density decreased relatively rapidly and stabilized between −0,7 and −0,9 µA/cm^2.

The current density for the AA6082 sample exposed at 10 °C fluctuated slightly the first 250 hours of exposure, after this the behavior was stable between −2,3 and −2,6 µA/cm^2. The AA6082 sample exposed at 32 °C experienced a small increase the first 150 hours of exposure, reaching a maximum current density of −3,9 µA/cm^2. Then the current density decreased slowly, and stabilized at −1,7 µA/cm^2.

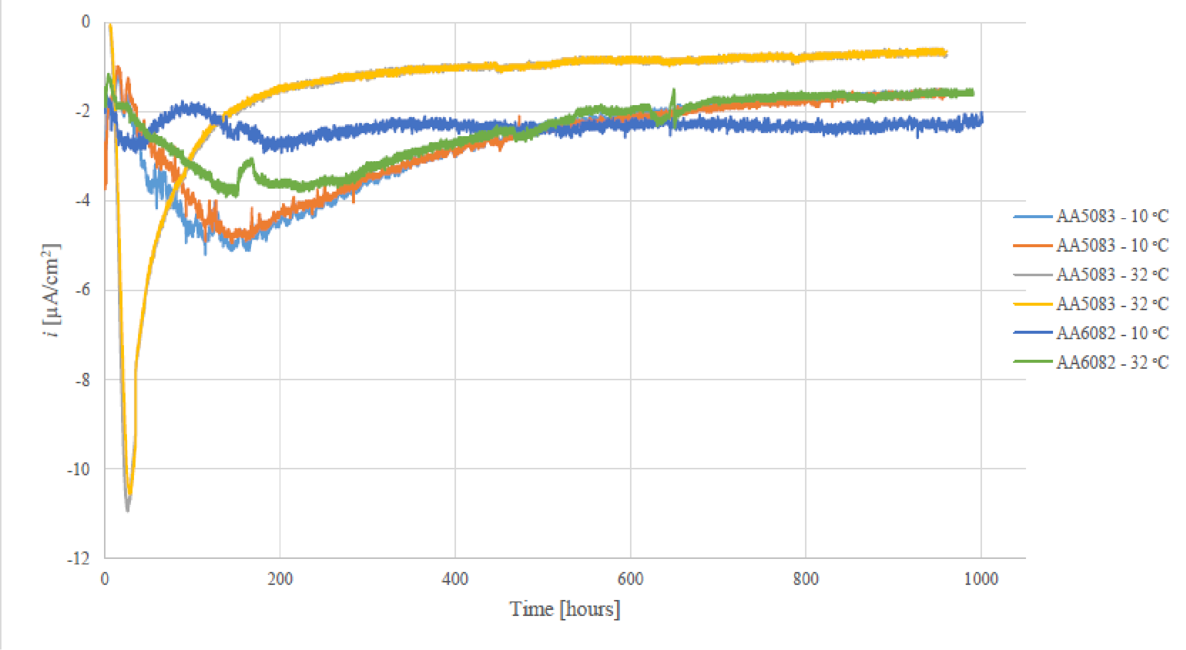

Figure 23: Current density for the samples coupled to sacrificial anode (potential of approximately −1050 mV vs Ag/AgCl)

−1500 mV vs Ag/AgCl (−1580 mV vs Ag/AgCl)

The cathodic current density curves for the samples polarized to −1500 mV vs Ag/AgCl are shown in Figure 24.

As it can be seen from Figure 24 common for all the samples was that the current density started at high values. The current density for the AA5083 samples exposed at 10 °C started at approximately −200 µA/cm^2, and then decreased rapidly to −35 to −40 µA/cm^2 before it decreased more slowly and stabilized. One of the samples stabilized between −8 and −10 µA/cm^2, and one between −12 and −14 µA/cm^2. The current density for the AA5083 samples exposed at 32 °C started at −300 µA/cm^2, and then decreased rapidly to between −15 and −25 µA/cm^2. Between 90 and 160 hours of exposure, the current density had a fluctuating behavior for these samples. After this, the current density stabilized, one stabilized at −12 to −13 µA/cm^2 and the other stabilized at −14 to −15 µA/cm^2. Figure 24 indicates that one of the samples exposed at 32 °C experienced increased current density at the end of the exposure time.

The current density for the AA6082 sample exposed at 10 °C was completely different from the other samples. The current density started at −220 µA/cm^2, and was relatively stable around −240 µA/cm^2 for the first 150 hours. After 150 hours, the current density suddenly dropped to −97 µA/cm^2 before it increased for the rest of the exposure time, reaching values of −320 µA/cm^2. The current density for the AA6082 sample exposed at 32 °C started at −240 µA/cm^2 and then decreased rapidly. The current density stabilized between −6 and −8 µA/cm^2.

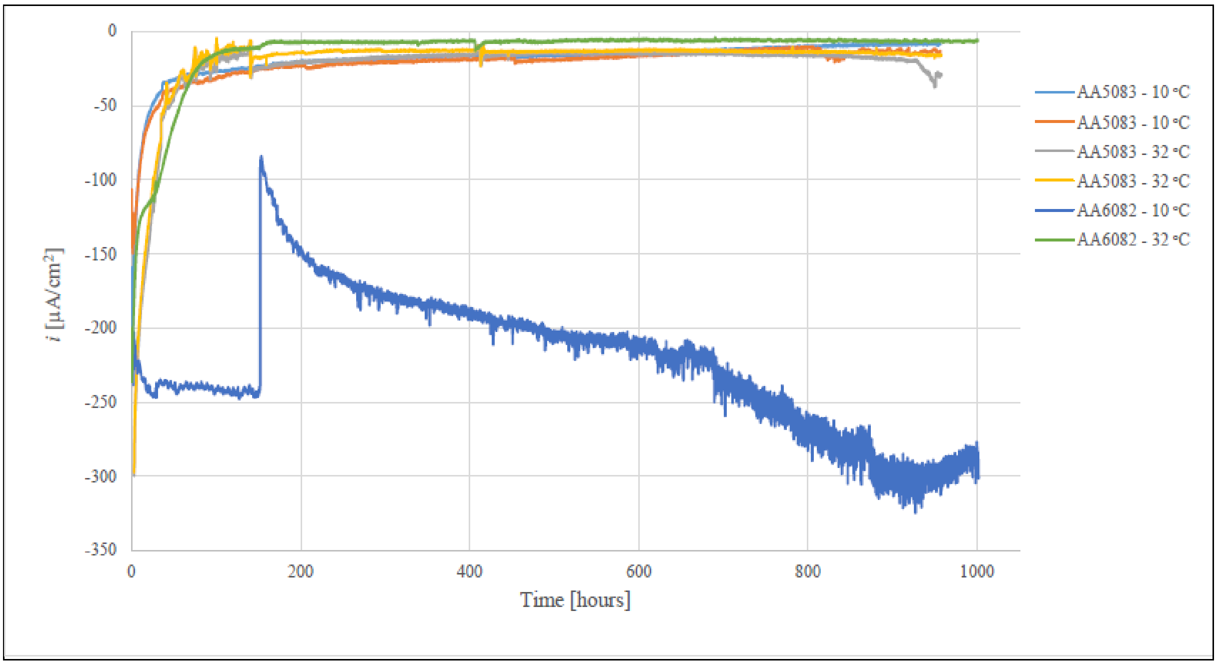

Figure 24: Current density for samples cathodic polarized to −1500 mV vs Ag/AgCl.

5.1.3 Potentiodynamic polarization curves

Potentiodynamic polarization curves were recorded for the freely exposed AA5083- and AA6082 samples at 10 °C and 32 °C. The procedure for recording the potentiodynamic polarization curves is explained in Section 4.4.

It should be mentioned that the complete polarization curves for AA6082 (at both temperatures) are recorded on freely exposed samples that have not been polarized previous during the exposure, which is the case for AA5083.

AA5083 – 10 °C

The recorded anodic- and cathodic polarization curves for the freely exposed AA5083 sample at 10 °C are shown in Figure 25. The complete polarization curve recorded at the end of the exposure time is also included in Figure 25.

As it can be seen from Figure 25 the cathodic polarization curve for day 1 had the lowest current density for potentials more negative than −1100 mV vs Ag/AgCl. For the cathodic curves, more positive than −1100 mV vs Ag/AgCl, it tends that day 1, week 4 and week 5 had fairly the same current densities, and that week 1, week 2 and week 3 had fairly the same.

The anodic polarization curve for day 1 had clearly the largest current density, and the pitting potential was also easy to see at approximately −720 mV vs Ag/AgCl. The other anodic curves were relatively unified. However, the tendency was that the current density was reduced and that the pitting potential increased with increasing exposure time.

Figure 25 also shows the complete polarization curve recorded after 1000 hours of exposure. The cathodic part of the curve is very similar to the cathodic curve recorded for week 5. The current changed direction at −1120 mV vs Ag/AgCl, which is well below the original OCP; −820 mV vs Ag/AgCl. The current density in the passive region in the anodic direction was almost one magnitude larger than the current density in the same region for the anodic curve for week 5. The current density for the pitting potential was also almost one magnitude larger, but the pitting potential was just slightly larger for the complete polarization curve than for the anodic curve for week 5.

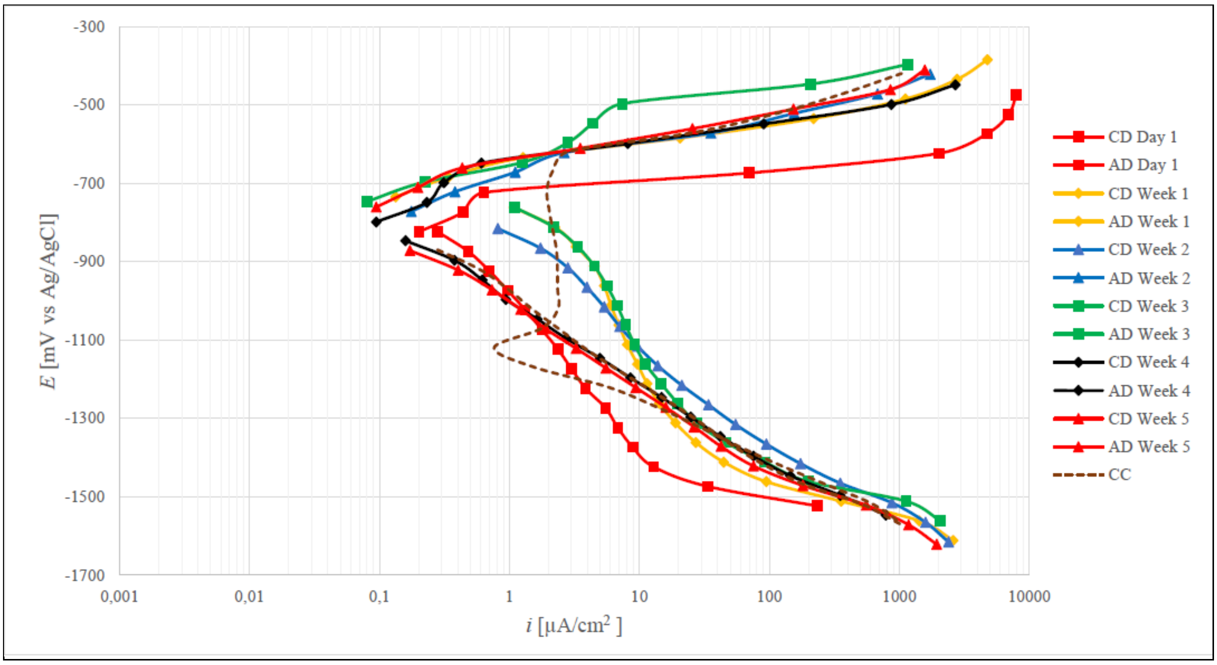

Figure 25: Recorded anodic- and cathodic polarization curves for the freely exposed AA5083 sample at 10 °C, the complete polarization curve recorded at the end of the exposure time is also included. AD and CD means anodic direction and cathodic direction, respectively. CC means the complete polarization curve. All the curves were recorded on the same sample.

AA5083 – 32 °C

Figure 26 shows the recorded anodic- and cathodic polarization curves for the freely exposed AA5083 sample at 32 °C. The complete polarization curve recorded at the end of exposure is also included.

From Figure 26 it can be seen that the cathodic curves for week 1 and week 3 had the largest current density. The cathodic curves for day 1, week 2, week 4 and week 5 are relatively unified and had the same current density for the potentials from OCP and down to approximately −1300 mV vs Ag/AgCl. At this potential, the current density for the day 1 curve increased and the curve became more unified with week 1 and week 3.

Figure 26 indicates that the anodic curve at day 1 had the largest current density and the lowest pitting potential. The current density for the anodic polarization curves decreased with time, and the pitting potential increased with time.

Figure 26 also shows the complete polarization curve recorded for AA5083 at 32 °C after 1000 hours of exposure. The cathodic part of the curve is slightly to the left of the recorded cathodic curves, this implies lower current density for the cathodic part. The current changed direction at −1120 mV vs Ag/AgCl. The current density for the transition to pitting was approximately the same for the complete polarization curve as for the anodic curve for week 5. The pitting potential was about 50 mV larger for the complete polarization curve compared to the anodic curve for week 5.

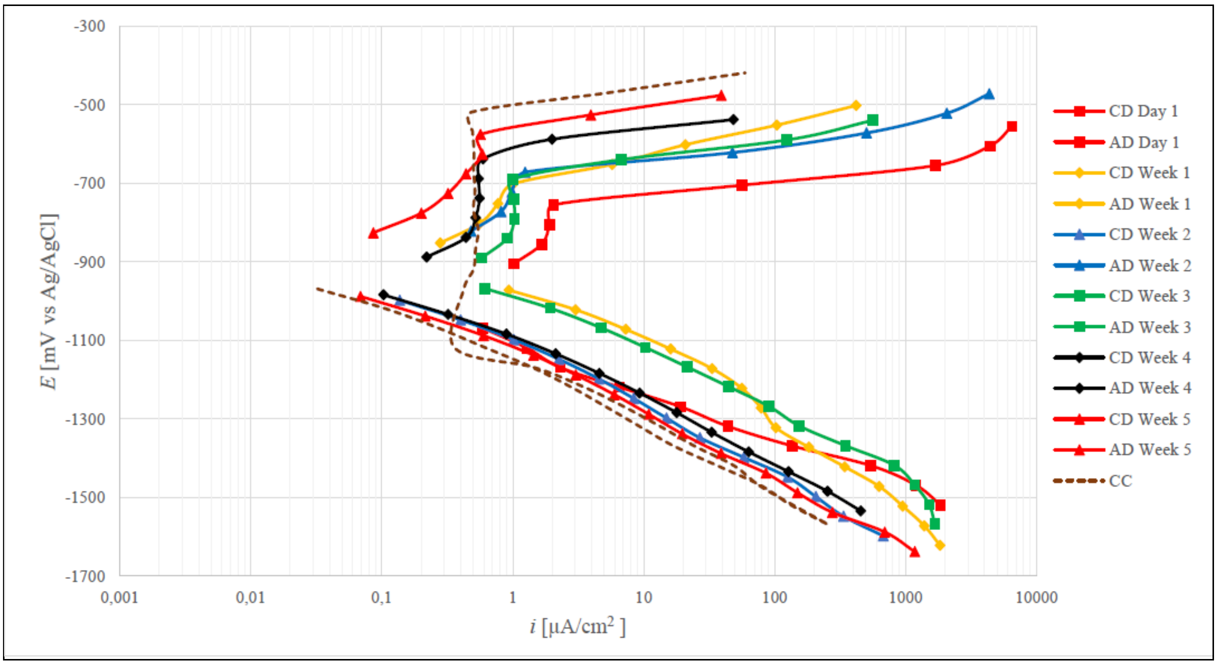

Figure 26: Recorded anodic- and cathodic polarization curves for the freely exposed AA5083 sample at 32 °C, the complete polarization curve recorded at the end of the exposure time is also included. AD and CD means anodic direction and cathodic direction, respectively. CC means the complete polarization curve. All the curves were recorded on the same sample.

AA6082 – 10 °C

The recorded anodic- and cathodic polarization curves, and the complete polarization curve for the freely exposed AA6082 sample at 10 °C are shown in Figure 27. Note that there are no recorded curves for week 2 for this alloy.

The cathodic curve for day 1 had the lowest current density, while the other cathodic curves are relatively unified. The current density at potentials near OCP was clearly lowest for week 2.

The anodic curves are relatively unified, but the curve for day 1 had the lowest pitting potential. The highest pitting potential is found for week 2 and week 5. For the anodic curve for week 4, no clear pitting potential can be seen.

The cathodic part of the complete polarization curve in Figure 27 is very similar to the recorded cathodic polarization curves, expect for the one recorded for day 1. The current direction changed at −995 mV vs Ag/AgCl, this change happend at a significantly lower current density than for the other curves. The anodic part of the complete polarization curve is very similar to the recorded anodic polarization curves, but the pitting potential was more positive for the complete polarization curve.

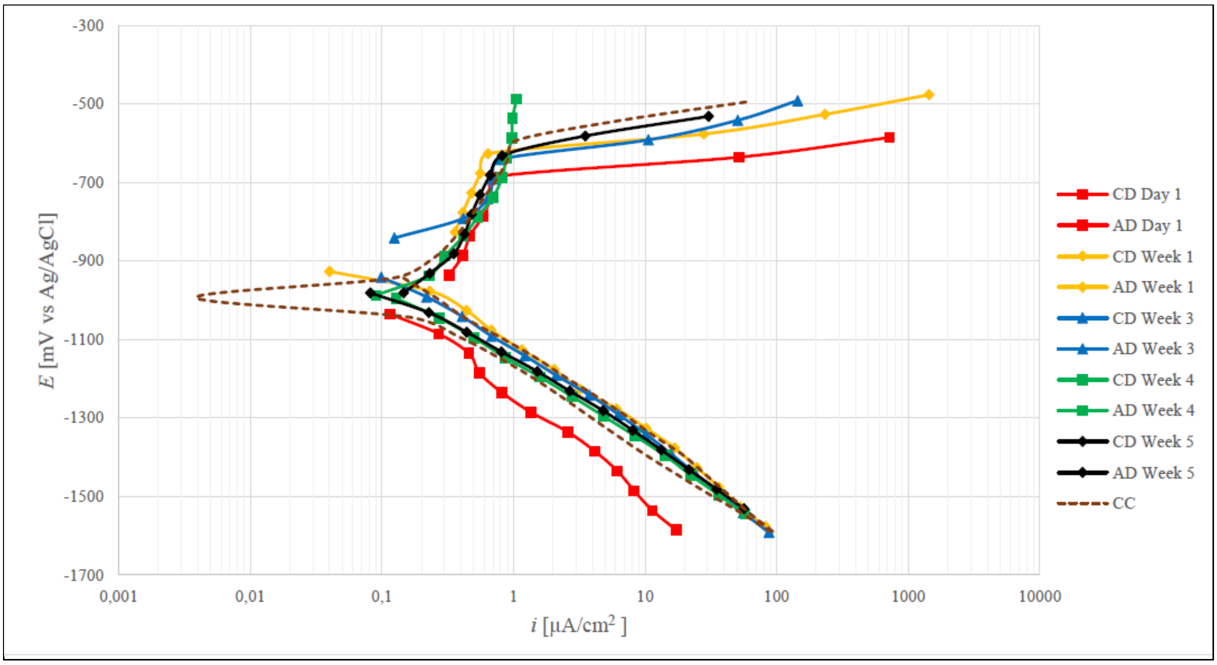

Figure 27: Recorded anodic- and cathodic polarization curves for the freely exposed AA6082 sample at 10 °C, the complete polarization curve recorded at the end of the exposure time is also included. AD and CD means anodic direction and cathodic direction, respectively. CC means the complete polarization curve. A new sample, that only had been freely exposed for 1000 hours, was used for recording the complete polarization curves.

AA6082 – 32 °C

The recorded anodic- and cathodic polarization curves, and the complete polarization curve for the freely exposed AA6082 sample at 32 °C are shown in Figure 28.

The cathodic curves are relatively unified, but the trend is that they were moved more to the left with time. This implies that the current density was reduced over time. The cathodic curve for day 1 had a bit different behavior than the other cathodic curves.

The anodic curves showed a rather different behavior. The anodic curves for day 1 and week 1 showed similar behavior, but the current density was slightly decreased and the pitting potential was slightly increased with time. The anodic curves for week 3 and 4 are moved significantly to the left and no clear transition to pitting can be seen. The current density is somewhat increased (moved to the right) for the anodic curve for week 5, but no clear transition to pitting can be seen for this curve either.

The cathodic part of the complete polarization curve in Figure 28 is similar to the recorded cathodic curves, and shows no significant difference in current density compared to the cathodic curves. The current direction changed at −1125 mV vs Ag/AgCl. The anodic part of the complete polarization curve is most similar to the anodic curves for day 1 and week 1. The current density in the passive region is slightly lower for the complete polarization curve. The transition to pitting happend in the same potential area as for the curves for day 1 and week 1.

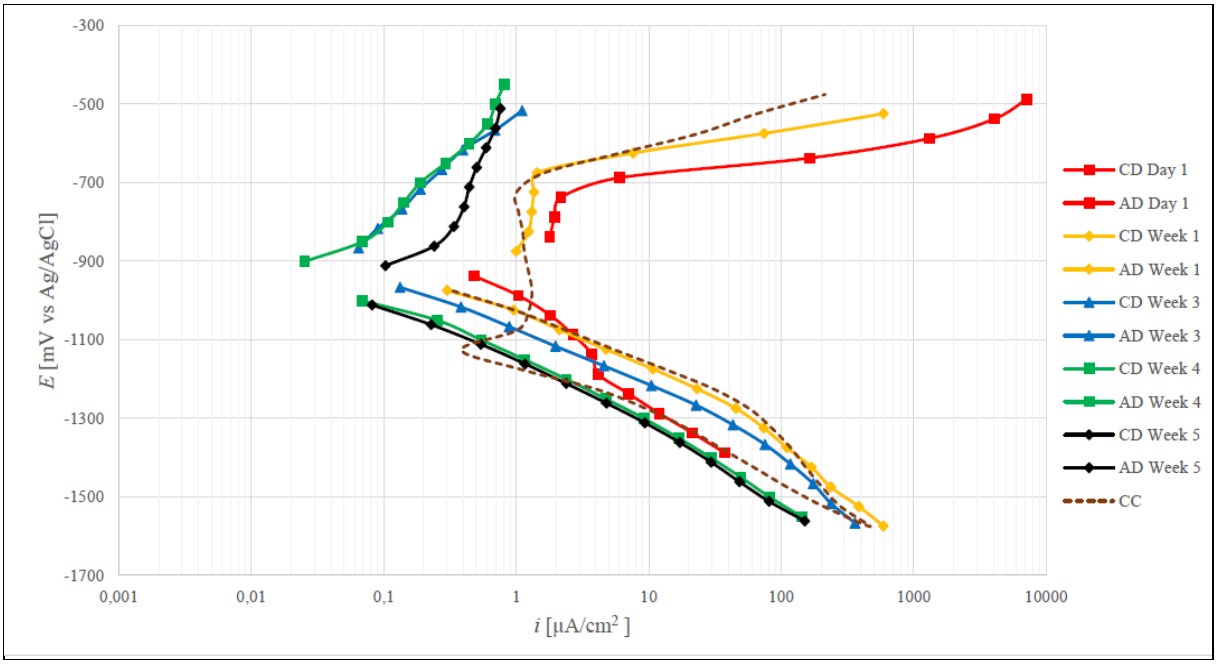

Figure 28: Recorded anodic- and cathodic polarization curves for the freely exposed AA6082 sample at 32 °C, the complete polarization curve recorded at the end of the exposure time is also included. AD and CD means anodic direction and cathodic direction, respectively. CC means the complete polarization curve. A new sample, that only had been freely exposed for 1000 hours, was used for recording the complete polarization curves.

Characteristic values from the polarization curves for AA5083 and AA6082 after 168 hours (one week) of exposure and after 1000 hours (six weeks) of exposure are shown in Table 8 and Table 9.

Table 8: Characteristic values for AA5083 during anodic- and cathodic polarization after 168 hours (one week) and 1000 hours (six weeks) of exposure.

	AA5083			
	10 °C		32 °C	
	1 week	6 weeks	1 week	6 weeks
E_{OCP} [mV vs Ag/AgCl]	−712	−820	−922	−919
E_{pit} [mV vs Ag/AgCl]	−585	−620	−700	−519
$\Delta E_{pit\text{-}OCP} = E_{pit} - E_{OCP}$ [mV]	127	200	222	400
i_{pass} [µA/cm^2]	0,3 – 1,3	1,95 – 2,45	0,4 – 0,9	0,4 – 0,55

Table 9: Characteristic values for AA6082 during anodic- and cathodic polarization after 168 hours (one week) and 1000 hours (six weeks) of exposure.

	AA6082			
	10 °C		32 °C	
	1 week	6 weeks	1 week	6 weeks
E_{OCP} [mV vs Ag/AgCl]	−877	−894	−915	−926
E_{pit} [mV vs Ag/AgCl]	−627	−594	−675	−726
$\Delta E_{pit\text{-}OCP} = E_{pit} - E_{OCP}$ [mV]	250	300	240	200
i_{pass} [µA/cm^2]	0,35 – 0,65	0,15 – 1,05	1,0 – 1,45	0,95 – 1,35

The complete polarization curves recorded for AA6082, on samples that had not experienced the previous polarizations, at 10 and 32 °C are plotted in the same diagram in Appendix D. This plot is included to see the effect of the temperature.

5.1.4 SEM images and EDS analyses

In this section, the results from SEM and EDS for the examination of the exposed surface of the samples are presented. SEM images of AA5083 and AA6082 samples prior to exposure can be seen in Appendix E. The results of the surface examination of the cross-sections in SEM are also presented in this section. By investigating the cross-sections of the samples in SEM one can only access a very small fraction of the exposed surface area; the edge of the cross-section face. However, the pits observed along this edge is a good indication of the severity and depth of the pits.

Freely exposed AA5083 at 10 °C

Figure 29 shows a SEM image of an AA5083 sample freely exposed in natural seawater at 10 °C and Figure 30 shows the EDS spectra of the marked area in Figure 29. The result from the EDS analysis can be seen in Table 10.

As it can be seen from Figure 29 both pits and particles were observed on the surface of the freely exposed AA5083 sample in natural seawater at 10 °C. The EDS analysis of the marked pit in Figure 29 revealed that inside the pit there was an intermetallic Al(Mn,Fe,Cr) particle (precipitate).

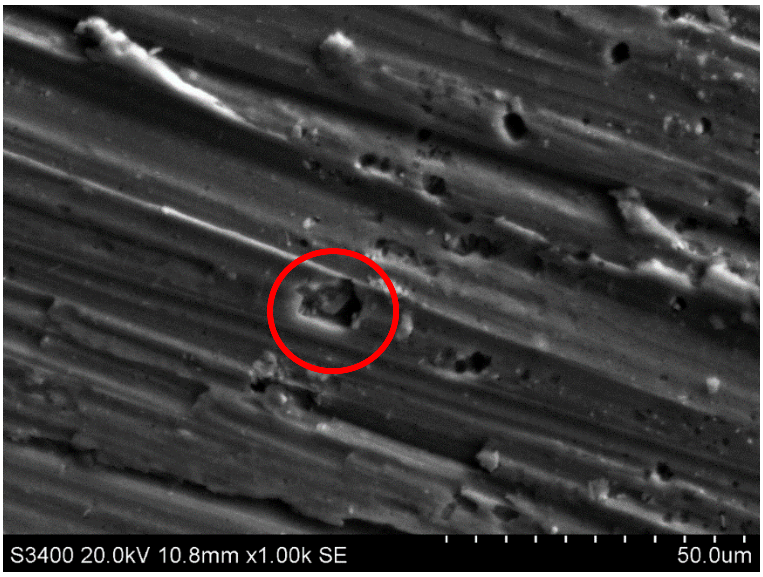

Figure 29: SEM image of an AA5083 sample freely exposed in natural seawater at 10 °C. An EDS analysis is performed for the pit inside the marked area.

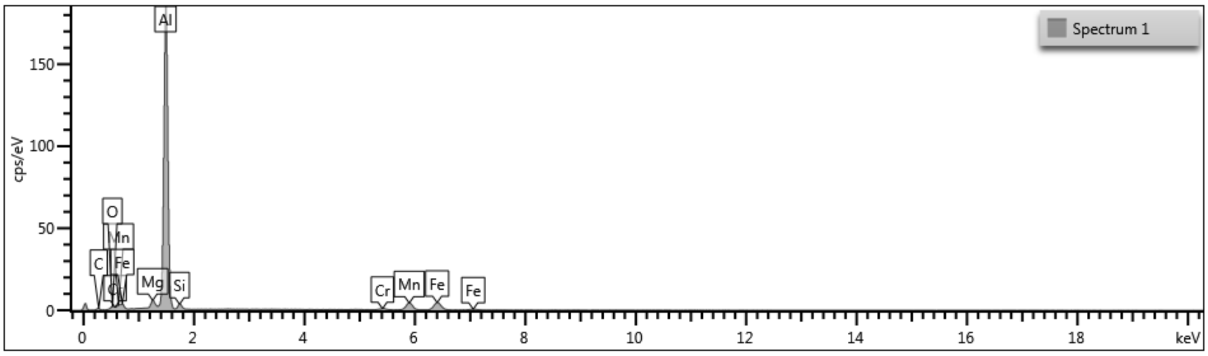

Figure 30: EDS spectra for the marked area in Figure 29.

Table 10: EDS analysis of the marked area in Figure 29.

Element	C	O	Mg	Al	Si	Cr	Mn	Fe
[wt%]	8,31	2,27	1,72	67,73	2,41	1,03	7,58	8,95

Freely exposed AA5083 at 32 °C

Figure 31 shows SEM images and EDS spectra for an AA5083 sample freely exposed in natural seawater at 32 °C. The image a) is magnified 500 times and shows several pits. The marked area in a) is further magnified in image b). An EDS analysis was performed on the marked area in image b) and the EDS spectra can be seen in image c) in Figure 31. The result from the EDS analysis can be seen in Table 11. According to the EDS analysis, the particle in the pit is a Fe-rich intermetallic.

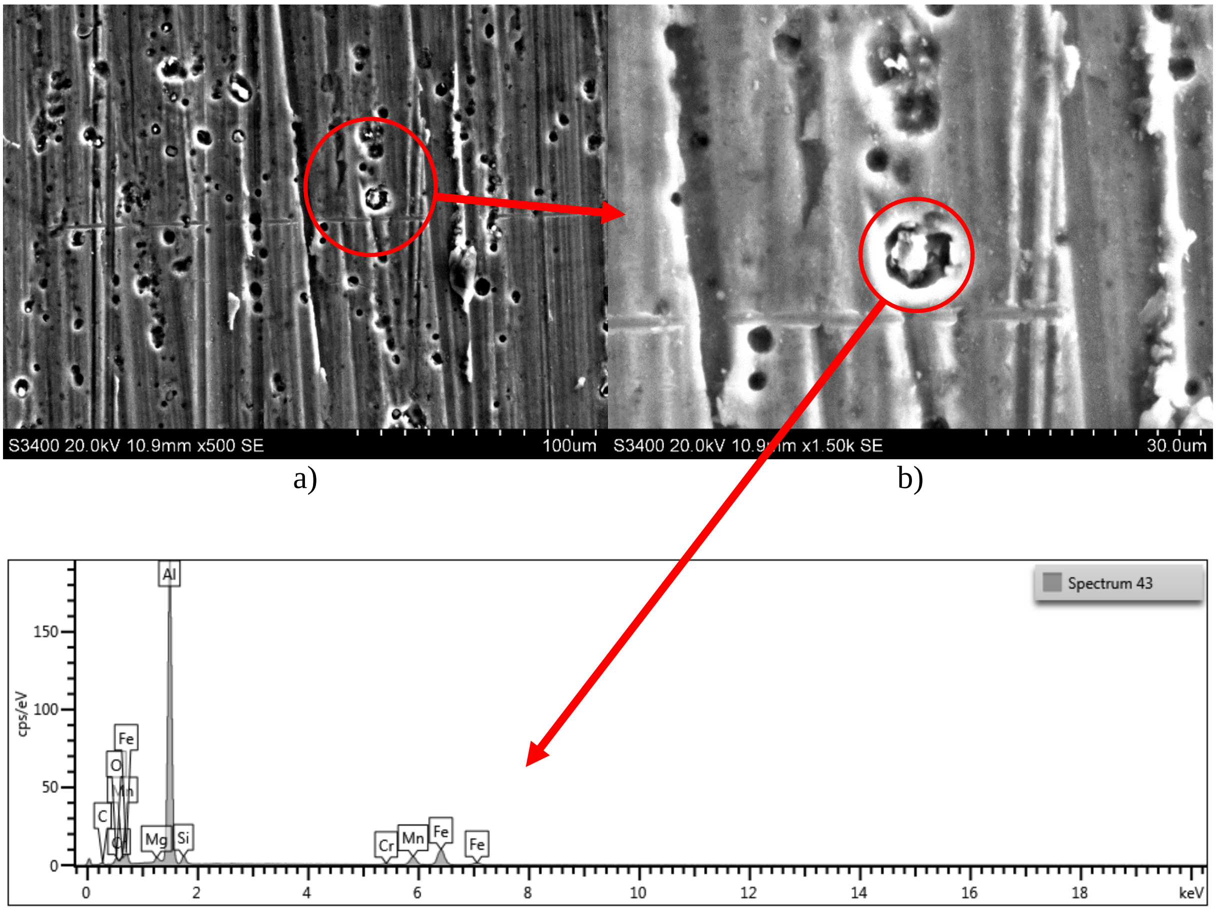

a)

b)

c)

Figure 31: SEM images and EDS spectra of freely exposed AA5083 in natural seawater at 32 °C.

Table 11: EDS analysis of the freely exposed AA5083 in Figure 31.

Element	C	O	Mg	Al	Si	Cr	Mn	Fe
[wt%]	7,62	3,95	1,03	60,84	2,9	0,64	7,23	15,8

Freely exposed AA6082 at 10 °C

In Figure 32, SEM images of an AA6082 sample freely exposed in natural seawater at 10 °C in SEALAB are shown. In image a), which is magnified 500 times, several pits and some particles can be seen. The marked area in image a) is magnified in image b). EDS was performed on the two most pronounced particles in image b) and the EDS spectra can be seen in part c). The particles were found to be corrosion products.

EDS was also performed on the marked pit in image b). The EDS spectra can be seen in part d) of Figure 32 and the result from the EDS analysis is presented in Table 12. The EDS indicates that this pit was initiated due to an Al(Fe,Mn) intermetallic.

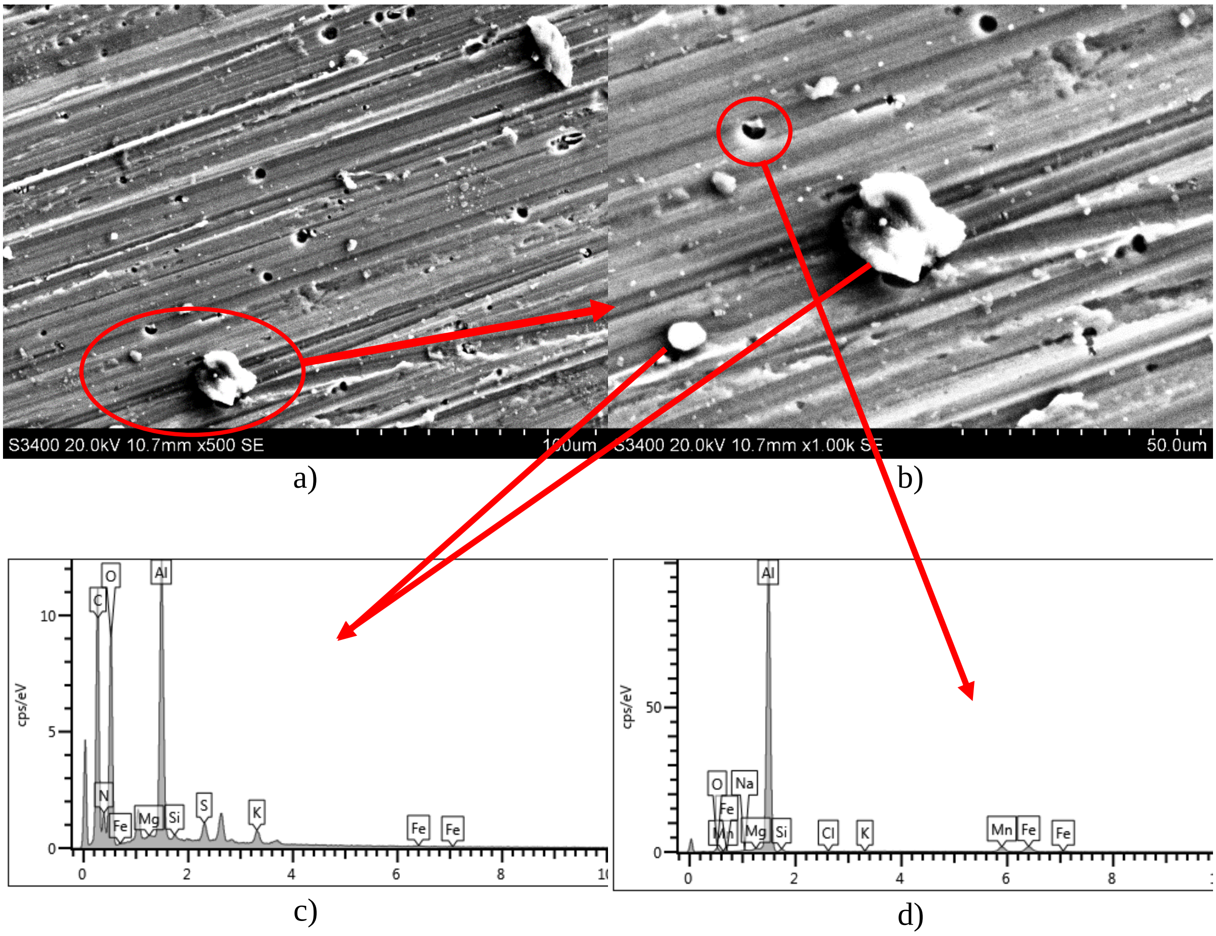

a) b)

c) d)

Figure 32: SEM images and EDS spectra for freely exposed AA6082 in natural seawater at 10 °C.

Table 12: EDS analysis for the indicated pit in image b) in Figure 32.

Element	O	Mg	Al	Si	Mn	Fe	Salts/impurities
[wt%]	4,14	0,36	78,67	1,63	6,65	7,73	Rest

Freely exposed AA6082 at 32 °C

In Figure 33 a SEM image of an AA6082 sample freely exposed in natural seawater at 32 °C is shown. Three pits with their associated intermetallics are indicated in the SEM image. EDS was performed on the indicated pits, and the EDS spectra's are also presented in Figure 33.

The results from the EDS, presented in Table 13, indicates that the intermetallics were Al(Fe,Mn,Si) precipitates.

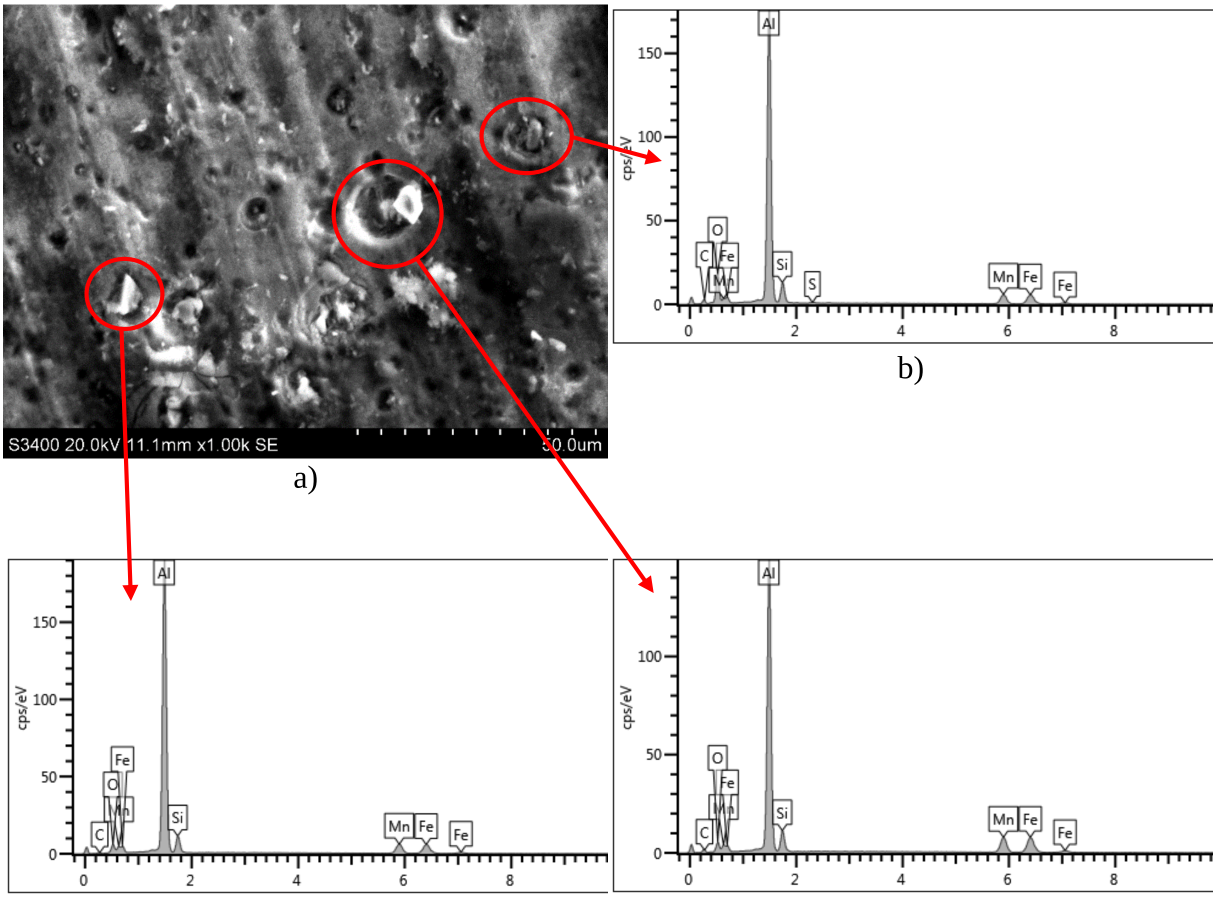

a)

b)

c)

d)

Figure 33: SEM image and EDS spectra for AA6082 freely exposed in natural seawater at 32 °C.

Table 13: Results of EDS of the indicated pits in image a) in Figure 33.

	Element	C	O	Al	Si	Mn	Fe
EDS b)	[wt%]	11,75	18,05	48,87	5,75	7,43	7,98
EDS c)	[wt%]	4,96	6,07	62,43	6,96	9,58	10
EDS d)	[wt%]	10,44	5,55	52,25	6,36	12,23	13,18

Cross-sections of the freely exposed samples

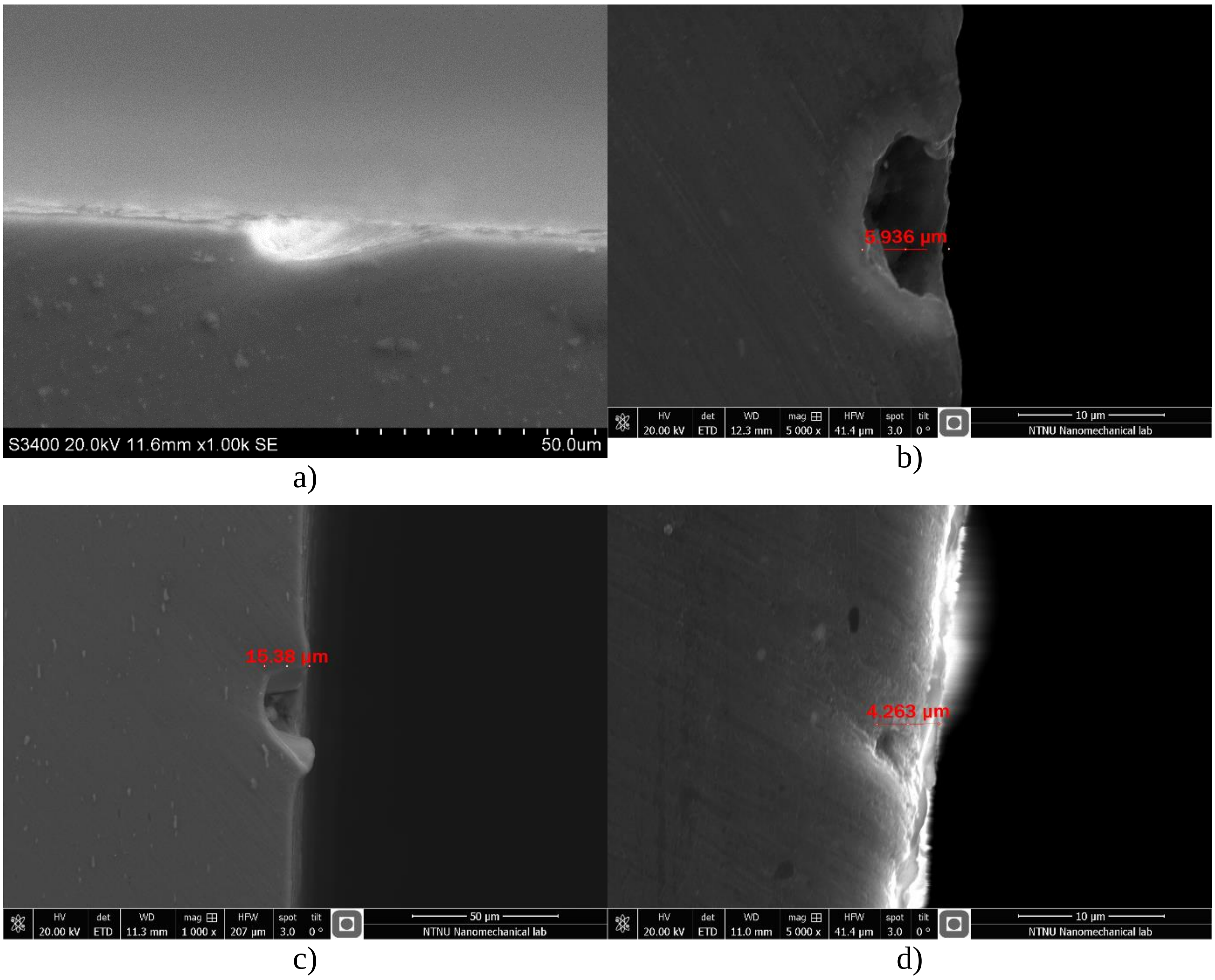
S3400 20.0kV 11.6mm x1.00k SE
50.0um
5.936 µm
HV 20.00 kV det ETD WD 12.3 mm mag 5 000 x HFW 41.4 µm spot 3.0 tilt 0 °
10 µm
NTNU Nanomechanical lab
15.38 µm
HV 20.00 kV det ETD WD 11.3 mm mag 1 000 x HFW 207 µm spot 3.0 tilt 0 °
50 µm
NTNU Nanomechanical lab
4.263 µm
HV 20.00 kV det ETD WD 11.0 mm mag 5 000 x HFW 41.4 µm spot 3.0 tilt 0 °
10 µm
NTNU Nanomechanical lab

a) b)

c) d)

Figure 34: SEM images of cross-sections of the freely exposed samples in SEALAB, a) AA5083 at 10 °C, b) AA5083 at 32 °C, c) AA6082 at 10 °C and d) AA6082 at 32 °C. Note that the magnification is not the same for all the images. Image a) is from another SEM.

Figure 34 shows the results of examination of the cross-section of the freely exposed samples. Two different SEM's have been used. As Figure 34 indicates the pits were only of microscopic scale with pitting depths of 5 and 15 µm. The deepest pit was found on the AA6082 sample exposed at 10 °C, it was expected to observe the deepest pits on the samples exposed at 32 °C. As earlier mentioned, the cross-section only represent a small fraction of the exposed surface area.

−700 mV vs Ag/AgCl

On the samples polarized to −700 mV vs Ag/AgCl corrosion was observed on the edge, beneath the coating, this can be seen in Figure 60 and Figure 64 in Appendix B.

5.1 SEALAB

The SEM images a) and c) in Figure 35 indicates that the surface of the AA5083 samples anodic polarized to −700 mV vs Ag/AgCl were covered by a significant amount of corrosion products, and as image b) indicates the corrosion was to a large extent concentrated on the edges, beneath the coating. EDS analysis indicated that the marked particles were corrosion products.

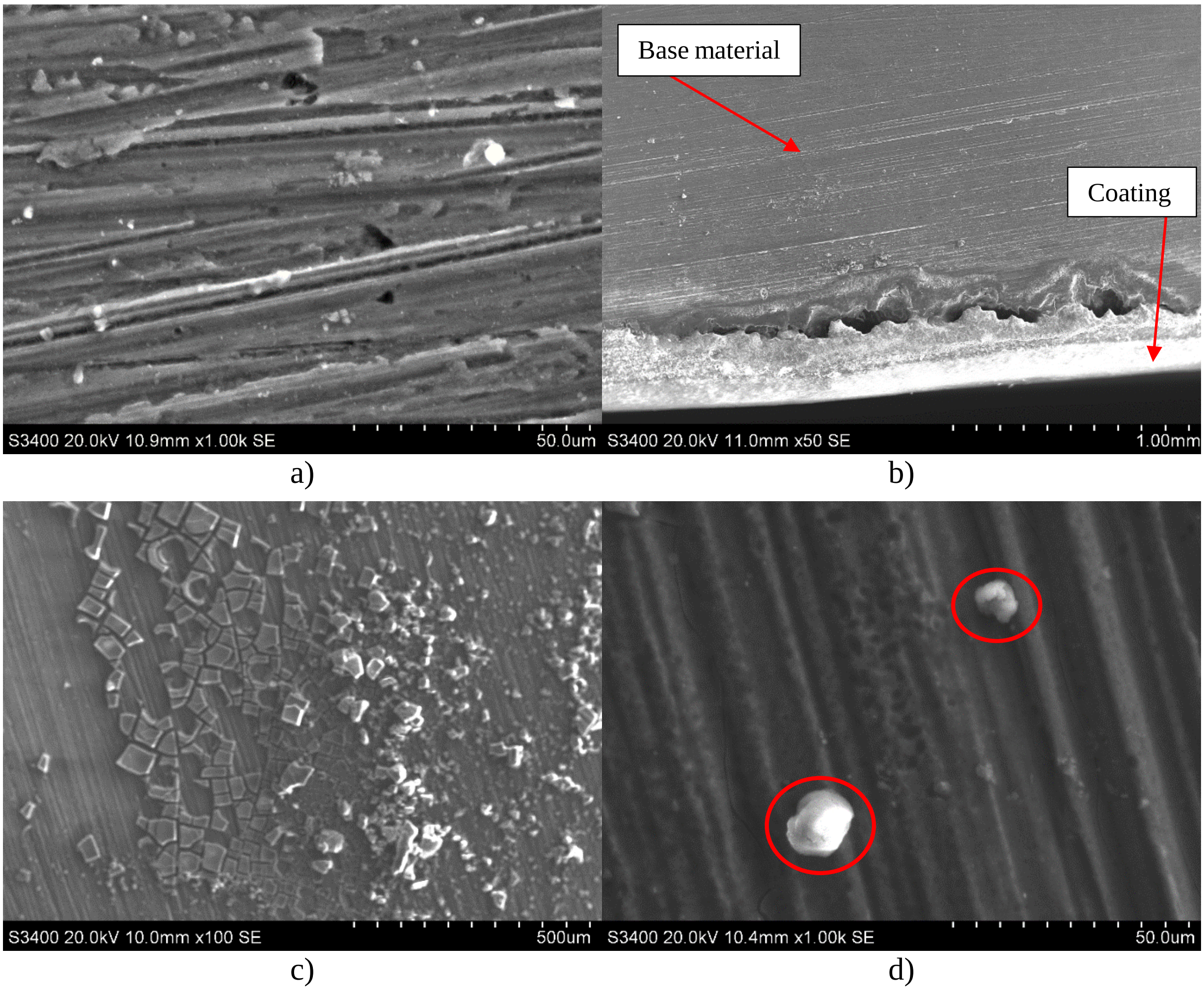
S3400 20.0kV 10.9mm x1.00k SE
50.0um
a)
Base material
Coating
S3400 20.0kV 11.0mm x50 SE
1.00mm
b)
S3400 20.0kV 10.0mm x100 SE
500um
c)
S3400 20.0kV 10.4mm x1.00k SE
50.0um
d)

Figure 35: SEM images of AA5083 anodic polarized to −700 mV vs Ag/AgCl in natural seawater in SEALAB. a) and b) at 10 °C, and c) and d) at 32 °C.

The SEM images in Figure 36 for AA6082 anodic polarized to −700 mV indicates that pits and intermetallics were observed. EDS was performed on the marked particles in image a) and in image b) the EDS spectra is shown. The EDS analysis indicated that the particles are Al(Fe,Mn,Si) precipitates.

For the AA6082 sample exposed at 32 °C severe pits were found, this can be seen in image c). The light particles that can be observed in image a) were examined to be Al(Fe,Mn,Si) precipitates. For this sample severe crystallographic pitting was also observed, this can be seen in image e) in Figure 36 and in Figure 38.

Image d) shows that a significant degree of the corrosion was concentrated to edge beneath the coating for AA6082 also. This corrosion was in form of crevice corrosion, Figure 37 shows how the coating formed a crevice.

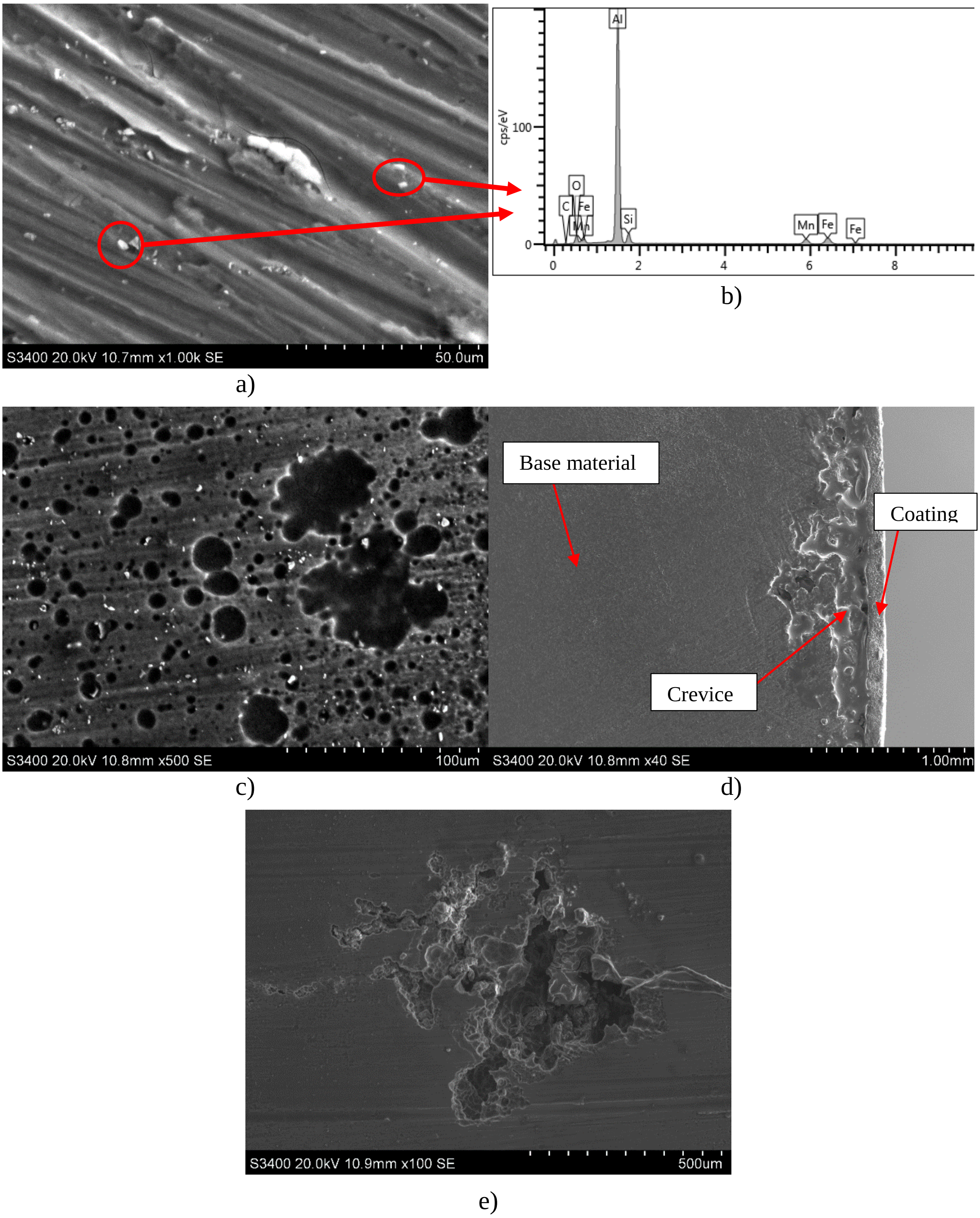
S3400 20.0kV 10.7mm x1.00k SE
50.0um
a)
cps/eV
100
0
Al
O
C
Fe
Mn
Si
Mn
Fe
Fe
0
2
4
6
8
b)
S3400 20.0kV 10.8mm x500 SE
100um
c)
Base material
Coating
Crevice
S3400 20.0kV 10.8mm x40 SE
1.00mm
d)
S3400 20.0kV 10.9mm x100 SE
500um
e)

Figure 36: SEM images and EDS of AA6082 anodic polarized to −700 mV vs Ag/AgCl in natural seawater in SEALAB. Image a) and b) for 10 °C and c), d) and e) for 32 °C.

5.1 SEALAB

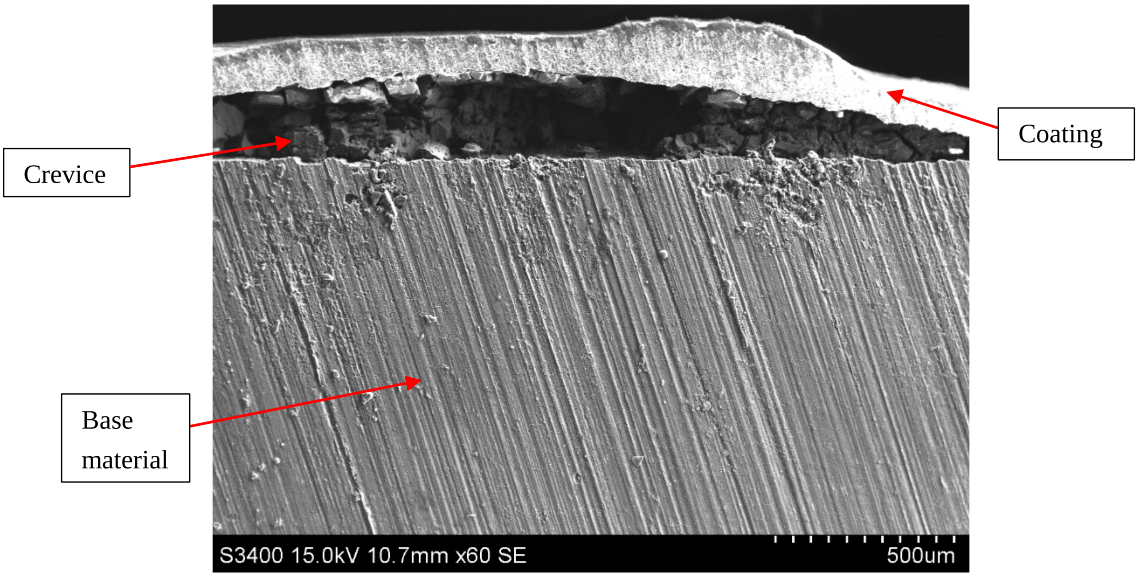
Crevice
Coating
Base material
S3400 15.0kV 10.7mm x60 SE
500um

Figure 37: Crevice formed beneath the coating.

Cross-section of samples anodic polarized to −700 mV vs Ag/AgCl

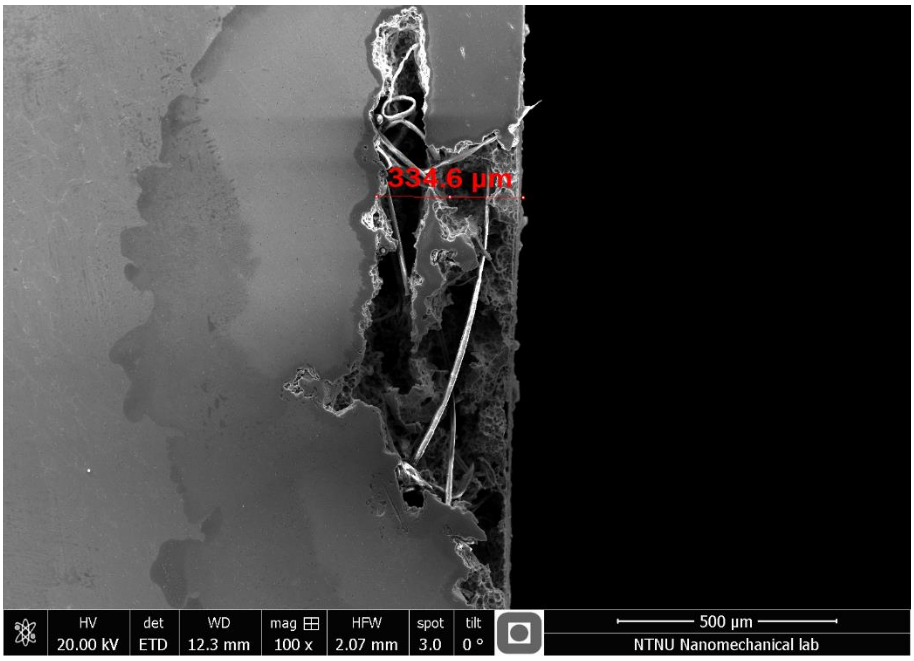
334.6 µm
HV
20.00 kV
det
ETD
WD
12.3 mm
mag
100 x
HFW
2.07 mm
spot
3.0
tilt
0 °
500 µm
NTNU Nanomechanical lab

Figure 38: SEM image of crystallographic pitting on the cross-section of AA6082 anodic polarized to −700 mV vs Ag/AgCl at 32 °C.

Figure 38 shows a severe pit observed on the cross-section of the AA6082 sample anodic polarized to −700 mV vs Ag/AgCl at 32 °C.

−1050 mV vs Ag/AgCl (coupled to sacrificial anode)

The photos in Figure 61 and Figure 65 in Appendix B shows no visible corrosion on the samples coupled to a sacrificial anode, but when examined in SEM microscopic pits were observed. Calcareous deposit was not observed on these samples.

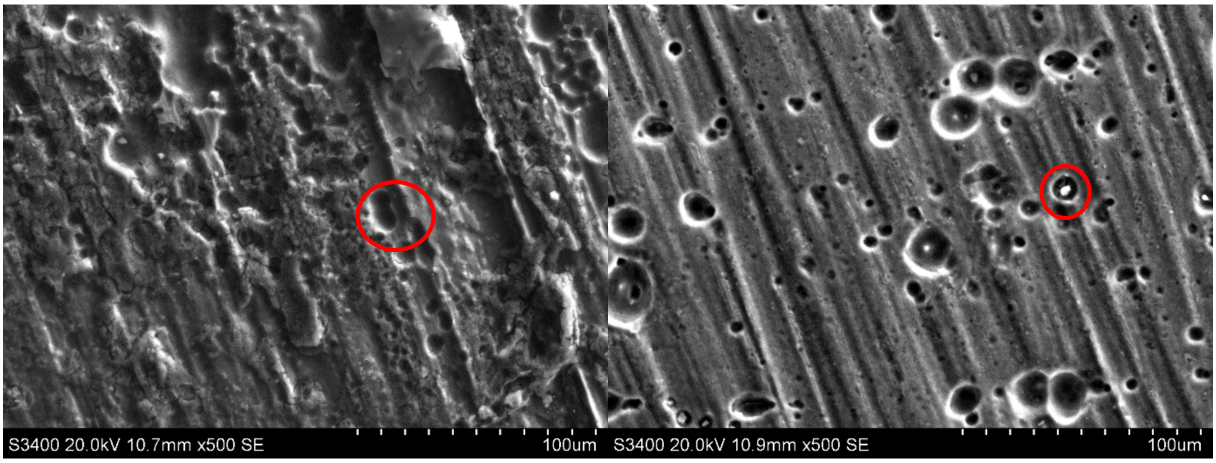

a) b)

Figure 39: SEM images of AA5083 coupled to sacrificial anode in natural seawater, a) at 10 °C and b) at 32 °C.

Image a) in Figure 39 shows some small pits on the AA5083 sample coupled to a sacrificial anode in natural seawater at 10 °C. The marked pit in image a) was analyzed by use of EDS. The EDS analysis indicated that the composition in the pit was Al-Mg.

Image b) in Figure 39, which is a SEM image of an AA5083 sample coupled to a sacrificial anode in natural seawater at 32 °C, shows that this sample had both more and bigger pits compared to the sample exposed at 10 °C. EDS was performed on the marked pit in image b), and the analysis indicated that the intermetallic was an Al(Fe,Mg,Si,Cr,Mn) precipitate. The results from the EDS for image a) and b) can be seen in Table 14.

Table 14: Results from EDS of marked areas in Figure 39.

	Element	C	O	Mg	Al	Si	Cr	Mn	Fe	Salts/impurities
EDS a)	[wt%]	3,52	10,36	4,35	79,13	-	-	0,37	-	Rest
EDS b)	[wt%]	4,54	27,19	1,06	48,4	2,05	0,63	5,18	5,97	Rest

SEM images and EDS spectra of AA6082 coupled to a sacrificial anode in natural seawater at 10 °C and at 32 °C are shown in Figure 40. Image a) and b) shows that pits are observed on the samples at both temperatures. However, the amount of pits was significantly larger for the sample exposed at 32 °C compared to the sample exposed at 10 °C.

EDS was performed on the marked area in image a) and image b). As it can be seen for the sample exposed at 10 °C the analyzed particle was an Al(Fe,Si,Mn) precipitate. The analyzed particles on the sample exposed at 32 °C consisted mainly of Al and Si, and some amount of Mg, which is also the main elements for this alloy.

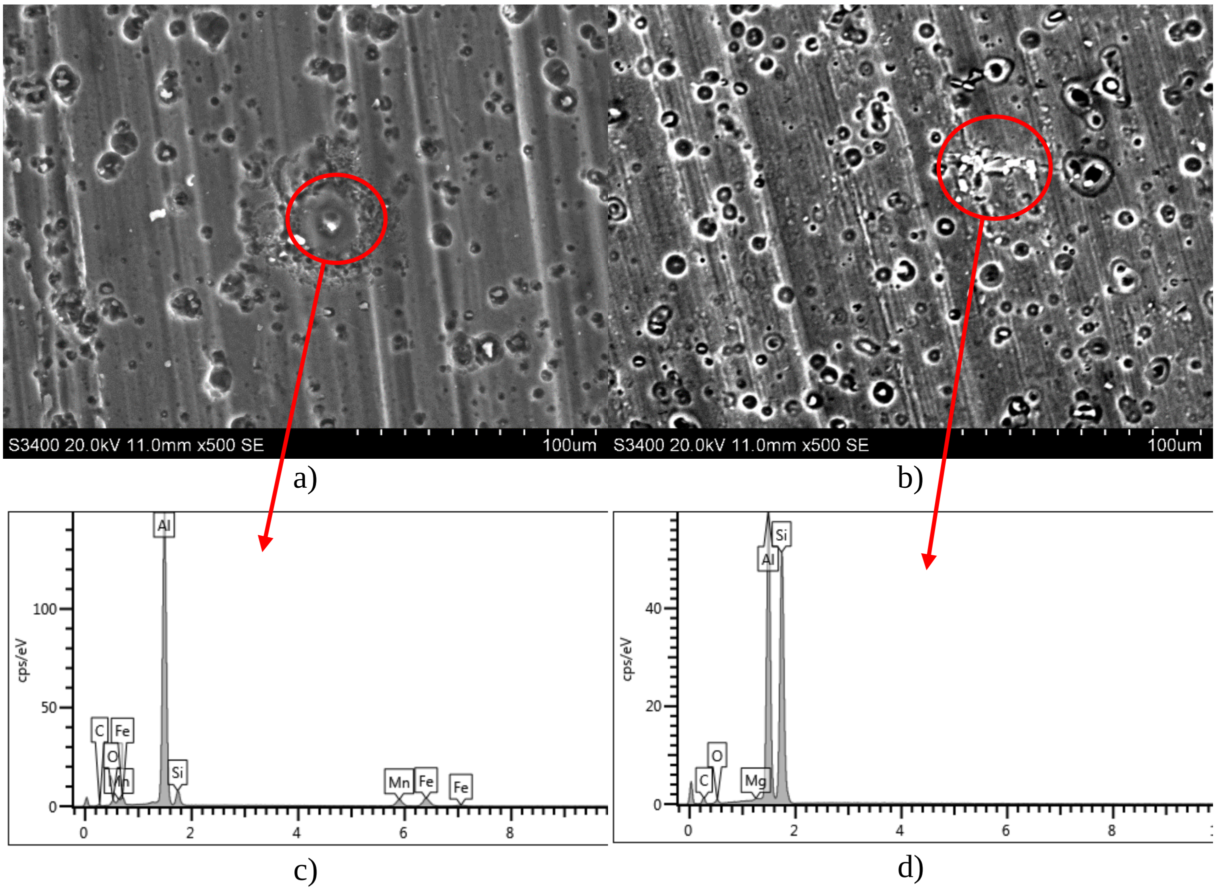

Figure 40: SEM images and EDS spectra for AA6082 coupled to a sacrificial anode in natural seawater, a) and c) at 10 °C, and b) and d) at 32 °C.

Cross-sections of samples coupled to a sacrificial anode

Figure 41 shows the SEM images of pits observed in the cross-section face of the samples coupled to a sacrificial anode exposed in SEALAB. No pits were observed on the AA5083 sample exposed at 10 °C. From Figure 41 one can see that the pits observed on the samples exposed at 32 °C are significantly deeper than the pit observed on the sample exposed at 10 °C.

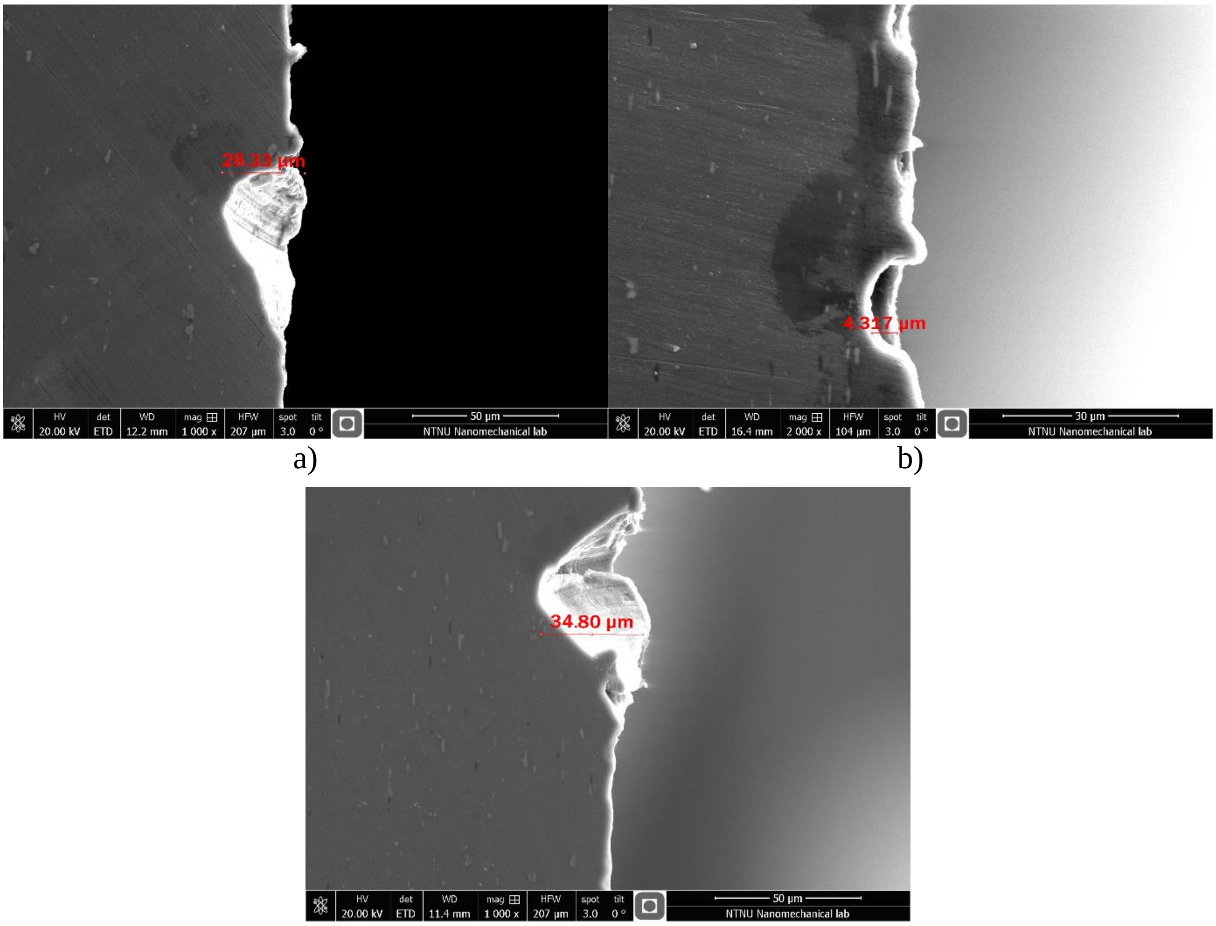
28.33 µm
HV 20.00 kV det ETD WD 12.2 mm mag 1 000 x HFW 207 µm spot 3.0 tilt 0 °
50 µm
NTNU Nanomechanical lab
4.317 µm
HV 20.00 kV det ETD WD 16.4 mm mag 2 000 x HFW 104 µm spot 3.0 tilt 0 °
30 µm
NTNU Nanomechanical lab
34.80 µm
HV 20.00 kV det ETD WD 11.4 mm mag 1 000 x HFW 207 µm spot 3.0 tilt 0 °
50 µm
NTNU Nanomechanical lab

a) b)

c)

Figure 41: SEM images of the cross-sections for the samples coupled to a sacrificial anode; a) AA5083 at 32 °C, b) AA6082 at 10 °C and c) AA6082 at 32 °C.

−1500 mV vs Ag/AgCl

From Figure 62 and Figure 66 in Appendix B it can be seen that the samples cathodic polarized to −1500 mV vs Ag/AgCl have suffered from severe corrosion, this can be seen because of the significant amount of corrosion products. The AA6082 sample exposed at 10 °C has not suffered from the same severe corrosion, but this sample is not representative and has not been further investigated.

The corrosion products were difficult to remove in a proper way on these samples due to the significant amount. The corrosion products on the AA5083 sample exposed at 10 °C were the easiest to remove, but as it can be seen in image a) in Figure 42 there was still a layer of corrosion products covering the particles and pits on the surface.

Image b) and image c) in Figure 42 shows magnified images of the corrosion products on the AA5083- and AA6082 sample, respectively, both exposed at 32 °C. The etching of these two samples in HNO_3 did not remove the corrosion products.

EDS analysis (mapping) of the corrosion products on these samples can be found in Appendix F. The corrosion products for AA5083 mainly consisted of Al, O and Mg, and Na, Cl and S from the seawater. The corrosion products for AA6082 consisted of Al, O, Si and C, in addition to Na from the seawater.

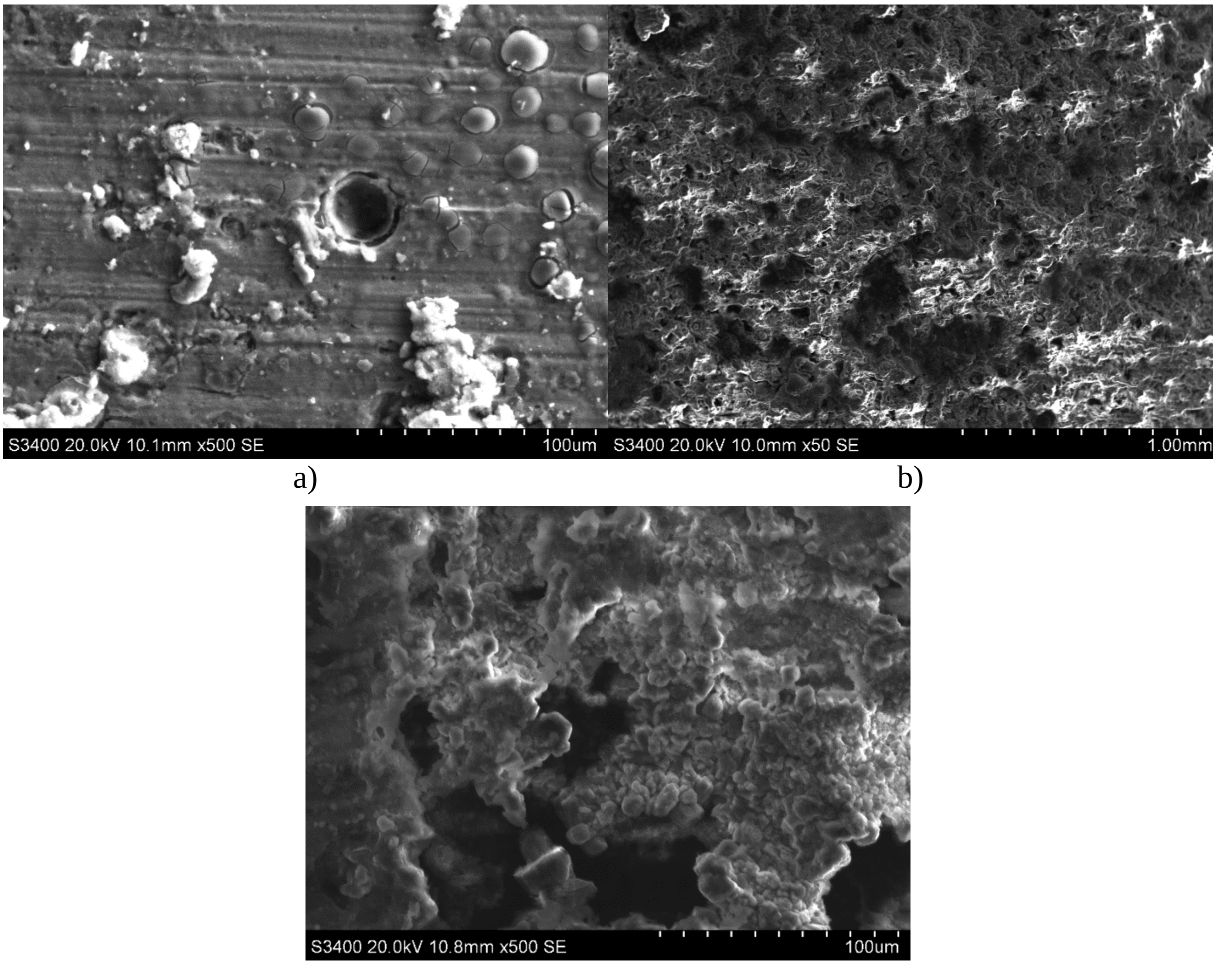
S3400 20.0kV 10.1mm x500 SE
100um
S3400 20.0kV 10.0mm x50 SE
1.00mm
S3400 20.0kV 10.8mm x500 SE
100um

a) b)

c)

Figure 42: SEM images of the samples cathodic polarized to −1500 mV vs Ag/AgCl in natural seawater, a) AA5083 at 10 ^{o}C, b) AA5083 at 32 ^{o}C and c) AA6082 at 32 ^{o}C.

Cross-section of the samples cathodic polarized to −1500 mV vs Ag/AgCl

Figure 43 shows SEM images of the cross-sections of the samples cathodic polarized to −1500 mV vs Ag/AgCl. The AA5083 sample exposed at 10 ^{o}C was the only sample of the ones cathodic polarized to −1500 mV vs Ag/AgCl where the corrosion products were fairly removed during rinsing in HNO_3. Thus, this was the only sample where pits may be observed.

Image a) in Figure 43 shows two pits observed on the cross-section of the AA5083 sample exposed at 10 ^{o}C. In image b) a cross-section view of the corrosion products on AA5083 exposed at 32 ^{o}C can be seen, the thickness of the corrosion products layer was measured to be above 1 mm. Image c) shows the corrosion products on AA6082 exposed at 32 ^{o}C, the thickness of this was measured to be about 410 µm. As earlier mentioned, the AA6082 sample exposed at 10 °C is not representative, thus it has not been examined in SEM.

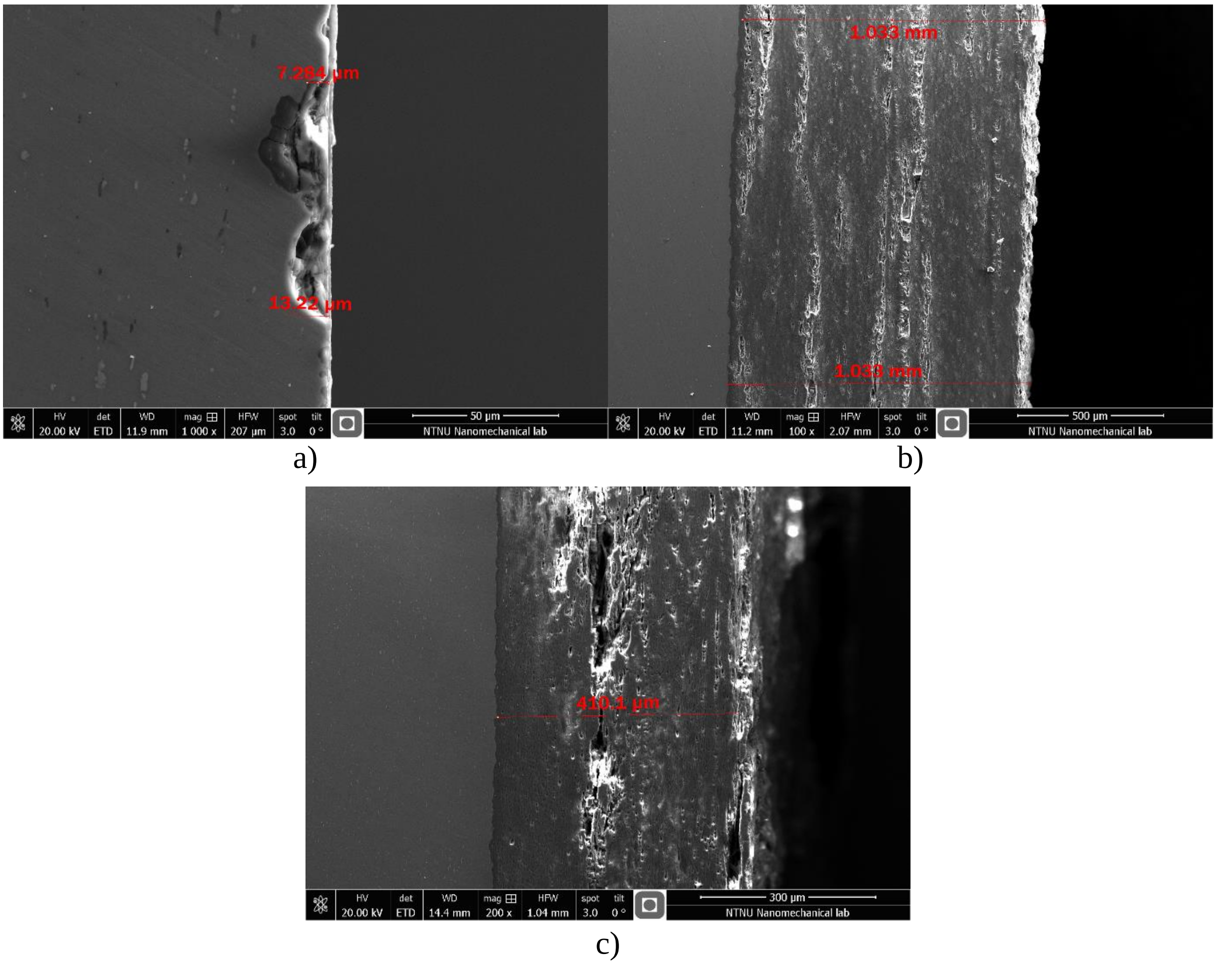
7.284 µm
13.22 µm
HV 20.00 kV det ETD WD 11.9 mm mag 1 000 x HFW 207 µm spot 3.0 tilt 0 °
50 µm
NTNU Nanomechanical lab
1.033 mm
1.033 mm
HV 20.00 kV det ETD WD 11.2 mm mag 100 x HFW 2.07 mm spot 3.0 tilt 0 °
500 µm
NTNU Nanomechanical lab
a)
b)
410.1 µm
HV 20.00 kV det ETD WD 14.4 mm mag 200 x HFW 1.04 mm spot 3.0 tilt 0 °
300 µm
NTNU Nanomechanical lab
c)

Figure 43: SEM images of the cross-sections of the samples cathodic polarized to −1500 mV vs Ag/AgCl; a) AA5083 at 10 °C, b) AA5083 at 32 °C and c) AA6082 at 32 °C.

5.2 Corrosion Laboratory Perleporten

The experiments that are performed in the corrosion laboratory at NTNU were mainly to examine the effect of pH on the corrosion behavior.

5.2.1 Open Circuit Potential

The OCP for the samples freely exposed in SSW with pH 8,2 can be found in Appendix G.

In Figure 44 the OCP development of AA5083 and AA6082 in SSW with pH 3 at room temperature are shown.

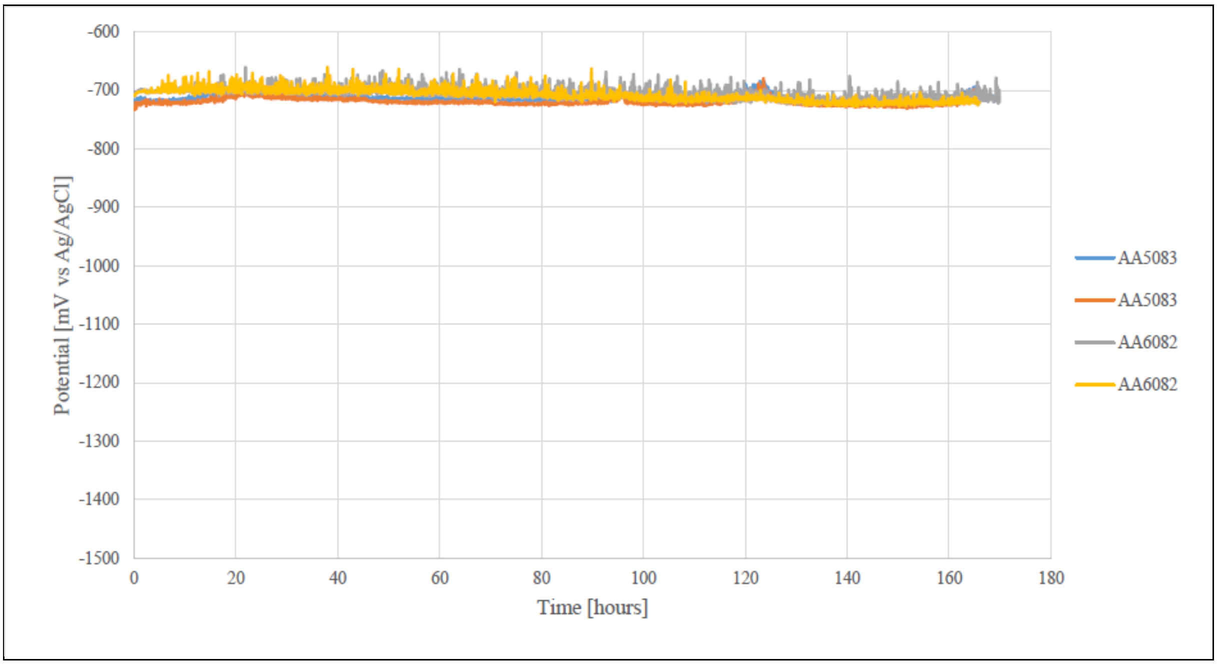

Figure 44: OCP for freely exposed AA5083 and AA6082 in SSW with pH 3 at room temperature.

As seen in Figure 44 the OCP for AA5083 and AA6082 in SSW with pH 3 showed a fluctuating (disturbing) behavior, but were concentrated around −700 mV vs Ag/AgCl. The OCP for AA5083 started at −725 mV vs Ag/AgCl, and then increased slightly and stabilized in the range −715 to −720 mV vs Ag/AgCl. It is difficult to see in Figure 44, but every 24th hour of exposure the OCP reached a maximum value of about −680 to −685 mV vs Ag/AgCl. These peaks are present because this was the time the pH was adjusted. The pH was not monitored and adjusted during night, thus, the most significant changes in pH occurred due to adjustment every morning. The effect of this significant change in pH can also be seen in the current density plots in Section 5.2.2.

The OCP for AA6082 started at −710 mV vs Ag/AgCl, and then it showed a stable, but fluctuating behavior in the range −695 to −705 mV vs Ag/AgCl for the rest of the exposure period. It is difficult to see, but the OCP for AA6082 also showed some peaks every 24th hour, reaching maximum values of −660 mV vs Ag/AgCl.

Figure 45 shows the OCP development of AA5083 and AA6082 in SSW with pH 10 at room temperature. The significant changes after 70 and 125 hours of exposure are due to significant adjustment of the pH. After 70 hours the pH was adjusted from 9,55 to 10,84, and after 125 hours it was adjusted from 9,78 to 11,5.

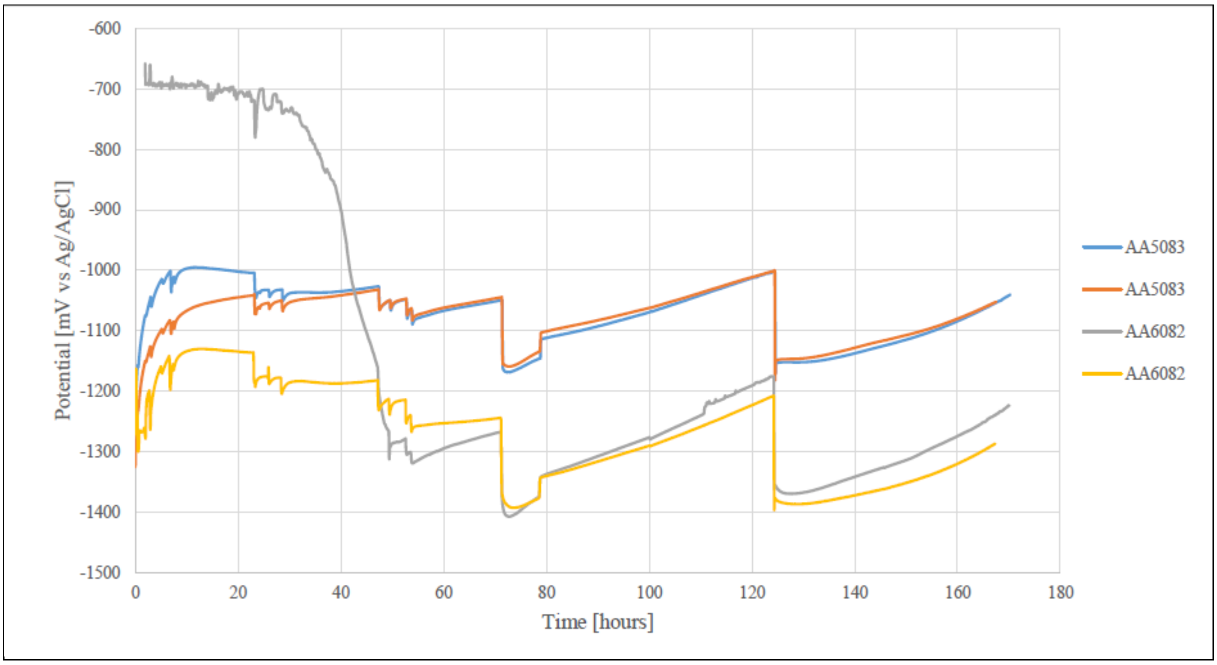

Figure 45: OCP for freely exposed AA5083 and AA6082 in SSW with pH 10 at room temperature.

The OCP-curves for AA5083 and AA6082 in SSW with pH 10 in Figure 45 were more spread out than the OCP-curves for SSW with pH 8,2 and pH 3. The OCP for AA5083 started at −1250 mV vs Ag/AgCl, and then increased relatively fast at the same time as the two curves separated. The curves increased to values of −1000 mV vs Ag/AgCl and −1040 mV vs Ag/AgCl. After 23 hours of exposure, the curves were unified and had the same behavior for the rest of the exposure period. The OCP experienced a little fluctuation, but after 50 hours, the tendency was that the OCP slightly increased and then suddenly had a significant drop after 70 hours. After this, between 80 and 125 hours of exposure, the OCP had a stable increase from −1100 mV vs Ag/AgCl to −1000 mV vs Ag/AgCl. Then, a sudden and significant drop down to −1150 mV vs Ag/AgCl occurred. After this, the OCP had a stable increase until the end of the exposure time.

The OCP curves for AA6082 started completely different, one started at −1300 mV vs Ag/AgCl and the other one started at −700 mV vs Ag/AgCl. The yellow curve followed the same tendency as the OCP for AA5083, but lied in the range −1500 to −2000 mV below the AA5083 curves. The grey curve was relative stable around −700 mV vs Ag/AgCl the first 20 hours of exposure, and then it started to decrease towards the AA6082-curve. After 30 hours, the grey curve decreased relative rapidly and after 50 hours, it reached −1310 mV vs Ag/AgCl, which is about 700 mV below the other AA6082-curve. After 70 hours, the two AA6082-curves were unified and followed the same trend for the rest of the exposure period. However, differences up to 70 mV between the two curves could be observed for the last 100 hours of exposure.

5.2.2 Current density curves

The specified potentials in this study were as following: −700 mV vs Ag/AgCl, −1050 mV vs Ag/AgCl (coupled to sacrificial anode) and −1500 mV vs Ag/AgCl. The current density curves for the samples exposed in SSW with pH 8,2 can be found in Appendix G.

−700 mV vs Ag/AgCl

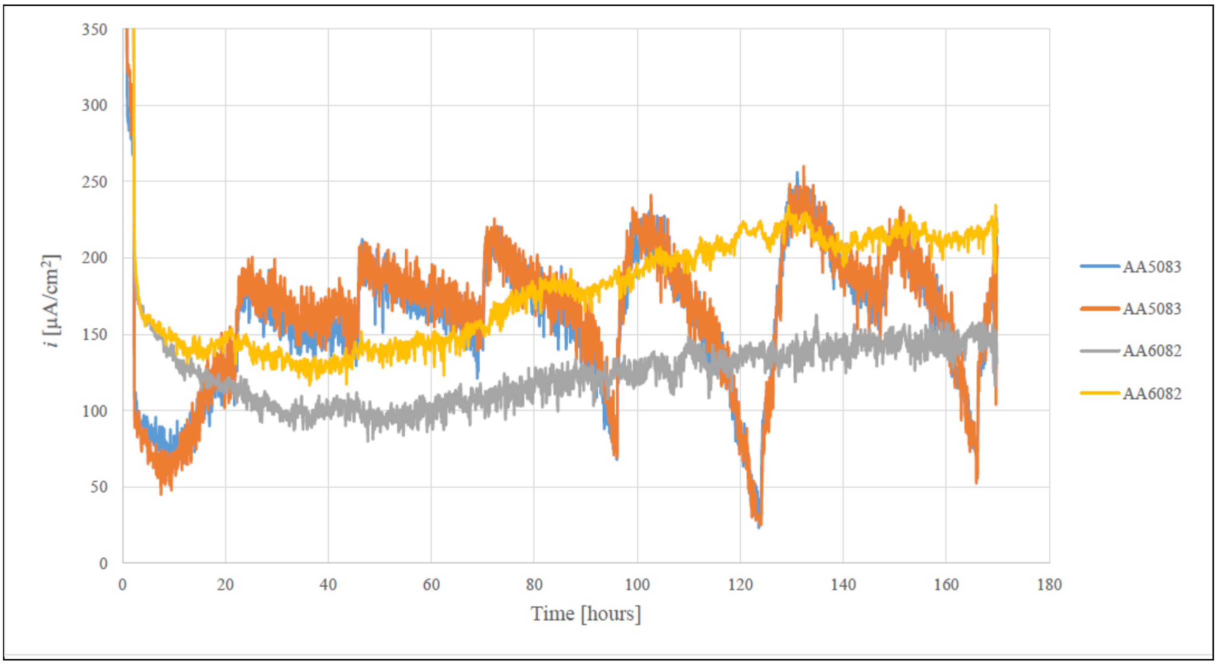

Figure 46: Current density for samples anodic polarized to −700 mV vs Ag/AgCl in SSW with pH 3.

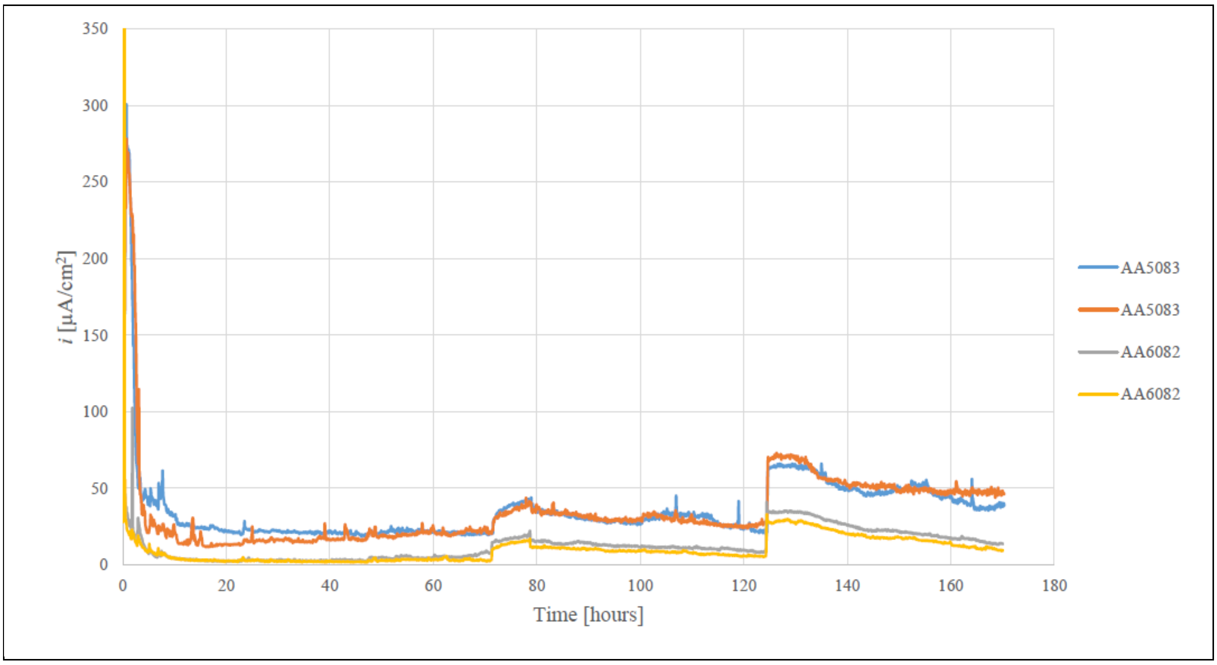

Figure 47: Current density for samples anodic polarized to −700 mV vs Ag/AgCl in SSW with pH 10.

Figure 46 and Figure 47 show the anodic current density for the samples polarized to −700 mV vs Ag/AgCl in SSW with pH 3 and pH 10. The sudden changes that can be seen in Figure 46 and Figure 47 are due to adjustment of the pH.

−1050 mV vs Ag/AgCl (samples coupled to sacrificial anode)

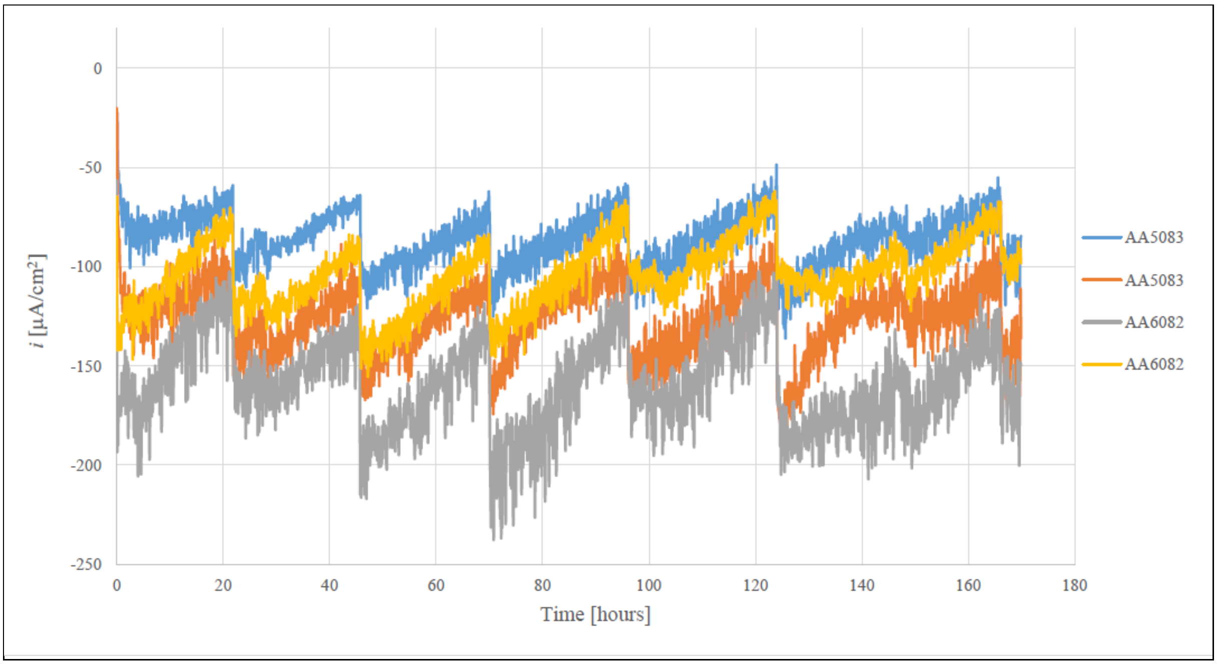

Figure 48: Current density for the samples cathodic polarized to −1050 mV vs Ag/AgCl in SSW with pH 3.

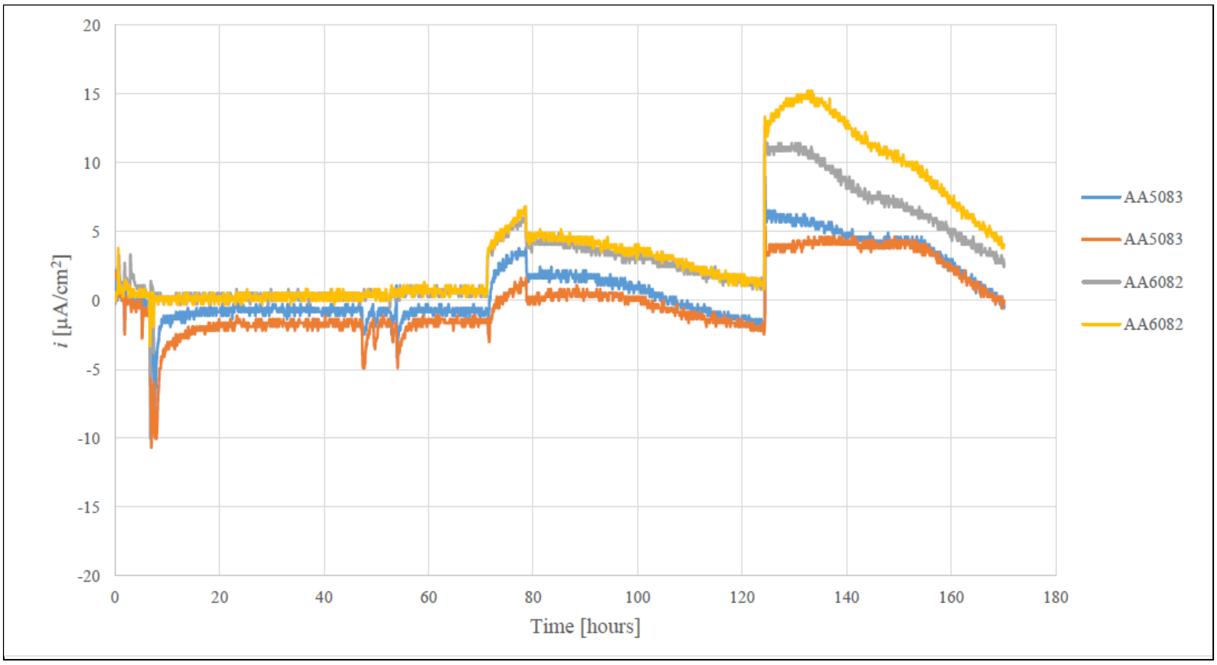

Figure 49: Current density for the samples cathodic polarized to −1050 mV vs Ag/AgCl in SSW with pH 10.

Figure 48 and Figure 49 show the current density for the samples coupled to a sacrificial anode in SSW with pH 3 and pH 10. The sudden changes that can be seen in Figure 48 and Figure 49 are due to adjustment of the pH.

−1500 mV vs Ag/AgCl

Figure 50 and Figure 51 show the current density for the samples polarized to −1500 mV vs Ag/AgCl in SSW with pH 3 and pH 10. The sudden changes that can be seen in Figure 50 is due to adjustment of the pH.

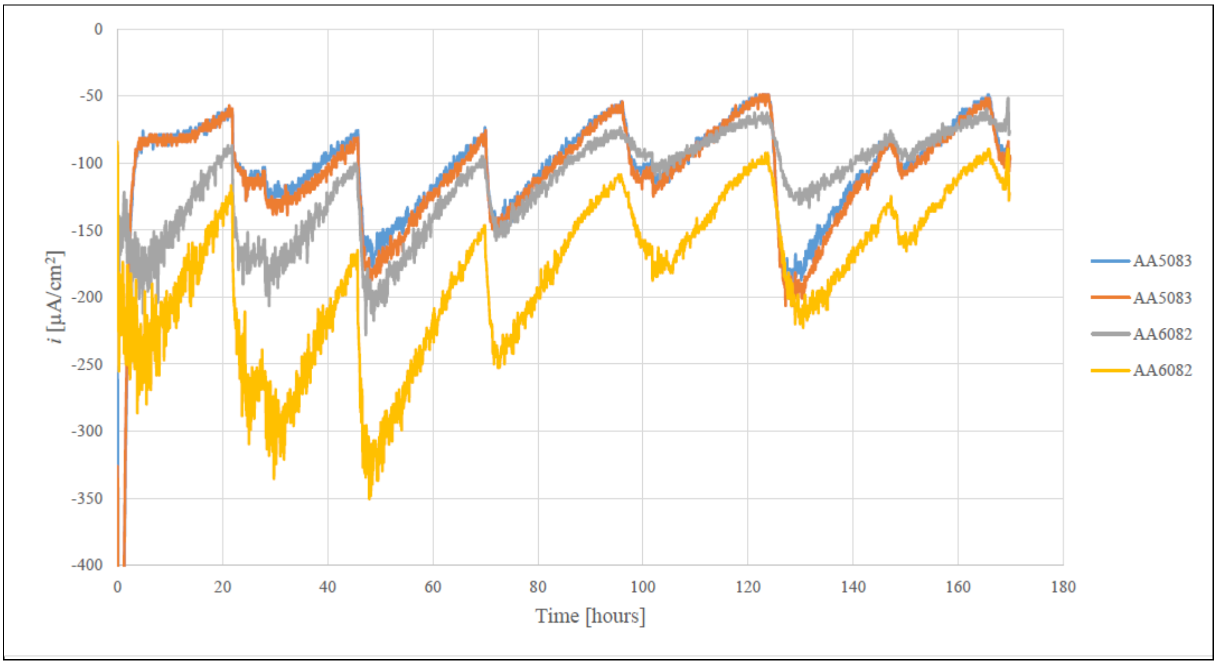

Figure 50: Current density for the samples cathodic polarized to −1500 mV vs Ag/AgCl in SSW with pH 3.

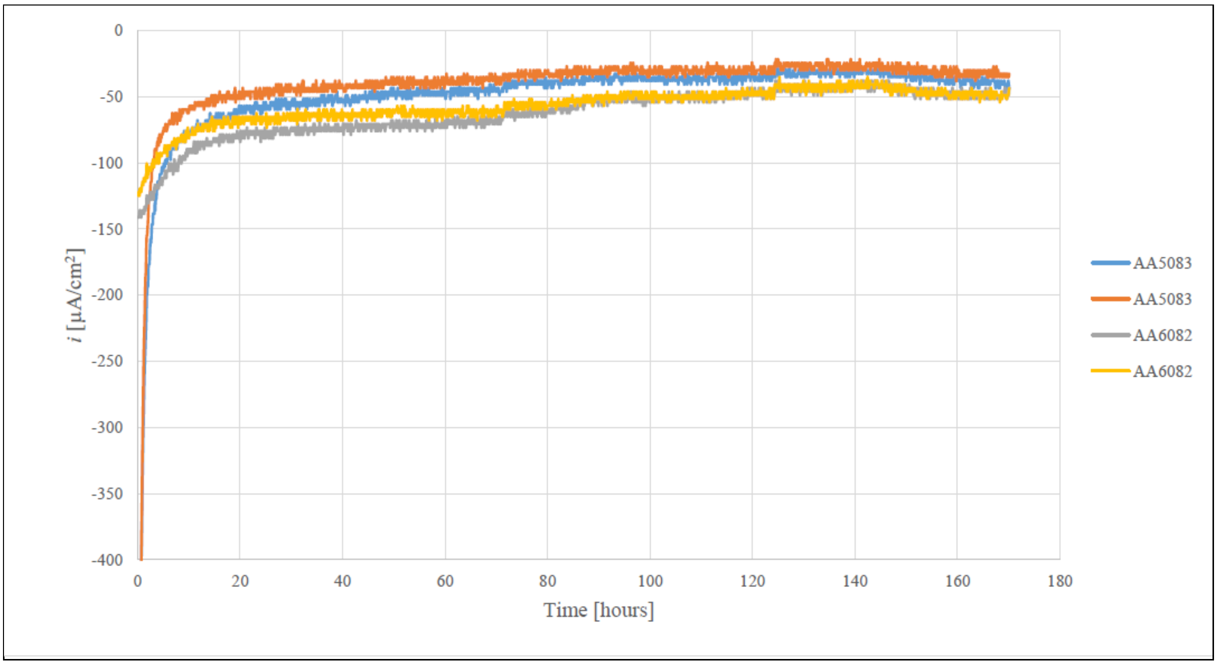

Figure 51: Current density for the samples cathodic polarized to −1500 mV vs Ag/AgCl in SSW with pH 10.

5.2.3 Potentiodynamic polarization curves

In this section, the recorded potentiodynamic polarization curves for the different alloys at the different pH-values after 24 hours and 168 hours of exposure are presented. In Appendix H the recorded polarization curves after 24 hours and 168 hours of exposure for pH 3 and 10 are presented in another way in an attempt to highlight the effect of exposure time.

AA5083 after 24 hours of exposure

The complete polarization curves recorded for AA5083 after 24 hours of exposure in SSW with the different pH values are shown in Figure 52.

As it can be seen from Figure 52 the OCP was the same for pH 3 and pH 8,2; −720 mV vs Ag/AgCl, while it was lower for pH 10; −1080 mV vs Ag/AgCl. The curve for pH 3 had the largest current density for the cathodic part, between OCP and −1200 mV vs Ag/AgCl the difference in current density between pH 3 and pH 8,2 is above one magnitude. The cathodic part of the curve for pH 10 has similar current density values as the curve for pH 8,2. However, due to the low OCP for pH 10 the shape of the cathodic part of this curve is slightly different.

The passive part of the curve for pH 3 showed a more fluctuating behavior than the other curves. The pitting potentials for the three pH-values were relatively similar. The curve for pH 8,2 had the highest pitting potential, −685 mV vs Ag/AgCl, while the curve for pH 10 had the lowest pitting potential, −710 mV vs Ag/AgCl.

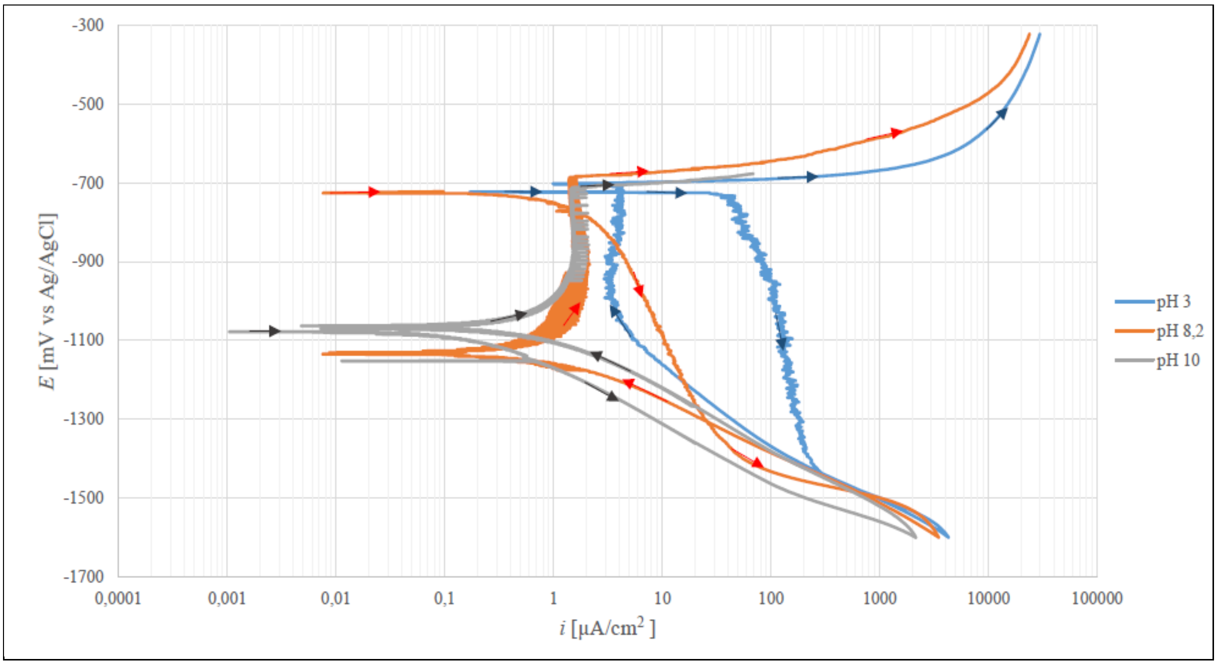

Figure 52: Complete polarization curves recorded for AA5083 after 24 hours exposure in SSW at room temperature.

AA5083 after 168 hours of exposure

The complete polarization curves recorded for AA5083 after 168 hours of exposure in SSW with the different pH values are shown in Figure 53.

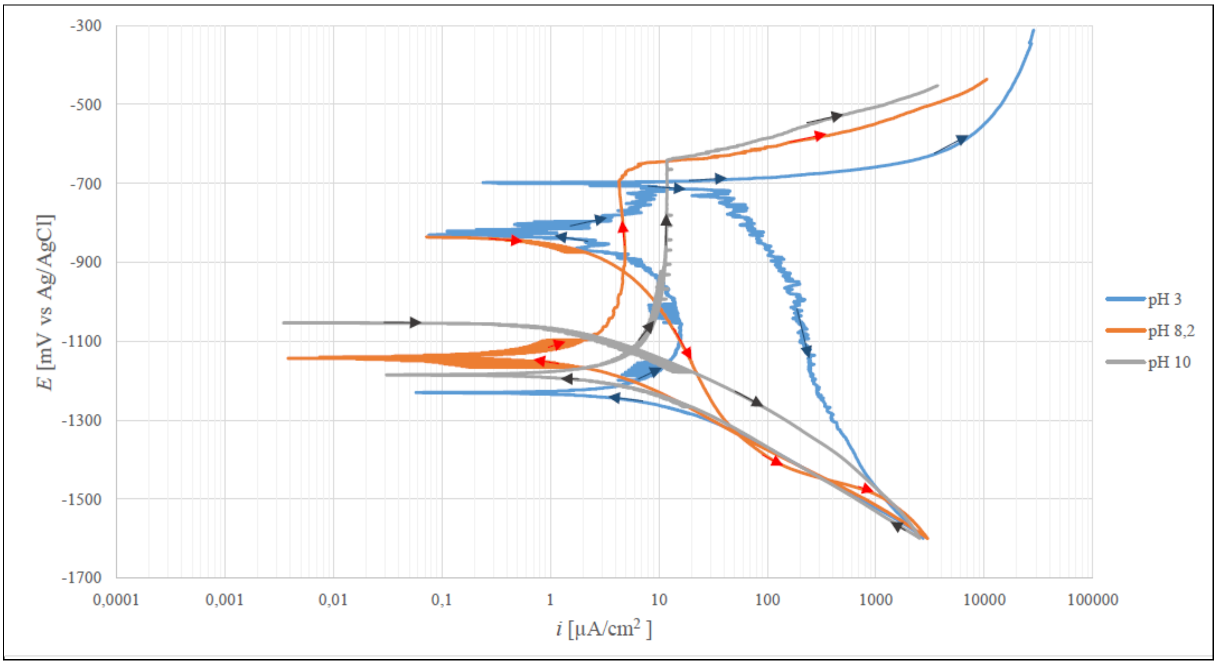

Figure 53: Complete polarization curves recorded for AA5083 after 168 hours exposure in SSW at room temperature.

The curve for pH 3 had the highest OCP; −710 mV vs Ag/AgCl, while the curve for pH 10 had the lowest; −1055 mV vs Ag/AgCl. The OCP for pH 8,2 was −835 mV vs Ag/AgCl.

The cathodic part of the curve for pH 3 had largest current density. Between OCP and −1190 mV vs Ag/AgCl the cathodic curve for pH 10 had the lowest current density. However, between −1190 and −1600 mV vs Ag/AgCl pH 10 had larger current density than pH 8,2. At −1600 mV vs Ag/AgCl, all the curves had approximately the same current density.

The passive part of the curve for pH 3 showed a more fluctuating behavior than the other curves. The pitting potential for pH 8,2 and 10 were approximately the same, −670 mV vs Ag/AgCl. The pitting potential for pH 3 was −700 mV vs Ag/AgCl. In the passive part, pH 8,2 tended to have the lowest and most stable current density.

AA6082 after 24 hours of exposure

The complete polarization curves recorded for AA6082 after 24 hours of exposure in SSW with the different pH values are shown in Figure 54. From Figure 54 one can see that there was a significant difference in the OCP for pH 10 and the OCP for pH 3 and pH 8,2. The OCP for pH 10 was −1180 mV vs Ag/AgCl and the OCP for pH 3 and pH 8,2 was −710 mV vs Ag/AgCl.

The curve for pH 3 had clearly the largest current density and the curve for pH 10 has clearly the lowest current density. At −1600 mV vs Ag/AgCl the difference is above one magnitude. In the passive part of the curves, the difference between pH 3 and pH 10 is approximately two magnitudes.

The pitting potential for pH 8,2 was the highest, −660 mV vs Ag/AgCl. The pitting potential for pH 3 was −700 mV vs Ag/AgCl. The curve for pH 10 did not reach the pitting potential; this is due to the low OCP.

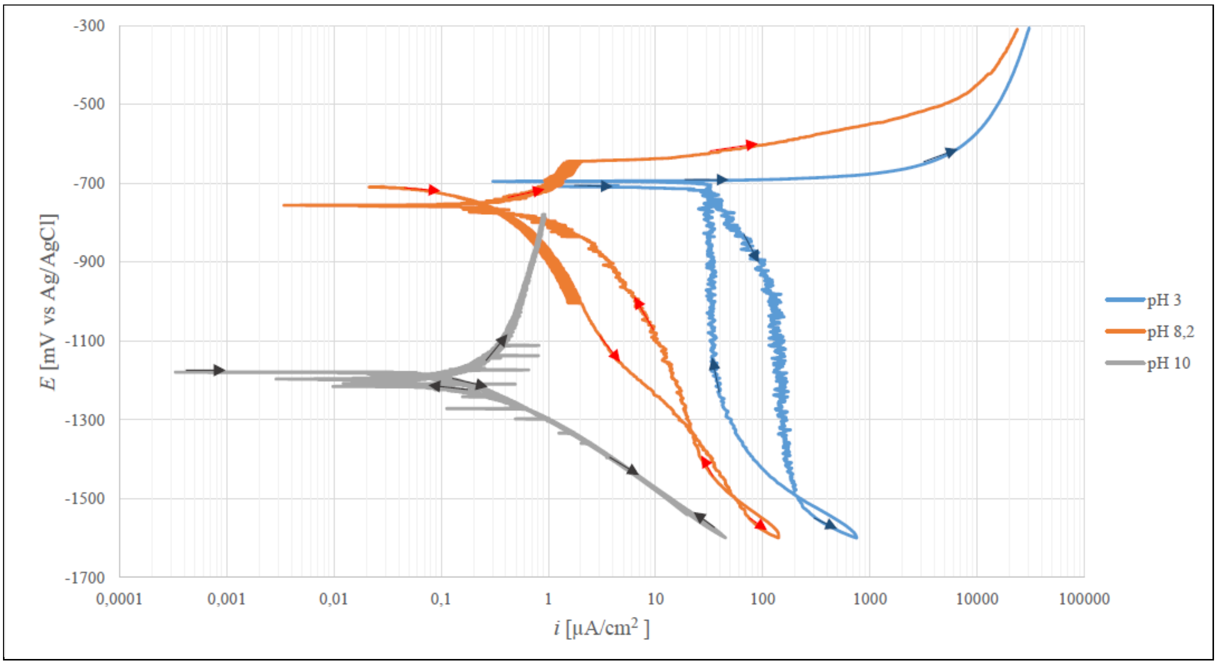

Figure 54: Complete polarization curves recorded for AA6082 after 24 hours exposure in SSW at room temperature.

AA6082 after 168 hours of exposure

The complete polarization curves recorded for AA6082 after 24 hours of exposure in SSW with the different pH values are shown in Figure 55. It can be seen from Figure 55 that the OCP for pH 3, 8,2 and 10 were as following; −725, −855 and −1290 mV vs Ag/AgCl. The curve for pH 3 had clearly the largest current density. The curve for pH 8,2 had the lowest current density in the passive part of the curve, but the current density for pH 10 in the passive part tended to be more stable.

The pitting potential for pH 8,2 was −665 mV vs Ag/AgCl. The pitting potential for pH 3 was −690 mV vs Ag/AgCl. The curve for pH 10 does not reach the pitting potential.

Characteristic values from the polarization curves for AA5083 and AA6082 after one day (24 hours) of exposure and after one week (168 hours) of exposure are shown in Table 15 and Table 16.

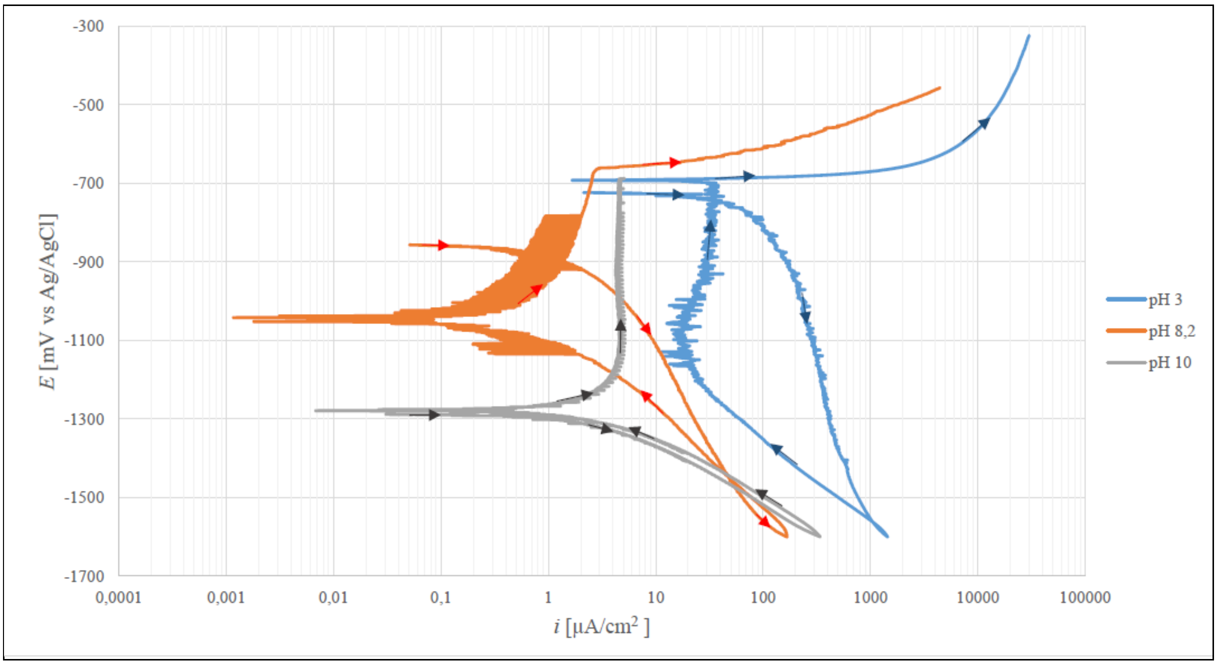

Figure 55: Complete polarization curves recorded for AA6082 after 168 hours exposure in SSW at room temperature.

Table 15: Characteristic values for AA5083 during anodic- and cathodic polarization after 1 day (24 hours) and 1 week (168 hours) of exposure.

	AA5083					
	pH 3		pH 8,2		pH 10	
	1 day	1 week	1 day	1 week	1 day	1 week
E_{OCP} [mV vs Ag/AgCl]	−723	−711	−722	−836	−1077	−1053
E_{pit} [mV vs Ag/AgCl]	−703	−706	−685	−655	−717	−640
$\Delta E_{\mathrm{pit\text{-}OCP}} = E_{\mathrm{pit}} - E_{\mathrm{OCP}}$ [mV]	20	5	37	181	360	413
i_{pass} [µA/cm^2]	3,0 – 5,0	3,0 – 10,0	0,5 – 2,0	3,0 – 7,0	0,7 – 1,7	6,8 – 13,2

Table 16: Characteristic values for AA6082 during anodic- and cathodic polarization after 1 day (24 hours) and 1 week (168 hours) of exposure.

	AA6082					
	pH 3		pH 8,2		pH 10	
	1 day	1 week	1 day	1 week	1 day	1 week
E_{OCP} [mV vs Ag/AgCl]	−706	−724	−709	−857	−1179	−1288
E_{pit} [mV vs Ag/AgCl]	−697	−696	−668	−663	-	-
$\Delta E_{\mathrm{pit\text{-}OCP}} = E_{\mathrm{pit}} - E_{\mathrm{OCP}}$ [mV]	9	28	41	194	-	-
i_{pass} [µA/cm^2]	30,0 – 60,0	14,0 – 40,0	0,5 – 2,0	0,5 – 3,0	0,2 – 1,0	3,0 – 5,0

5.2.4 SEM images

The freely exposed samples were examined in SEM to determine the degree of pits with the different pH-values.

AA5083

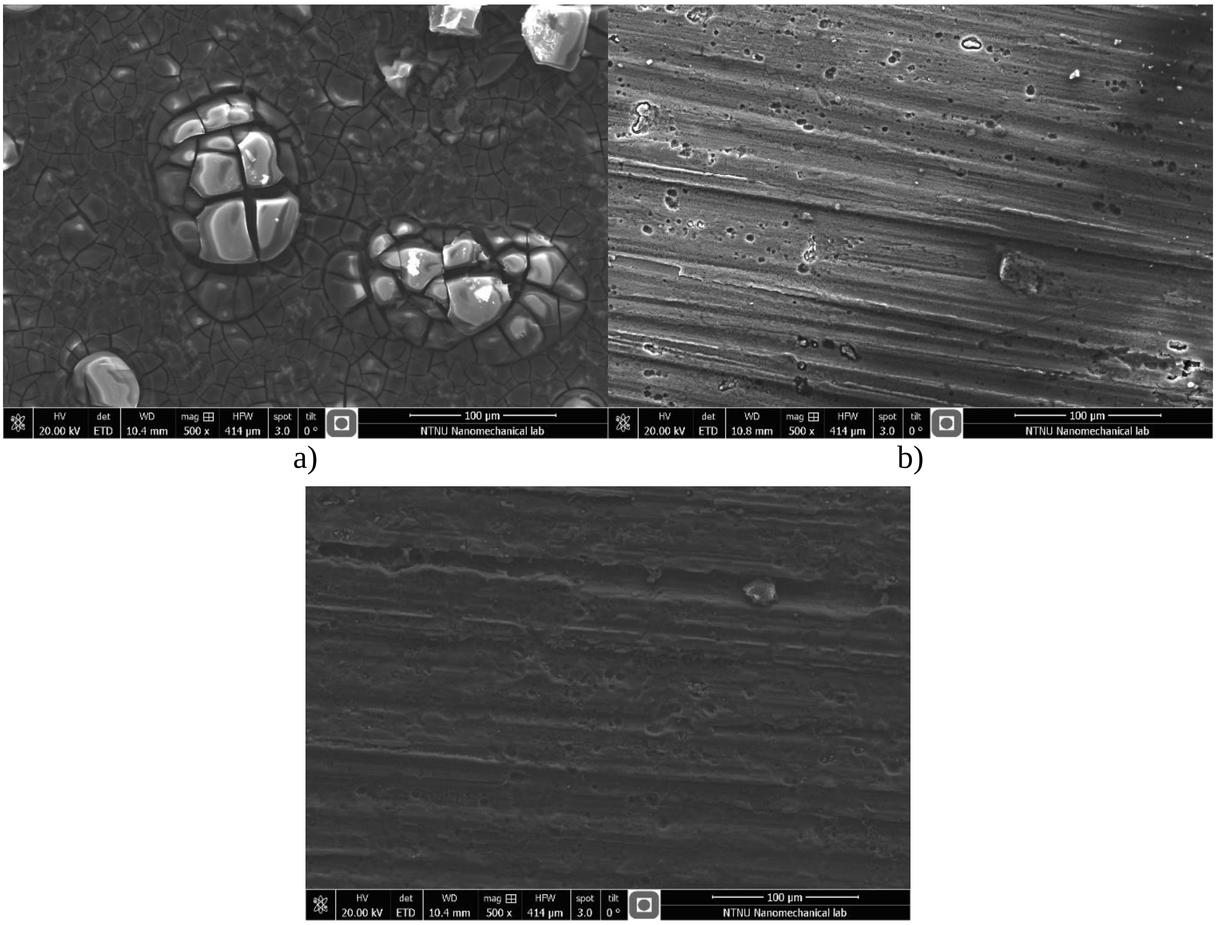
HV 20.00 kV det ETD WD 10.4 mm mag 500 x HFW 414 µm spot 3.0 tilt 0 °
100 µm
NTNU Nanomechanical lab
HV 20.00 kV det ETD WD 10.8 mm mag 500 x HFW 414 µm spot 3.0 tilt 0 °
100 µm
NTNU Nanomechanical lab
HV 20.00 kV det ETD WD 10.4 mm mag 500 x HFW 414 µm spot 3.0 tilt 0 °
100 µm
NTNU Nanomechanical lab

a) b)

c)

Figure 56: SEM images of AA5083 freely exposed in SSW with different pH-values, a) pH 3, b) pH 8,2 and c) pH 10.

Figure 56 shows SEM images of AA5083 freely exposed in SSW with different pH-values. As it can be seen in image a) the surface of the sample exposed at pH 3 had a layer of a deposit or corrosion products, and the pits could not be observed due to this. The etching in 65% HNO_3 did not remove this layer. In image b) some minor pits on the sample exposed at pH 8,2 can be seen. Image c) show the surface of the sample exposed at pH 10, and as it can be seen some pits were observed and the pits tended to be less severe than for the sample exposed at pH 8,2.

AA6082

Figure 57 shows SEM images of AA6082 freely exposed in SSW with different pH-values. Image a) shows the surface of the sample exposed at pH 3. AA6082 also had a layer on the surface, but pits could be observed. In image b) the surface of the sample exposed at pH 8,2 can be seen and only minor pits are observed. Image c) shows the sample exposed at pH 10, and pits can be observed. For AA6082 the severity of pits was bigger on the sample exposed at pH 10 than the sample exposed at pH 8,2.

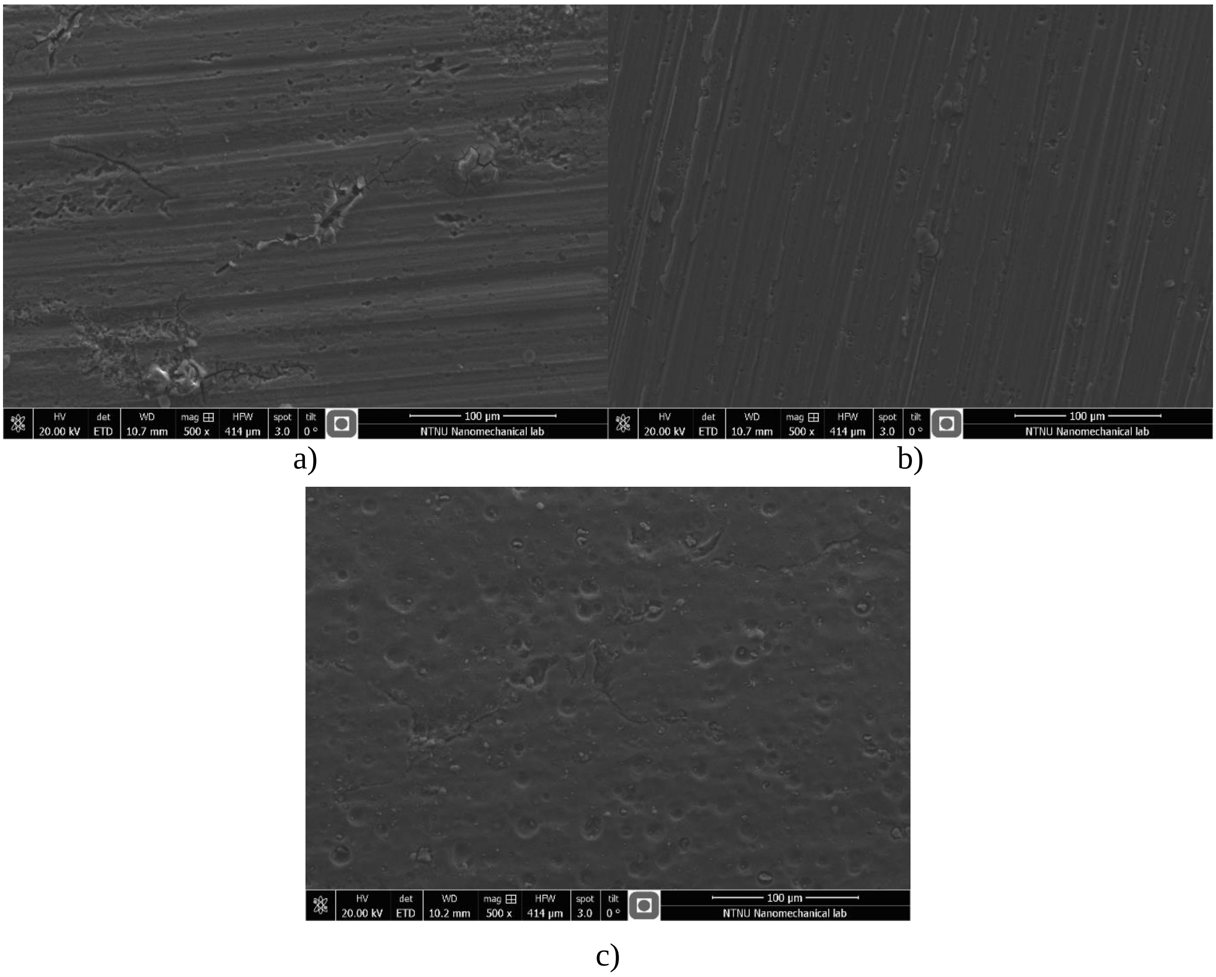
HV 20.00 kV
det ETD
WD 10.7 mm
mag 500 x
HFW 414 μm
spot 3.0
tilt 0 °
100 μm
NTNU Nanomechanical lab
HV 20.00 kV
det ETD
WD 10.7 mm
mag 500 x
HFW 414 μm
spot 3.0
tilt 0 °
100 μm
NTNU Nanomechanical lab
HV 20.00 kV
det ETD
WD 10.2 mm
mag 500 x
HFW 414 μm
spot 3.0
tilt 0 °
100 μm
NTNU Nanomechanical lab

a) b)

c)

Figure 57: SEM images of AA6082 freely exposed in SSW with different pH-values, a) pH 3, b) pH 8,2 and c) pH 10.

6 Discussion

6.1 Effect of temperature

6.1.1 OCP and pitting potential

The temperature has an effect on the OCP for the freely exposed samples, this can be seen in Figure 21 for both alloys. The tendency was that OCP for the samples exposed at 32 ^{o}C was more negative than OCP for the samples exposed at 10 ^{o}C. The literature provides little information about the temperature dependency of OCP for aluminium alloys, but it is reasonable to think that the behavior of the OCP is related to the behavior of the critical pitting potential with varying temperature. The OCP for the samples in this study behaved in accordance to how Z. A. Foroulis and M. J. Thubrikar [26], and J. Soltis, et al. [27] explains that the critical pitting potential behave with varying temperature[3].

The results from the recorded polarization curves presented in Section 5.1.3, Table 8 and Table 9, indicate the same effect of temperature on OCP as discussed above. The pitting potentials after one week for AA5083 are reasonable and in accordance with theory [25, 26]. The pitting potential for the sample exposed at 10 ^{o}C was −585 mV vs Ag/AgCl, and for the sample at 32 ^{o}C it was −700 mV vs Ag/AgCl. After six weeks of exposure, the pitting potential for AA5083 exposed at 10 ^{o}C and 32 ^{o}C were −620 and −519 mV vs Ag/AgCl, respectively. This is not in accordance with theory, because the sample exposed at the highest temperature is supposed to have the most negative pitting potential [26, 27]. The results show that the pitting potential for AA6082 behaved in accordance with theory, see Table 9.

$$\Delta E_{\text{pit-OCP}} = E_{\text{pit}} - E_{\text{OCP}} \tag{6.1}$$

The difference between OCP and pitting potential, Equation 6.1, is an interesting and important value considering resistance against pitting corrosion. The bigger this difference is the better. The characteristic values in Table 8 and Table 9 show this difference after one week and six weeks of exposure. For AA5083 after one week of exposure this difference was 127 mV for the sample at 10 ^{o}C and 222 mV for the sample at 32 ^{o}C. After six weeks of exposure, this difference was 200 mV at 10 ^{o}C and 400 mV at 32 ^{o}C. These results implies that the corrosion resistance was better for the sample exposed at 32 ^{o}C. This is somewhat conflicting with the surface examinations, discussed in Section 6.1.3, of these samples. Because more pits were observed on the sample exposed at 32 ^{o}C than on the sample exposed at 10 ^{o}C.

---

[3] When comparing the results of this study to other studies and theory, all electrochemical potential values are converted to the actual reference used, such that the basis for comparison is correct.

For AA6082 after one week the difference was 250 mV at 10 °C and 240 mV at 32 °C, and after six weeks, the difference was 300 mV at 10 °C and 200 mV at 32 °C. These results implies that the sample exposed at 10 °C exhibited the best resistance to corrosion, and this is more in accordance with the observations from the surface examinations, which shows more pits for the sample at 32 °C. As mentioned in Section 4.4.1 the complete polarization curves for AA6082 were recorded on samples that had only been freely exposed for six weeks, and not experienced the previous anodic- and cathodic polarizations. This was not the case for AA5083, the samples used for recording these complete polarization curves had experienced all the previous anodic- and cathodic polarizations. The previous polarizations may have made the AA5083 samples defect, and not representative, this may have affected the results. The ideal way to record potentiodynamic polarization curves is to have a new sample for every polarization. This could not be done in this study due to lack of test material. For further studies it is recommended to record the polarization curves on new samples for every polarization, this will provide more reliable and correct results.

6.1.2 Current density

The current density for the polarized samples can be seen in Figure 22, Figure 23 and Figure 24. As explained in Section 2.3 the cathodic current demand for aluminium is mainly restricted to the cathodic intermetallic sites, but when calculating/plotting the current density it was assumed that the current is supplied to the complete exposed aluminium surface area.

The temperature clearly had the biggest effect on the current density for the samples anodic polarized to −700 mV vs Ag/AgCl, and especially for the AA5083 samples. This can be seen in Figure 22. For the AA5083 samples there was a slightly difference in anodic current for 10 °C and 32 °C from the very beginning of the exposure, and the difference increased with increased exposure time. For the AA6082 samples, there was no significant difference in anodic current for 10 °C and 32 °C for the first 550 hours of exposure. After 550 hours of exposure, the anodic current for the sample exposed at 32 °C started to increase, and the anodic current tended to increase with increasing exposure time.

The significant effect of temperature on the anodic current for the samples polarized to −700 mV vs Ag/AgCl may be due to the following explanation. These samples were polarized to approximately the same potential as the critical pitting potential for aluminium in seawater which is about −0,75 V_{SCE} (−706 mV vs Ag/AgCl) [12]. The pitting potentials presented in Section 5.1.3 were generally in a range slightly more positive than −700 mV vs Ag/AgCl, but as these pitting potentials varied somewhat the samples may have been polarized more positive than the pitting potential for periods. As earlier discussed, the critical pitting potential of samples exposed at 32 °C should be more negative than for 10 °C. Thus, corrosion was more easily initiated on the samples exposed at 32 °C, and as the rate of corrosion increased, the anodic current increased. It should be mentioned that the corrosion on these samples to a large extent was crevice corrosion in crevices formed beneath the coating, this is discussed more in detail in Section 6.2. Due to the acidic environment, crevice corrosion is usually initiated at potentials more negative than the pitting potential. Thus, it can be concluded that the samples were polarized above the potential for crevice corrosion to initiate, and crevice corrosion was the main contributing factor for the increased anodic current.

In Figure 23 the current densities for the samples coupled to a sacrificial anode are shown. It can be seen that the current densities for the samples exposed at 32 ^{o}C decreased faster and were lower than for the samples exposed at 10 ^{o}C. As explained in Section 2.3, the cathodic current is mainly restricted to the cathodic intermetallic sites. As it can be seen from the results presented in Section 5.1.4 more pits and intermetallic particles were observed for the samples exposed at 32 ^{o}C. According to theory [34] is detachment and isolation of such cathodic intermetallic particles, Figure 12, the main factor for reducing the current demand, and thus the current density decreased fastest and was lowest for the samples exposed at 32 ^{o}C. The samples exposed at 10 ^{o}C had more positive OCP than the samples exposed at 32 ^{o}C. This implies that the change in potential, between OCP and the potential from the anode, is larger for the samples exposed at 10 ^{o}C than for the samples at 32 ^{o}C. This may also be a contributing factor for why the samples exposed at 32 ^{o}C had the lowest current density. The potentials from the sacrificial anodes in this study can be found in Appendix C.

In Figure 24 the current densities for the samples cathodic polarized to −1500 mV vs Ag/AgCl are shown. Remember that the samples exposed at 32 ^{o}C were polarized to −1580 mV vs Ag/AgCl. The AA6082 sample exposed at 10 ^{o}C is not representative, and will not be discussed. Due to lack of test-material, there was no redundancy for this sample at this condition. For the other samples it can be observed that for the cathodic current densities (after 800 hours) the AA6082 sample exposed at 32 ^{o}C had the lowest, −6 μA/cm^{2}. While for the AA5083 samples one can see that the samples exposed at 10 ^{o}C had lower current densities, −9,9 and −10,7 μA/cm^{2}, than the samples exposed at 32 ^{o}C, −13,3 and −16,3 μA/cm^{2}. The course of events for these samples were as following. The rate of the cathodic reaction was high due to the negative potential, this caused the high cathodic current density in the beginning. The cathodic intermetallic particles were detached and isolated from the aluminium matrix at a high rate, and hence the cathodic current density decreased rapidly. The exposed surface was covered with a layer of corrosion products, and the cathodic current density was kept at a low level. The samples exposed at 32 ^{o}C were polarized to a more negative potential than the samples at 10 ^{o}C, and this is probably why the current density was slightly larger for these samples.

6.1.3 Surface examinations

The results from the surface examinations presented in Section 5.1.4 clearly indicate that the temperature had an effect on the corrosion behavior. For the exposed samples, both AA5083 and AA6082, it was common that more severe corrosion was found on the samples exposed at 32 °C.

For the freely exposed samples, one can see from the SEM images that the number of pits were significantly higher and the pits were bigger for the samples exposed at 32 °C compared to the samples exposed at 10 °C. The same can be observed on the samples coupled to the sacrificial anode. It should be mentioned that the observed corrosion on these samples is of microscopic scale, and is not referred to as corrosion attacks.

For the samples anodic polarized to −700 mV vs Ag/AgCl it can be seen from Figure 60 and Figure 64 in Appendix B that more white deposit as a result of the corrosion process is escaping from under the coating on the samples exposed at 32 °C compared to the samples exposed at 10 °C. The crevice corrosion beneath the coating is discussed more in detail in Section 6.2.

For the samples cathodic polarized to −1500 mV vs Ag/AgCl, −1580 mV vs Ag/AgCl for the samples exposed at 32 °C, a thick layer of corrosion products was observed on the samples exposed at 32 °C. This can be seen both in Figure 43, and in Figure 66 in Appendix B. Corrosion was also observed on the AA5083 sample exposed at 10 °C, this can be seen in Figure 62 in Appendix B, but the severity was not of the same degree as for the samples exposed at 32 °C.

The explanation is the same as discussed earlier, at least for the samples polarized to −700 mV vs Ag/AgCl, increased temperature lower the critical pitting potential and the potential for crevice corrosion to initiate, and thus corrosion is more easily initiated on the samples exposed at the highest temperature. By use of the potentiodynamic polarization curves a reasonable explanation for the samples coupled to a sacrificial anode can be given. Considering the complete polarization curves for AA6082 in Figure 27 and Figure 28, a plot can be seen in Figure 69 in Appendix D, it can be seen that at a potential of −1050 mV vs Ag/AgCl the cathodic current density was larger for 32 °C than for 10 °C. This implies that there were more cathodic activity (corrosion activity), Figure 12, on the samples exposed at 32 °C and, thus more pits were observed on these samples. This confirms the discussion in Section 6.1.2 regarding why the cathodic current density for the samples exposed at 32 °C decreases faster and are lower than for the samples at 10 °C. The rate of the sequence in Figure 12 increases with increased temperature.

The samples polarized to −1500 mV vs Ag/AgCl were clearly in the pitting corrosion region of the diagram in Figure 3. By increasing the temperature, in addition to the fact that the samples exposed at 32 °C experienced at potential of −1580 mV vs Ag/AgCl, make it reasonable to suggest that these samples may alternated between the pitting corrosion region and the general attack region. Thus, such severe corrosion as observed on these samples will occur.

6.2 Effect of electrochemical potential

Based on the experimental potential – pH diagram, Figure 3, it was expected that the freely exposed samples would exhibit good corrosion resistance when exposed in SEALAB. Even though this diagram is originally based on data for AA5086, it was thought that it might be a good guideline for AA5083 and AA6082 also. From the results presented in Section 5.1.4 it can be seen that freely exposed samples did not suffer from corrosion. The observed corrosion is only of microscopic scale, the pits found on the cross-section faces, Figure 34, had depths of 5 and 15 µm. As it can be seen from the results the corrosion for AA5083 was mainly concentrated to areas around Al(Mg,Mn,Fe,Cr) precipitates, according to theory this is also as expected [12, 43, 44]. For AA6082 the intermetallics found in the pits also contained Si. The observed pits was of a hemispherical art, this is in accordance with what A. Aballe, et al. [43] and H. Ezuber, et al. [45] observed through similar experimental work.

The samples coupled to a sacrificial anode, with a potential of approximately −1050 mV vs Ag/AgCl, did not suffer from corrosion. The observed corrosion is only of microscopic scale; no pits were observed on the cross-section for the AA5083 sample exposed at 10 ^{o}C, for AA6082 at 10 ^{o}C a pit with depth 4,3 µm was observed. The samples exposed at 32 ^{o}C had pits with depths 28,3 and 34,8 µm. On the AA5083 samples, only minor pits were observed around the intermetallics, in the same way as discussed above. For the AA6082 samples, the severity of the corrosion tended to be of a larger degree than for the freely exposed samples. This can be seen by comparing Figure 40 to Figure 32 and Figure 33. This may be because the lowered potential from the anode increased the rate of the cathodic reaction such that the protective oxide was slightly destabilized, and hence more pits were observed on the AA6082 sample coupled to the sacrificial anode. Based on the results it is clearly that when AA5083 and AA6082 are exposed to seawater, without metallic contact to more noble metals, the corrosion resistance is good both when freely exposed and with CP.

The corrosion on the samples anodic polarized to −700 mV vs Ag/AgCl was in a large extent concentrated to the edges beneath the coating, in the form of crevice corrosion. Figure 37 shows how the coating formed crevices. According to the theory [22] an acid environment develops in the crevice. The low pH inside the crevice results in an aggressive environment. When polarizing the samples to −700 mV vs Ag/AgCl by the use of a potentiostat, one is simulating the samples being coupled to a big cathode, e.g. galvanic coupling with steel, thus the samples acts as anodes. The corrosion is initiated by the more positive potential caused by the coupling to the “big cathode” and will then start in weak spots on the samples, often in weak spots in the oxide layer. For this case, the weakest spots were the crevices, with its acidic environment, beneath the coating, thus the corrosion was favored to occur there. Corrosion on the exposed surface was also observed, in weak spots in the oxide and around the intermetallics, but in a less degree than expected. For the AA6082 samples more corrosion was observed on the exposed surface, and the degree of crevice corrosion was not as severe as for the AA5083 samples. This may be related to the higher content of Si, according to theory [30], Si particles are resistant to both most acids and salts, hence the presence of Si may reduce the AA6082 samples susceptibility to corrosion in the acid environment in the crevices beneath the coating. Si containing particles will be cathodic to the aluminium matrix, and thus contribute to initiate corrosion around the intermetallics. This may be some of the reason for observing more pits on the AA6082 samples than on the AA5083 samples.

The study performed by A. Aballe, et al. [43] showed that for the formation of crystallographic pitting to be produced, it is necessary to polarize the alloy above the critical pitting potential. The results from this study agrees with that, severe crystallographic pitting was observed on the AA6082 sample exposed at 32 °C, Figure 38. Crystallographic pitting was not observed on the other samples anodic polarized to −700 mV vs Ag/AgCl, but this is in accordance with the results obtained from the potentiodynamic polarization curves. According to these result, the pitting potential of the other samples was more positive and has not been reached, thus crystallographic pitting was not observed. The results has clearly been affected by the fact that the samples were coated. In that manner the results can be of practical use by indicating what will happen to coated aluminium coupled to steel submerged in seawater. New experiments with uncoated samples should be performed to avoid crevice corrosion on the test samples.

The samples cathodic polarized to −1500 mV vs Ag/AgCl experienced severe corrosion attacks. As discussed in Section 6.1 the samples exposed at 32 °C experienced the most severe attack. Based on the experimental potential – pH diagram in Figure 3 a lot of corrosion was expected on these samples. As it can be seen from the diagram these samples have been in the pitting corrosion region, and as discussed earlier, the samples exposed at 32 °C may have altered between pitting attacks and general attack because the potential for these samples was −1580 mV vs Ag/AgCl. Based on the images in Figure 66 in Appendix B the samples at 32 °C seems to have suffered from a general corrosion attack. The thickness of the corrosion products layer was measured for the samples exposed at 32 °C, Figure 43, and for AA5083 it was found to be above 1 mm, while for AA6082 it was measured to be about 410 µm. For AA5083 the corrosion products consisted of the main elements Al and Mg, in addition to O. Elements from the seawater, like Cl and Na, were also present. For AA6082 the corrosion products consisted of the main elements Al, Mg and Si, in addition to O. Elements from the seawater were also present. No indication of calcareous deposits, $CaCO_3$ or $Mg(OH)_2$, was found.

Based on theory about corrosion of aluminium [12, 17, 22, 50] the explanation for the samples cathodic polarized to −1500 mV vs Ag/AgCl is as following. The low potential increases the rate of the cathodic reaction and the high rate of the cathodic reaction leaves the metal surface alkaline due to the production of OH^-. Hence, the protective oxide, which is amphoteric, is destabilized. The destabilized oxide leads to higher corrosion rate, often called cathodic pitting. For this study, the potential of −1580 mV vs Ag/AgCl for the samples exposed at 32 °C tended to increase the rate of the cathodic reaction so much that the bulk of the oxide was destabilized, causing a general corrosion attack. It should be mentioned that the general attack also included corrosion beneath the coating. The potential of −1500 mV vs Ag/AgCl for the AA5083 sample exposed at 10 °C tended to cause a severe pitting corrosion attack, but as this corrosion was in form of pitting, a pronounced layer of corrosion products was not found of this sample.

6.3 Effect of pH

The results presented in Section 5.2 indicates that the pH clearly affects the corrosion behavior of AA5083 and AA6082. The results obtained for the experiment in SSW with pH 8,2 as electrolyte should be used as basis for comparison, because this can be seen as standardized conditions [49].

6.3.1 OCP and pitting potential

The experiments performed in SSW indicated that the pH clearly has an effect on the OCP. When the pH was lowered from 8,2 to 3, the OCP for AA5083 and AA6082 was increased by approximately 140 to 180 mV. Figure 44 shows the development in OCP at pH 3, and one can see that the OCP had a fluctuating behavior, but it was concentrated around −700 mV vs Ag/AgCl. The explanation for this behavior is given by use of the experimental potential – pH diagram in Figure 3[4]. When the AA5083 and AA6082 samples (freely exposed) are submerged in SSW with pH 3 the protective oxide becomes destabilized [12], thus the OCP will be in the imperfect passivity region and may alternate to the pitting region of the diagram. Due to the low pH, the samples cannot manage to build a sufficient oxide, such that passivity is secured. The samples will try to build a sufficient protective oxide that will break down by the low pH, therefore, the OCP for these samples will show a fluctuating behavior in the imperfect passivity region. It is worth mentioning that from Figure 75 in Appendix G one can see that the OCP for the samples exposed in SSW with pH 8,2 also started in the imperfect passivity region of the diagram in Figure 3. However, due to the different pH, these samples managed to build a sufficient protective oxide and the OCP was lowered into the passive region.

When the pH was increased to 10 the OCP was lowered, this can be seen in Figure 45. The OCP for AA6082 was more negative than for AA5083. The samples were in the pitting corrosion region of the diagram in Figure 3. It can be seen, Figure 45, that the development of OCP followed the development of pH. Because, after 50 hours of exposure the pH was significantly adjusted (increased from about 9,55 to 10,84) and at the same time the OCP dropped significantly. From 80 to 125 hours exposure the pH decreased gradually, while the OCP increased gradually until the pH was adjusted again. According to theory [12, 17] the alloying elements Mg and Mn have oxides which becomes increasingly passive with increased pH, and this is some of the reason for that aluminium can be passive in the slightly alkaline seawater environment with pH 8,2. In this study the passivating effect of these alloying elements tended to fade with increasing pH, even if the alloying elements itself becomes more passive. From Table 7 it can be seen that AA5083 and AA6082 contains approximately the same amount of Mn, but AA5083 contains much more Mg than AA6082. This may be the reason for why the OCP for AA6082 became more negative than the OCP for AA5083 in SSW with pH 10.

---

[4] The lowest pH-value in the diagram in Figure 3 is used in the discussion of AA5083 and AA6082 at pH 3, and the highest pH-value in the diagram is used in the discussion of AA5083 and AA6082 at pH 10.

The results from the recorded polarization curves presented in Section 5.2.3 indicate the same effect of pH on OCP as discussed above. The pitting potential, Table 15 and Table 16, was slightly lowered when the pH decreased from 8,2 to 3. At pH 10 the behavior of the pitting potential was more unpredictable. The difference between OCP and pitting potential ($\Delta E_{\text{pit-OCP}}$), Equation 6.1, is interesting. The samples exposed at pH 3 had the lowest $\Delta E_{\text{pit-OCP}}$, this was as expected and in accordance to theory [12, 17, 50]. Because low $\Delta E_{\text{pit-OCP}}$ implies a larger extent of corrosion, which is also expected when the pH is decreased to 3. The SEM images, Figure 56 and Figure 57, confirms the low $\Delta E_{\text{pit-OCP}}$.

For the samples exposed at pH 10 the $\Delta E_{\text{pit-OCP}}$ was large. For AA5083 it was 360 mV after 24 hours and 413 mV after 168 hours. For AA6082 no pitting potentials were observed during recording of potentiodynamic polarization curves, Figure 54 and Figure 55. Considering the procedure for recording of these curves, explained in Section 4.4.2, this implies that $\Delta E_{\text{pit-OCP}}$ was larger than 400 mV for AA6082. The big difference in OCP and pitting potential means that these samples experienced good corrosion resistance during exposure. The SEM images presented in Section 5.2.4 also indicates a low degree of pitting corrosion on the samples exposed at pH 10. The results are conflicting the theory; according to Figure 3 should a severe pitting attack occur on the samples, and relevant theory [12] explains that the protective oxide will be broken down in alkaline environments (pH 10).

6.3.2 Current density

As earlier mentioned, the pH was not monitored and adjusted during nighttime, thus for pH 3 some significant changes (often from 3,35 to 2,80) in pH occurred due to adjustment every morning. From the current density plots presented in Section 5.2.2 it can be seen that the current densities were very sensitive for changes in pH when the pH was in the low range of 2,7 to 3,4. The current densities for the samples anodic polarized to −700 mV vs Ag/AgCl in Figure 46 indicate that AA6082 did not experience the same sensitivity for sudden changes in pH. As discussed in Section 6.2 when polarizing to −700 mV vs Ag/AgCl one is simulating a galvanic coupling to steel (cathode), and the corrosion is initiated by this cathode connection and will start in the weakest spots on the samples. The corrosion for these samples was mainly in forms of crevice corrosion, this goes also for the samples exposed in the Corrosion Laboratory. The proposed explanation is therefore that the larger content of Si in AA6082 makes this alloy less sensitive to low pH. This is in accordance to Mondolfo [30] that documented that Si is resistant to most acids and salts.

For the samples polarized in cathodic direction, coupled to sacrificial anode and −1500 mV vs Ag/AgCl, both AA5083 and AA6082 were sensitive to sudden changes in pH. For these samples, the corrosion process is mainly restricted to the intermetallic sites, and one thought is that Si may become inferior in these precipitates. Such that the positive effect against low pH for AA6082 fades, and AA6082 becomes sensitive to these changes such as AA5083. It should also be mentioned that Si is cathodic to aluminium, and will then act as a site for the cathodic reaction.

The current density for the samples exposed in SSW with pH 10 did not show the same sensitivity as for pH 3. An interesting thing regarding the current density for the samples exposed at pH 10 can be seen in Figure 49. The current density for the samples coupled to the sacrificial anode alternated between anodic- and cathodic current. The simple explanation for this is that the OCP varies, and will sometimes be more positive and sometimes more negative than the potential of the sacrificial anode. From the low current, one can also see that the OCP and the anode had potential values close to each other for this pH.

6.3.3 Surface examination

The results presented in Section 5.2.4 indicate that the different pH-values affected the corrosion behavior of AA5083 and AA6082. For AA5083 exposed in SSW with pH 3, Figure 56, a layer was observed on the surface. This layer is most likely corrosion products because of high corrosion rate. For AA6082 exposed at pH 3, Figure 57, big pits were observed. These results are as expected, and in accordance with theory [12, 17].

From Figure 56 it can be seen that more pits were observed for AA5083 exposed at pH 8,2 than for AA5083 at pH 10. According to theory [12, 17] more corrosion should be expected on the sample exposed at pH 10 because of the amphoteric behavior of the protective aluminium oxide. One thought is therefore that the sample exposed at pH 10 may suffered from a general corrosion attack, thus fewer pits were observed for this sample. This is an imperfect explanation, and similar experimental work where weight loss is included should be performed to confirm this.

From Figure 57 it can be seen that the observed pits on AA6082 were as expected and in accordance with theory. More severe pits were observed on the sample exposed at pH 10, than on the sample exposed at pH 8,2.

6.4 Effect of exposure time

The exposure time did not have a significant effect on the OCP development for the exposed samples rather than the fact that the OCP behavior stabilized with increased exposure time.

According to theory [12, 17, 34], will cathodic intermetallic particles detach from the aluminium matrix during exposure, which implies that the current density will be reduced. This was observed for the samples coupled to a sacrificial anode and the samples cathodic polarized to −1500 mV vs Ag/AgCl, Figure 23 and Figure 24. From Table 8 and Table 9 it can be seen from the passive current values that the AA6082 samples behaved in accordance with theory. The AA5083 sample exposed at 32 ^{o}C tended to behave as expected, but for the AA5083 sample exposed at 10 ^{o}C the passive current was increased rather than decreased. This was probably due to the harsh treatment. Based on the potentiodynamic polarization curves it can be concluded that AA5083 was more resistant to the harsh treatment than AA6082. The current density, Figure 22, for the samples anodic polarized to −700 mV vs Ag/AgCl increased with exposure time. This is, as discussed earlier, because of the localized crevice- and pitting corrosion.

The intuitive thought was that pitting potentials would increase with exposure time for freely exposed AA5083 and AA6082, because of the protective oxide and the reduced amount of cathodic intermetallics. This was not the case for neither AA5083 nor AA6082. For the characteristic values for AA6082 in Table 9, which is the most reliable because a new sample was used for recording the complete polarization curves, see Section 4.4.1, it can be seen that at 10 ^{o}C the pitting potential increased and at 32 ^{o}C it decreased. One thought is that the pitting potential is determined by the types of intermetallic particles enriched on the surface, and remaining in the surface of the aluminium matrix. The type of detached and remaining intermetallic particles may vary from sample to sample, thus the pitting potential may vary from sample to sample. However, this proposed explanation is imperfect and more experimental work should be performed regarding this topic. For further work on this topic it is recommended to increase the number of samples, such that one sample does not have to undergo several potentiodynamic polarizations.

It is also interesting to see how the exposure time affects the samples freely exposed in SSW with pH 3 and pH 10. Aluminium may experience pH 3 when exposed in soil, and pH 10 is likely to occur on the surface of cathodic polarized samples in seawater due to the cathodic reaction. In Appendix H the potentiodynamic polarization curves for pH 3 and pH 10 are plotted such that the effect of exposure time is emphasized. For pH 3, Figure 79 and Figure 80, it can be seen that there were no significant changes after 168 hours of exposure. The OCP and pitting potential were more or less the same. Some differences can be seen in the passive current, after 168 hours of exposure the samples showed a more fluctuating and unpredictable behavior regarding the passive current. AA5083 showed a more fluctuating behavior than AA6082, this may be due to the different content of Si, the effect of Si has been discussed earlier.

For pH 10, Figure 81 and Figure 82, the differences between 24 and 168 hours of exposure were more obvious. For AA5083, it can be seen that the pitting potential increased from −717 to −640 mV vs Ag/AgCl, and the passive current increased by almost one decade, from approximately 1,7 to 13,2 µA/cm^2. But, the alloy was passive in a wider potential range after 168 hours. There was no pronounced difference in OCP for AA5083. For AA6082 the OCP decreased from −1179 to −1288 mV vs Ag/AgCl, and the passive current increased significantly, but not as much as for AA5083. One can see that AA6082 also was passive in a wider potential range after 168 hours. Due to the negative OCP for AA6082 in SSW with pH 10 these samples did not reach the pitting potential during recording of complete potentiodynamic polarization curves. The development in the polarization curves over time for pH 3 and pH 10 implies that the rate of corrosion increased with increased exposure time.

6.5 Current density required for protection

As mentioned, the use of sacrificial anodes is a common way to achieve corrosion protection for structures in seawater. In Figure 23 the current density for the samples coupled to a sacrificial anode (approximately −1050 mV vs Ag/AgCl) in this study is shown. The current density for these samples, except for AA6082 at 10 °C, behaved in accordance to what R. Gundersen and K. Nisancioglu explains [34]. They had initial current density peaks, and then the current density decreased. The increase in current density in the beginning is due to corrosion around the Fe-rich intermetallic particles in the surface of the matrix. Once these intermetallic particles are detached and isolated from the matrix they are not cathodic to the matrix anymore and corrosion will not occur around them, i.e. the demand for current is reduced. The current density for carbon steel St 52 coupled to a sacrificial anode exposed in natural seawater in SEALAB is shown in Figure 68 in Appendix C.

According to DNV RP B-401 [51], the recommended initial[5] current densities relevant for this study are as following:

---

[5] The initial design current densities from DNV are used, because the exposure period is relative short and the initial values provides the best basis for comparison. For aluminium the initial, final and mean design current density values are the same. The initial design current density refers to the cathodic current density that is required to effect polarization of an initially bare metal surface, typically for structural steel surfaces with some rusting and/or mill scale. The design current densities are used to determine the number and size of anodes [51].

6.5 Current density required for protection

Aluminium in seawater:

$$i = 0,010\,\text{A/m}^2 = 1,00\,\mu\text{A/cm}^2;\ \text{for } T \leq 25\,°\text{C}$$

$$i = 0,0114\,\text{A/m}^2 = 1,14\,\mu\text{A/cm}^2;\ \text{for } T = 32\,°\text{C}$$

Bare metal (carbon steel) in seawater with depth 0 – 30 m:

$$i = 0,200\,\text{A/m}^2 = 20,0\,\mu\text{A/cm}^2;\ \text{for } T = 7-11°\text{C}$$

$$i = 0,150\,\text{A/m}^2 = 15,0\,\mu\text{A/cm}^2;\ \text{for } T \geq 20\,°\text{C}$$

The recommended current densities from DNV are in accordance with the theory from R. Gundersen and K. Nisancioglu stating that the current densities required for protection of steel is one to two orders of magnitude larger than for aluminium [34].

Results from this study, Table 17, after 800 hours of exposure, shows that the current density for carbon steel exposed at 10 °C was −34,8 µA/cm^2, while it for AA5083 and AA6082 were −1,8 µA/cm^2 and −2,3 µA/cm^2, respectively. For 32 °C the current density, after 800 hours, for carbon steel in this study was −6,9 µA/cm^2, while for it for AA5083 and AA6082 were −0,75 µA/cm^2 and −1,7 µA/cm^2, respectively. From Figure 68 in Appendix C one can see that the current density for carbon steel still decreases after 800 hours, and after 2000 hours of exposure the current densities for 10 °C and 32 °C were −12 µA/cm^2 and −3 µA/cm^2, respectively. The main reason for the reduced current demand for protection of steel is the formation of calcareous deposit [22, 52]. The results from this study indicates that the recommended current density values for aluminium from DNV might be a little low. For carbon steel, the recommended current density at 10 °C is a little low, at least compared to the result after 800 hours, while it for 32 °C tends to be suitable. Compared to the results for carbon steel after 2000 hours of exposure one can see that the recommended current density for both temperatures are suitable. Based on Figure 23 it is reasonable to assume that the current density for AA5083 and AA6082 would have decreased more if the samples were exposed for another 1000 hours, such as the case for carbon steel. In that case, the recommended current density values from DNV will be more suitable.

Table 17: Current density values, *i* [µA/cm^2], for the samples coupled to a sacrificial anode in natural seawater.

	10 °C			32 °C		
Exposure time [hours]	AA5083	AA6082	CS	AA5083	AA6082	CS
800	−1,8	−2,3	−34,8	−0,75	−1,7	−6,9
2000	-	-	−12	-	-	−3

6.6 AA5083 vs AA6082

In general, AA5083 and AA6082 tended to show rather similar corrosion behavior with the different conditions, but some differences were also observed. The recording of OCP during exposure in SEALAB showed that AA6082 had a more negative OCP than AA5083. This was not as expected, because AA5083 contains a significantly larger amount of Mg and as it can be seen in Table 6 intermetallics containing Mg have rather negative OCP. The overall effect of the temperature tended to be the same for both alloys.

For the samples anodic polarized to −700 mV vs Ag/AgCl it can be seen in the results that the AA6082 samples exhibited better resistance to the crevice corrosion that occurred on the samples at this condition. As earlier discussed, this may be because AA6082 contains more Si than AA5083. The two alloys experienced fairly the same current density behavior when coupled to a sacrificial anode in natural seawater at 32 ^{o}C. When coupled to a sacrificial anode at 10 ^{o}C the current density behavior was a little more different for the two alloys, the current demand for AA6082 was 1 µA/cm^2 larger than for AA5083. This is a reasonable difference, because of the larger amount of Mg in AA5083. Selective dissolution of Mg protects the Al remaining at surface sacrificially against pitting [17], thus the lower current demand. For the samples cathodic polarized to −1500 mV vs Ag/AgCl both AA5083 and AA6082 suffered from severe corrosion. This was as expected according to theory [12], because the rate of the cathodic reaction was so high that the pH increased and destabilized the protective oxide.

From the potentiodynamic polarization curves recorded for the samples exposed in SEALAB, it can be seen that AA5083 had a more pronounced tendency than AA6082. The curves, especially the anodic curves, were moved to the left with increased exposure time and the pitting potential tended to increase with increased exposure time. This implies that the current density is reduced and that the cathodic intermetallics are detached and isolated from the aluminium matrix. For AA6082 this tendency was not so pronounced. However, by considering the curve for week 1 and the complete polarization curve at the end it can be seen that this tendency was almost the case for AA6082 also. It may be concluded that for the freely exposed samples, AA5083 became more passivated during exposure than AA6082.

From the surface examinations it could be seen that the pitting corrosion for AA5083 was mainly concentrated to areas around Al(Mg,Mn,Fe,Cr) precipitates. For AA6082 the intermetallics found in the pits also contained Si. Based on the theory explained in Section 2.2.1 and 2.2.6 this was as expected. For the freely exposed samples, the severity of the microscopic pitting tended to be the same for both alloys. For the cathodic polarized samples, the pits were more severe on the AA6082 samples than on the AA5083 samples. This was as expected, because according to basic theory about aluminium [3] the Al-Mg (5xxx) series is known to be the alloys most suitable for applications in seawater. However, for the samples cathodic polarized to −1500 mV vs Ag/AgCl at 32 °C the corrosion products layer was thicker for AA5083 than for AA6082.

As discussed earlier, AA6082 tended to be less affected by the variations in pH due to the presence of Si. By considering the recorded potentiodynamic polarization curves for the samples exposed in SSW with different pH-values the tendency was the opposite. Significantly larger differences in the potentiodynamic polarization curves with varying pH were observed for AA6082 than for AA5083. This implies that AA6082 is more sensitive to the varying pH than AA5083.

7 Conclusion

This master's thesis emphasized on studying the corrosion behavior for the aluminium alloys AA5083 and AA6082. The following conclusions can be drawn from the experimental work:

Temperature

- Increased temperature increases the severity and rate of corrosion.
- The open circuit potential (OCP) of AA5083 and AA6082 in natural seawater decreases to more negative values when the temperature is increased.
- Results from this study showed that increased temperature increases the difference between pitting potential and OCP, $\Delta E_{\text{pit-OCP}}$, for AA5083 and decreases $\Delta E_{\text{pit-OCP}}$ for AA6082. For AA5083 exposed for 1000 hours at 10 ^{o}C $\Delta E_{\text{pit-OCP}}$ = 200 mV, and at 32 ^{o}C $\Delta E_{\text{pit-OCP}}$ = 400 mV. For AA6082 exposed for 1000 hours at 10 ^{o}C $\Delta E_{\text{pit-OCP}}$ = 300 mV, and at 32 ^{o}C $\Delta E_{\text{pit-OCP}}$ = 200 mV.

Electrochemical potential

- AA5083 and AA6082 exhibits good resistance to corrosion when freely exposed in seawater, both at 10 and 32 ^{o}C.
- The results showed that AA5083 and AA6082 do not suffer from corrosion when coupled to sacrificial anodes, neither at 10 nor 32 ^{o}C.
- Anodic polarization to −700 mV vs Ag/AgCl (simulating galvanic coupling to steel) causes severe corrosion on AA5083 and AA6082. The corrosion starts in the weakest spots on the samples. Crystallographic pitting was observed on AA6082 exposed at 32 ^{o}C
- Cathodic polarization to −1500 mV vs Ag/AgCl causes severe cathodic corrosion attacks on AA5083 and AA6082. For AA5083 exposed at 32 ^{o}C the thickness of the corrosion products layer was above 1 mm, and the thickness of this layer for AA6082 exposed at 32 ^{o}C was 410 µm.
- For seawater conditions (pH 8,2) the potential – pH diagram in Figure 3 is a good guideline for AA5083 and AA6082.

pH

- The OCP for AA5083 and AA6082 increases to more positive values when the pH is lowered from 8,2 to 3.
- When the pH is increased from 8,2 to 10 the OCP for AA5083 and AA6082 decreases.
- Results from this study showed that when pH is lowered the difference between pitting potential and OCP, $\Delta E_{\text{pit-OCP}}$, for AA5083 and AA6082 decreases, and when pH is increased $\Delta E_{\text{pit-OCP}}$ for AA5083 and AA6082 increases.

- The left part of the potential – pH diagram in Figure 3 can be used as a rough guideline for AA5083 and AA6082 at pH 3. Based on the results the diagram is not valid for AA5083 and AA6082 at pH 10.

Current density for protection

- After 800 hours of exposure the required cathodic current density for cathodic protection (CP) in nearly stagnant natural seawater at 10 ^{o}C for AA5083 and AA6082 were −1,8 and −2,3 µA/cm^2, respectively.
- Required cathodic current density for CP in nearly stagnant natural seawater at 32 ^{o}C for AA5083 and AA6082 were −0,75 and −1,7 µA/cm^2, respectively.
- Calcareous deposit was not observed on AA5083 and AA6082 coupled to a sacrificial anode.

AA5083 vs AA6082

- The OCP in natural seawater for AA5083 is more positive than for AA6082, both at 10 and 32 ^{o}C.
- The overall effect of temperature and electrochemical potential is more or less the same for both AA5083 and AA6082.
- Results from this study showed that AA6082 is less sensitive to low pH than AA5083.
- Surface examinations showed that corrosion of AA5083 often occurs around Al(Mg,Mn,Fe,Cr) precipitates. For AA6082 the corrosion often occurs around Al(Mg,Mn,Fe,Cr,Si) precipitates.

8 Suggestions for further work

For further experimental work on this topic it is recommended to use uncoated samples. The formation of such crevices that were formed on some of the samples in this study, Figure 37, will not be possible on uncoated samples. Furthermore, it is strongly suggested to include more samples for recording potentiodynamic polarization curves, and each sample should only experience one recording. This will provide more correct and reliable results.

Suggestions for further work include:

- The same study should be performed on welded samples to examine the effect of welding.
- Study the corrosion behavior of AA5083 and AA6082 with temperatures above 40 ^{o}C.
- Perform experiments with increased exposure period.
- It would also be interesting to perform experimental work emphasized on studying crevice corrosion when AA5083 and AA6082 are galvanic coupled to a more noble metal in seawater.

References

[1] M. Collette and R. Sielski, "Aluminum Ship Structures," 2013.

[2] D. Lerman and T. Capaccio, "Navy Finds "Aggressive" Corrosion on Austal's Combat Ship," in *Bloomberg Business*, ed, 2011.

[3] Hydro. (2002, Aluminium in the marine environment.

[4] "Petroleum, petrochemical and natural gas industries -- Materials selection and corrosion control for oil and gas production systems," in *ISO21457*, ed: International Organization of Standardization, 2010.

[5] "Aluminium structural material," in *NORSOK M-121*, ed: Standard Norway, 2015.

[6] S. Alexey, "Properties of Pure Aluminum," in *Handbook of Aluminum*, ed: CRC Press, 2003.

[7] (11.02.2016). *European Aluminium Association and MATTER*. Available: http://aluminium.matter.org.uk/content/html/eng/default.asp?catid=&pageid=1

[8] TheEngineeringToolBox. (26.05.16). *Modulus of Elasticity or Young's Modulus - and Tensile Modulus for common Materials*. Available: http://www.engineeringtoolbox.com/young-modulus-d_417.html

[9] W. D. J. Callister and D. G. Rethwisch., "Materials science and engineering; an introduction, 8th ed.," 2010.

[10] T. Furu, "Aluminium in marine environments," presented at the Lecture in Offshore materials, NTNU, 2015.

[11] ESAB-Knowledge-Center. (2014). *Understanding the Aluminum Alloy Designation System*. Available: http://www.esabna.com/us/en/education/blog/understanding-the-aluminum-alloy-designation-system.cfm

[12] K. Nisancioglu, "Corrosion and protection of aluminum alloys in seawater," *European Federation of Corrosion Publications,* vol. 50, pp. 145-155, 2007.

[13] TotalMateria. (2003). *Aluminum-Magnesium (5000) Alloys*. Available: http://www.totalmateria.com/Article75.htm

[14] I. The Aluminum Association. (1998, 20.10.2015). Aluminum Alloy Selection and Applications. Available: http://www.calm-aluminium.com.au/documents/aluminium-alloys.pdf

[15] K. F. Veium, "Effect of Cathodic Polarization on the Susceptibility to Hydrogen Embrittlement in 5xxx, 6xxx and 7xxx Series Aluminium Alloys," Master, Department of Materials and Engineering Science, NTNU, 2015.

[16] E. k. center. (2014). *The Difference Between Heat-Treatable and Non-Heat-Treatable Aluminum Alloys*. Available: http://www.esabna.com/us/en/education/blog/the-differences-between-heat-treatable-and-non-heat-treatable-aluminum-alloys.cfm

[17] K. Nisacioglu, "Corrosion of Aluminum and Aluminum Alloys - Lecture notes in TMM4170," 2014.

[18] P. P. Trzaskoma, "Pit Morphology of Aluminum Alloy and Silicon Carbide/Aluminum Alloy Metal Matrix Composites," *Corrosion,* vol. 46, pp. 402-409, 1990.

[19] J. G. Kaufman, "Aluminum Alloys," in *Mechanical Engineers' Handbook*, ed: John Wiley & Sons, Inc., 2006, pp. 59-116.

[20] K. Nisancioglu and H. Holtan, "Measurement of the critical pitting potential of aluminium," *Corrosion Science,* vol. 18, pp. 835-849, 1978/01/01 1978.

[21] A. Broli and H. Holtan, "Use of potentiokinetic methods for the determination of characteristic potentials for pitting corrosion of aluminium in a deaerated solution of 3%NaCl," *Corrosion Science,* vol. 13, pp. 237-246, 1973/01/01 1973.

[22] E. Bardal, *Korrosjon og korrosjonsvern*. Trondheim, 1994.

[23] TotalMateria. (2008). *Corrosion of Aluminum and Its Alloys: Forms of Corrosion*. Available: http://www.totalmateria.com/page.aspx?ID=CheckArticle&site=ktn&NM=187

[24] P. A. Brook, "Potential-pH diagrams at elevated temperatures," *Corrosion Science,* vol. 12, pp. 297-306, 1972/01/01 1972.

[25] A. Bjørgum, "Corrosion of Aluminum in Chloride Solutions Containing Carbon Dioxide, Bicarbonate, Copper and Hydrogen Sulfide," PhD, Laboratories of Industrial Electrochemistry, Norwegian Institute of Technology, Trondheim, 1993.

[26] Z. A. Foroulis and M. J. Thubrikar, "A Contribution to the Study of the Critical Pitting Potential of Oxide Covered Aluminum in aqueous chloride solutions," *Materials and Corrosion,* vol. 26, pp. 350-355, 1975.

[27] J. Soltis, N. J. Laycock, and D. Krouse, "Temperature dependence of the pitting potential of high purity aluminium in chloride containing solutions," *Corrosion Science,* vol. 53, pp. 7-10, 1// 2011.

[28] B. Nick, T. H. Muster, and G. B. Rudolph, "Corrosion of Aluminum Alloys," in *Corrosion Mechanisms in Theory and Practice, Third Edition,* ed: CRC Press, 2011, pp. 705-736.

[29] K. Nisancioglu, "Electrochemical Behavior of Aluminum-Base Intermetallics Containing Iron," *The Electrochemical Society,* vol. 137, pp. 69-77, 1990.

[30] L. F. Mondolfo, "3 - Aluminum–Magnesium, Aluminum–Manganese Alloys," in *Aluminum Alloys,* ed: Butterworth-Heinemann, 1976, pp. 806-841.

[31] S. Egtvedt, "Thermally Sprayed Aluminum (TSA) with Cathodic Protection as Corrosion Protection for Steel in Natural Seawater: Characterization of Properties on TSA and Calcareous Deposit," Materials Science and Engineering, Norwegian University of Science and Technology, Trondheim, 2011.

[32] R. Goswami, G. Spanos, P. S. Pao, and R. L. Holtz, "Precipitation behavior of the ß phase in Al-5083," *Materials Science and Engineering: A,* vol. 527, pp. 1089-1095, 2/15/ 2010.

[33] B. Sakshaug, "Korrosjonsoppførsel av AA5083- og AA6082-legeringer ved ulike temperaturer," NTNU, Trondheim, 2015.

[34] R. Gundersen and K. Nisancioglu, "Cathodic Protection of Aluminum in Seawater," *CORROSION,* vol. 46, pp. 279-285, 1990.

[35] C. Deslouis, A. Doncescu, D. Festy, O. Gil, V. Maillot, S. Touzain, *et al.*, "Kinetics and Characterisation of Calcareous Deposits under Cathodic Protection in Natural Sea Water," *Materials Science Forum,* vol. 289-292, pp. 1163-1180, 1998.

[36] A. Neville and A. P. Morizot, "Calcareous scales formed by cathodic protection—an assessment of characteristics and kinetics," *Journal of Crystal Growth,* vol. 243, pp. 490-502, 9// 2002.

[37] S. C. Dexter and S. H. Lin, "Calculation of seawater ph at polarized metal surfaces in the presence of surface films," *CORROSION,* vol. 48, 1992.

[38] D. A. Shifler, "Understanding material interactions in marine environments to promote extended structural life," *Corrosion Science,* vol. 47, pp. 2335-2352, 10// 2005.

[39] H. P. Hack and R. J. Guanti, "Effect of high flow on calcareous deposits and cathodic protection current denisty," *David Taylor Research Center,* 1988.

[40] W. H. Hartt, C. H. Culberson, and S. W. Smith, "Calcareous Deposits on Metal Surfaces in Seawater—A Critical Review," *Corrosion,* vol. 40, pp. 609-618, 1984.

[41] H. Möller, "The influence of Mg2+on the formation of calcareous deposits on a freely corroding low carbon steel in seawater," *Corrosion Science,* vol. 49, pp. 1992-2001, 4// 2007.

[42] C. Deslouis, D. Festy, O. Gil, V. Maillot, S. Touzain, and B. Tribollet, "Characterization of calcareous deposits in artificial sea water by impedances techniques: 2-deposit of Mg(OH)2 without CaCO3," *Electrochimica Acta,* vol. 45, pp. 1837-1845, 2/1/ 2000.

[43] A. Aballe, M. Bethencourt, F. J. Botana, M. J. Cano, and M. Marcos, "Localized alkaline corrosion of alloy AA5083 in neutral 3.5% NaCl solution," *Corrosion Science,* vol. 43, pp. 1657-1674, 9// 2001.

[44] K. A. Yasakau, M. L. Zheludkevich, S. V. Lamaka, and M. G. S. Ferreira, "Role of intermetallic phases in localized corrosion of AA5083," *Electrochimica Acta,* vol. 52, pp. 7651-7659, 10/10/ 2007.

[45] H. Ezuber, A. El-Houd, and F. El-Shawesh, "A study on the corrosion behavior of aluminum alloys in seawater," *Materials & Design,* vol. 29, pp. 801-805, // 2008.

[46] M. Händel, D. Nickel, and T. Lampke, "Effect of different grain sizes and textures on the corrosion behaviour of aluminum alloy AA6082

Einfluss unterschiedlicher Korngrößen und Texturen auf das Korrosionsverhalten der Aluminiumlegierung EN AW-6082," *Materialwissenschaft und Werkstofftechnik,* vol. 42, pp. 606-611, 2011.

[47] K. Blommedal, "Corrosion Development in Welded AA6082 Alloys," Materials Science and Engineering, NTNU, Trondheim, 2013.
[48] Jotun, "Jotamastic 87," ed, 2016.
[49] "Standard Practice for the Preparation of Substitute Ocean Water," ed: ASTM International, 2013.
[50] C. Vargel, *Corrosion of aluminium*, 1st ed., English ed ed. Amsterdam ; Boston: Amsterdam ; Boston : Elsevier, 2004.
[51] "Cathodic Protection Design," in *DNV-RP-B401*, ed: Det Norske Veritas, 2010.
[52] J. F. Yan, R. E. White, and R. B. Griffin, "Parametric Studies of the Formation of Calcareous Deposits on Cathodically Protected Steel in Seawater," *Journal of the Electrochemical Society*, vol. 140, pp. 1275-1280, 1993.
[53] K. Andersen, "HISC in Super Duplex Stainless Steels: A study of the relation between microstructure and susceptibility to hydrogen induced stress cracking," Department of Materials Science and Engineering, Norwegian University of Science and Technology, Trondheim, 2013.
[54] R. H. Jones, "The influence of hydrogen on the stress-corrosion cracking of low-strength Al-Mg alloys," *JOM*, vol. 55, pp. 42-46, 2003.

Appendix A

Hydrogen in aluminium alloys

CP represent a source of hydrogen, the hydrogen evolution reaction takes place at the anode. Hydrogen can diffuse into the protected material (cathode) and cause hydrogen embrittlement, also referred to as hydrogen induced stress cracking (HISC). Strictly speaking, hydrogen embrittlement is a type of failure; in response to applied or residual tensile stress brittle fracture occurs catastrophically as cracks grow and rapidly propagate. Hydrogen in its atomic form diffuses interstitially through the crystal lattice, and concentrations as low as several parts per million can lead to cracking [9].

Hydrogen embrittlement can only occur if the three factors illustrated in Figure 58 are present; hydrogen, stress and a susceptible material. In general, high strength materials like super duplex stainless steels are known to be susceptible to hydrogen embrittlement [53]. According to DNV-RP-B401, aluminium alloys are generally considered immune to HISC [51]. Due to the inherently high ductility of FCC alloys, like aluminium, they are relative resistant to the hydrogen embrittlement. However, strain hardening of these alloys will enhance their susceptibility to hydrogen embrittlement [9].

Experimental work performed by K. Veium indicated that cathodic polarization with an applied potential of -1093 mV_{SCE} tended to not affect the susceptibility to hydrogen embrittlement for the aluminium alloys EN AW 5083 H321 and EN AW 6082 T6, regardless of both composition and thermal history [15]. However, according to R. H. Jones there is considerable evidence that hydrogen is generated at the tip of a crack growing along grain boundaries of AA5083 that contain precipitated β phase. Thus, the following possibility must be considered as a viable crack-growth mechanism: Hydrogen-induced crack growth is responsible for crack growth through or around the β phase particles and along the grain boundary between the particles [54].

More information can be found in the references [15, 53, 54].

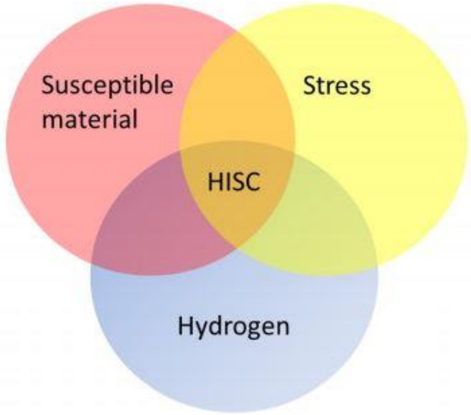

Figure 58: The three important factors for hydrogen embrittlement/HISC [53].

Appendix B

Photos of samples after exposure in SEALAB

Samples exposed in natural seawater at 10 °C

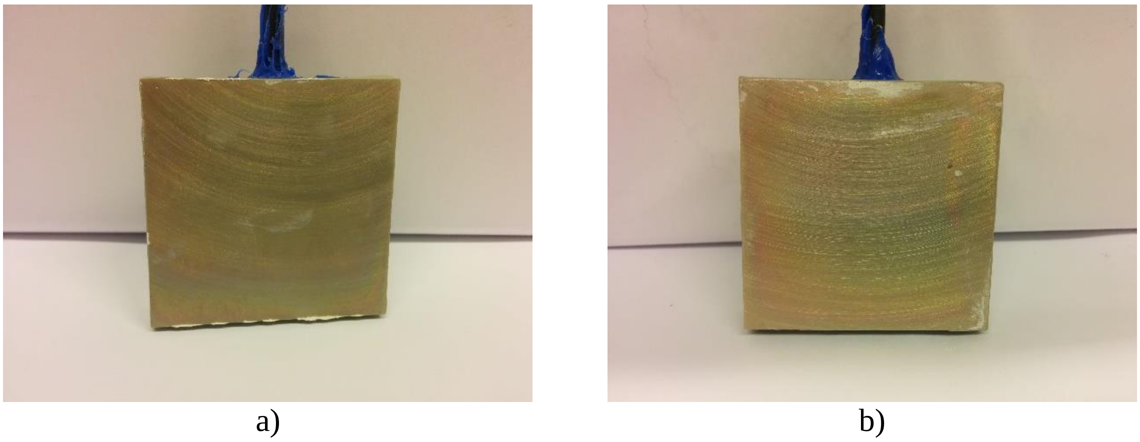
a) b)

Figure 59: Freely exposed samples in natural seawater at 10 °C in SEALAB; a) AA5083 and b) AA6082.

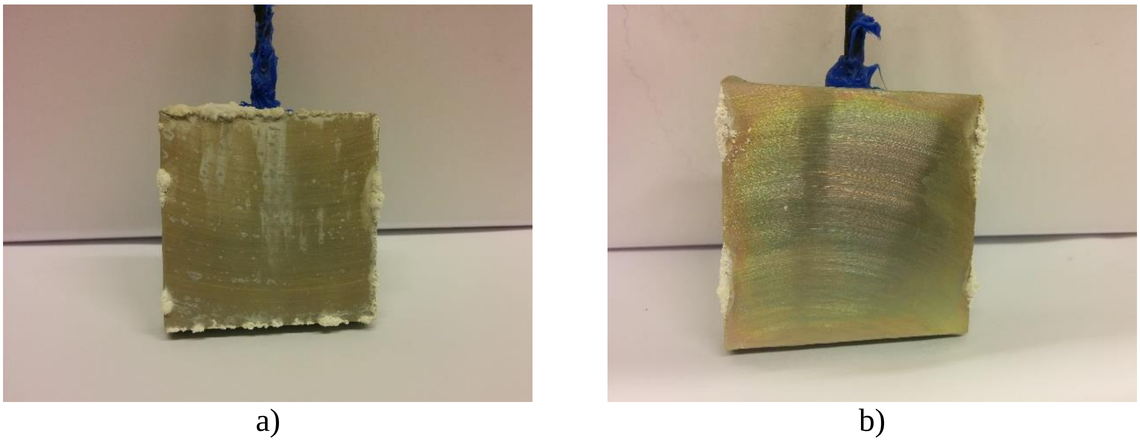
a) b)

Figure 60: Samples anodic polarized to −700 mV vs Ag/AgCl in natural seawater at 10 °C in SEALAB; a) AA5083 and b) AA6082.

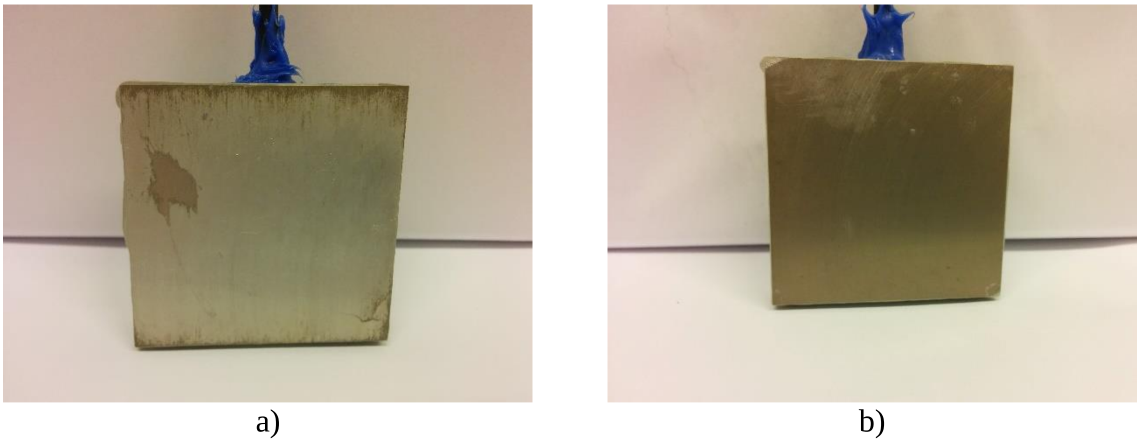
a) b)

Figure 61: Samples polarized coupled to a sacrificial anode (approximately −1050 mV vs Ag/AgCl) in natural seawater at 10 °C in SEALAB; a) AA5083 and b) AA6082.

Photos of samples after exposure in SEALAB

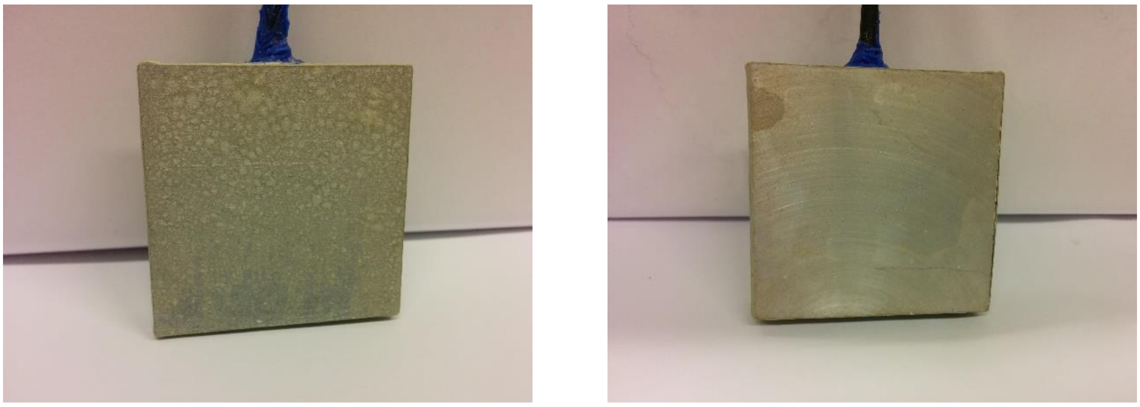
a) b)

Figure 62: Samples cathodic polarized to −1500 mV vs Ag/AgCl in natural seawater at 10 °C in SEALAB; a) AA5083 and b) AA6082.

Samples exposed in natural seawater at 32 °C

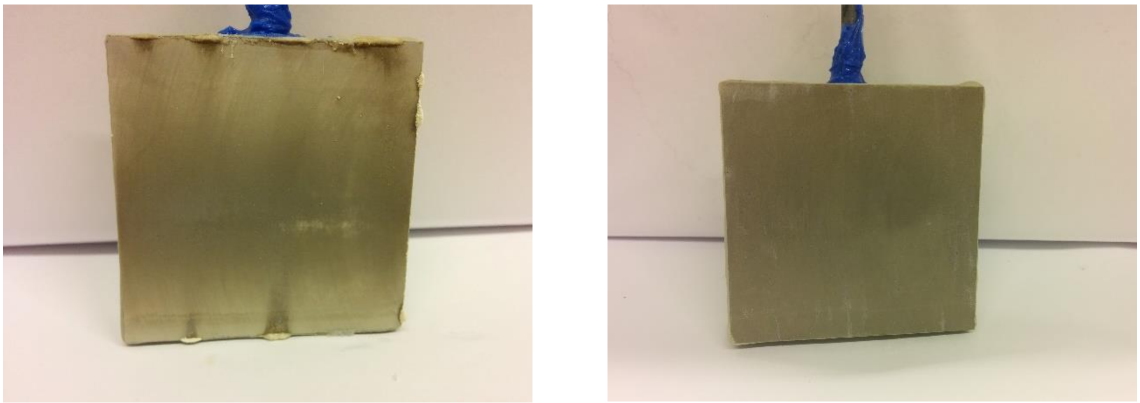
a) b)

Figure 63: Freely exposed samples in natural seawater at 32 °C in SEALAB; a) AA5083 and b) AA6082.

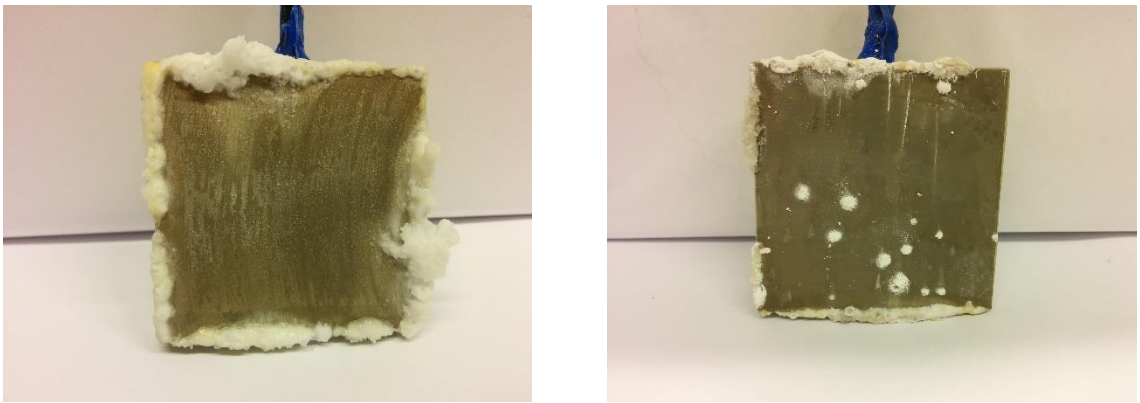
a) b)

Figure 64: Samples anodic polarized to −700 mV vs Ag/AgCl in natural seawater at 32 °C in SEALAB; a) AA5083 and b) AA6082.

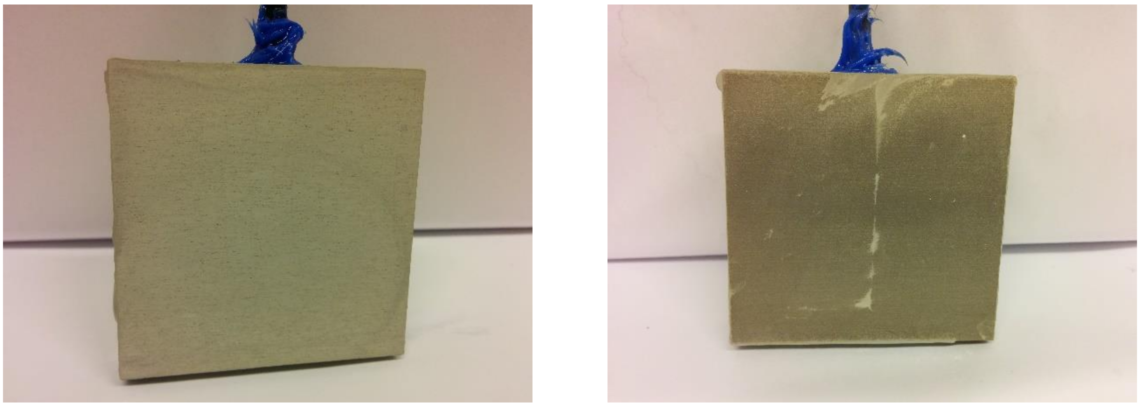

a) b)

Figure 65: Samples polarized coupled to a sacrificial anode (approximately −1050 mV vs Ag/AgCl) in natural seawater at 10 ^{o}C in SEALAB; a) AA5083 and b) AA6082.

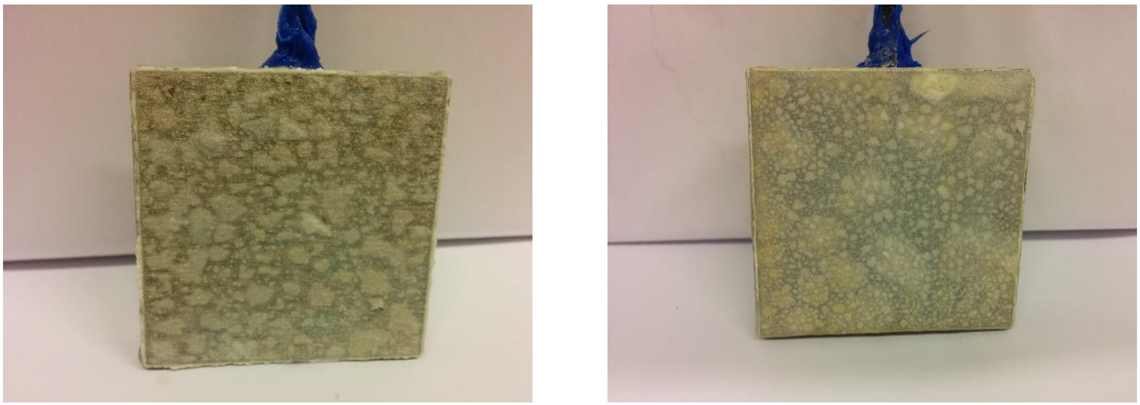

a) b)

Figure 66: Samples cathodic polarized to −1580 mV vs Ag/AgCl in natural seawater at 32 ^{o}C in SEALAB; a) AA5083 and b) AA6082.

Appendix C

Potential from sacrificial anode and current density for carbon steel coupled to sacrificial anode

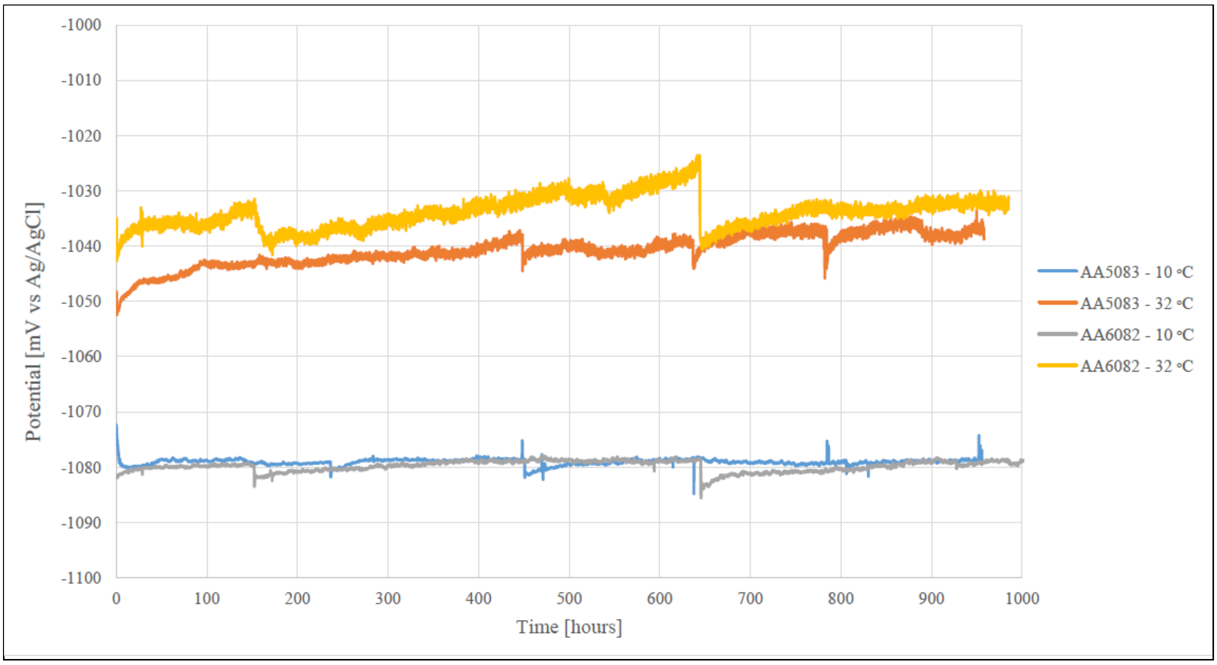

Figure 67: Potential from the sacrificial anode used in the experiments performed in SEALAB.

Figure 67 shows the potential from the sacrificial anode used in the experiments performed in SEALAB, the drop in the curve for AA6082 at 32 °C was due to poor contact between two cables. It did not affect the results. Figure 68 shows the current density for carbon steel coupled to a sacrificial anode in SEALAB, at 10 °C and 32 °C. The carbon steel samples were exposed for 2000 hours.

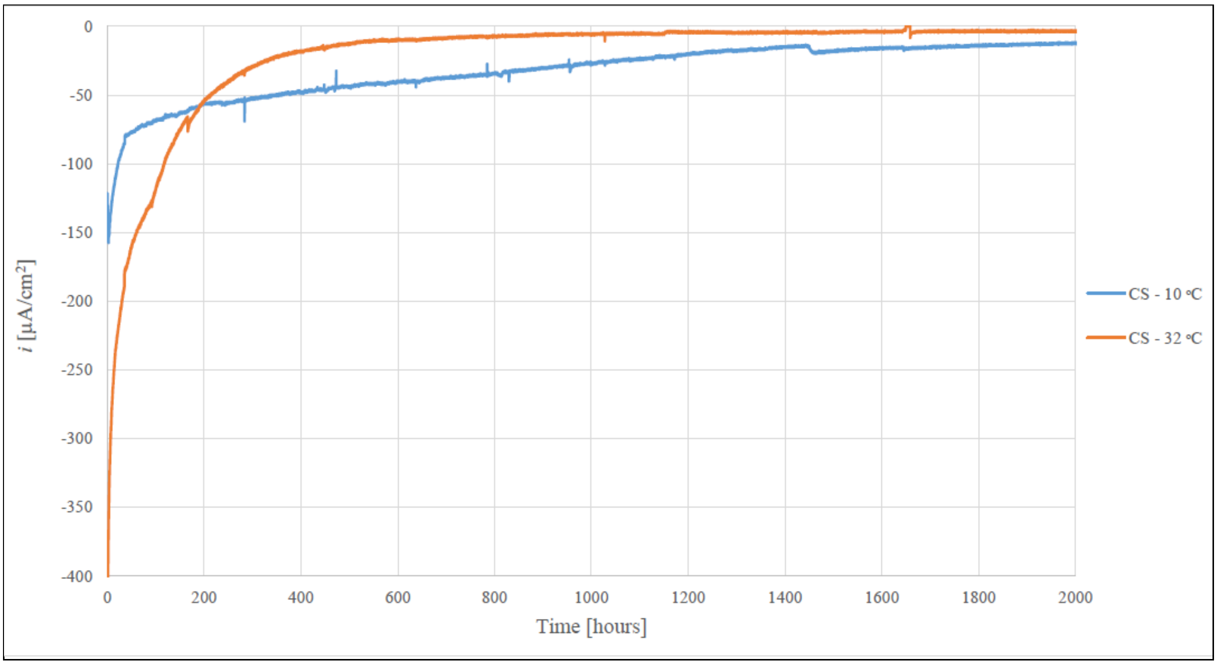

Figure 68: Current density for carbon steel coupled to sacrificial anode in SEALAB.

Appendix D

Complete polarization curves for AA6082 exposed at 10 °C and 32 °C

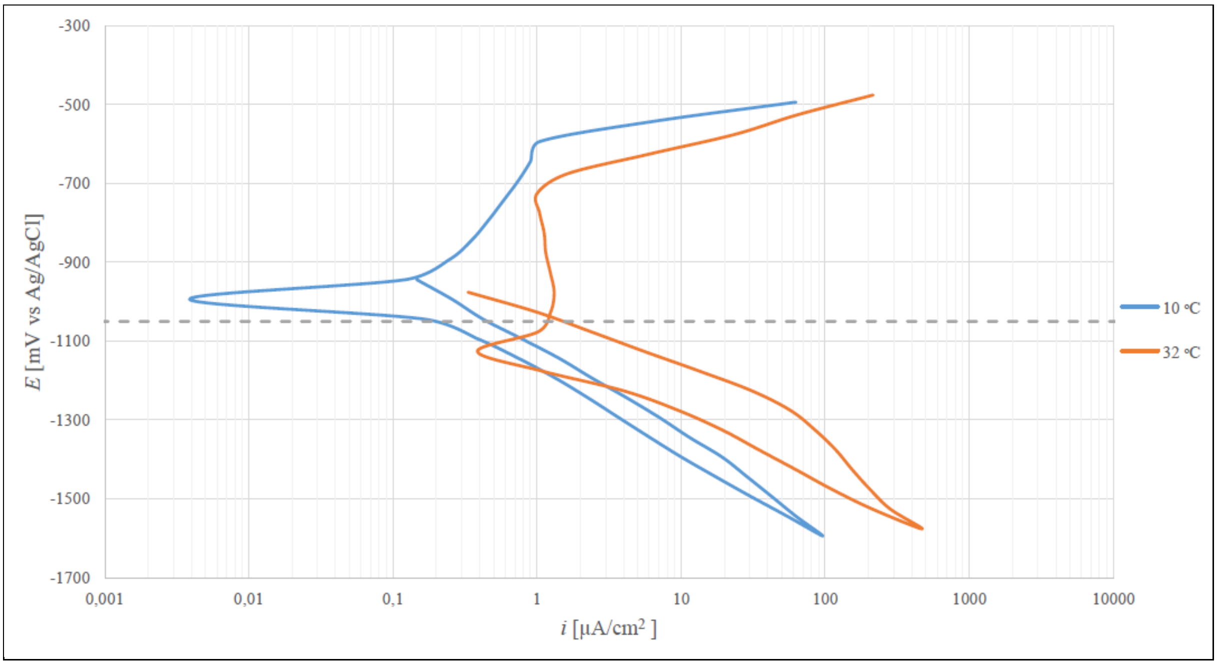

Figure 69: Complete polarization curves for AA6082 exposed at 10 °C and 32 °C in natural seawater.

Appendix E

SEM images of samples prior to exposure

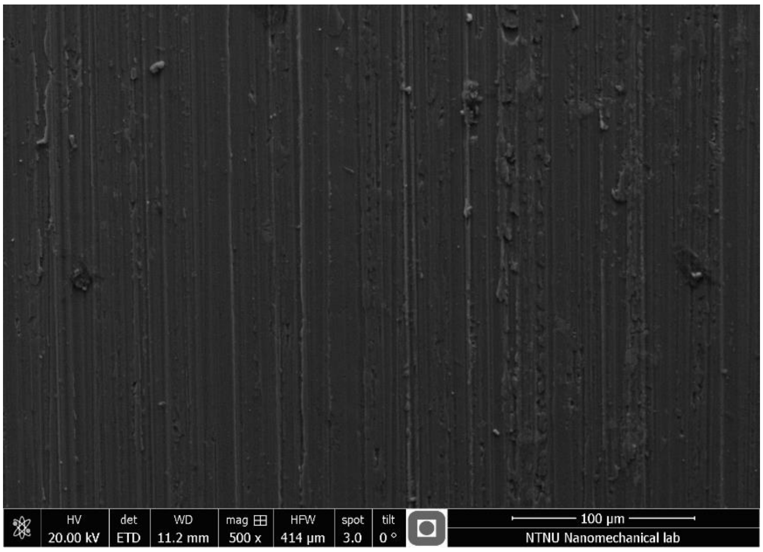
HV
20.00 kV
det
ETD
WD
11.2 mm
mag
500 x
HFW
414 µm
spot
3.0
tilt
0 °
100 µm
NTNU Nanomechanical lab

Figure 70: AA5083 sample prior to exposure.

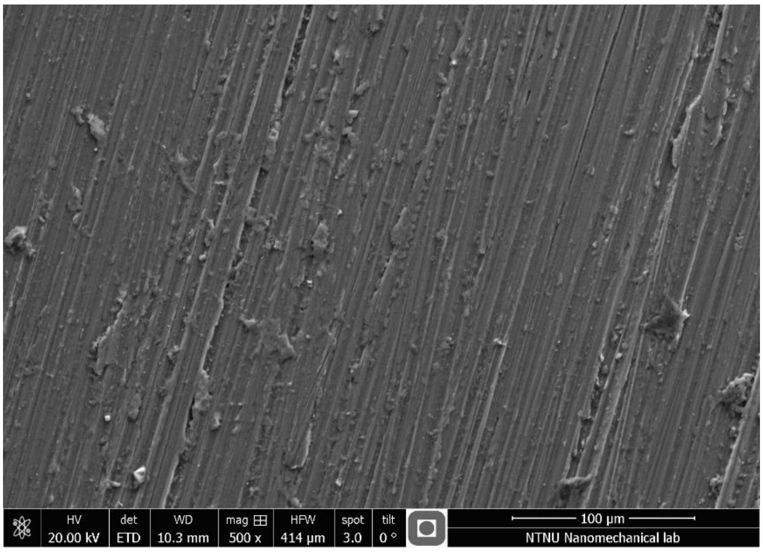
HV
20.00 kV
det
ETD
WD
10.3 mm
mag
500 x
HFW
414 µm
spot
3.0
tilt
0 °
100 µm
NTNU Nanomechanical lab

Figure 71: AA6082 sample prior to exposure.

Appendix F

EDS analysis of corrosion products on samples polarized to −1500 mV vs Ag/AgCl

AA5083 at 10 °C

Figure 72 presents an EDS analysis of the corrosion products on the AA5083 sample polarized to −1500 mV vs Ag/AgCl at 10 °C. As it can be seen, the corrosion products mainly consist of Al, O and Mg, but salts and elements from the seawater, like S and Cl.

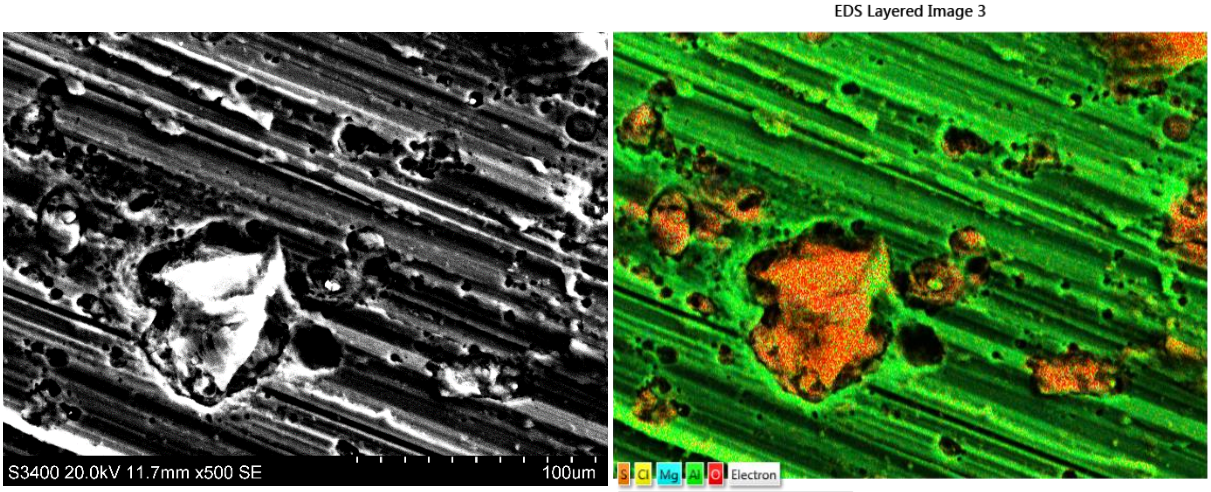

a)

b)

Figure 72: EDS analysis of corrosion products on AA5083 polarized to −1500 mV vs Ag/AgCl at 10 °C. Image a) is a SEM image of an area on the surface, b) indicates the composition of the same area.

AA5083 at 32 °C

Figure 73 presents the EDS analysis of the corrosion products on the AA5083 sample polarized to −1500 mV vs Ag/AgCl at 32 °C. The corrosion products consists of Al, O and Mg, with elements like Na and Cl from the seawater.

EDS analysis of corrosion products on samples polarized to −1500 mV vs Ag/AgCl

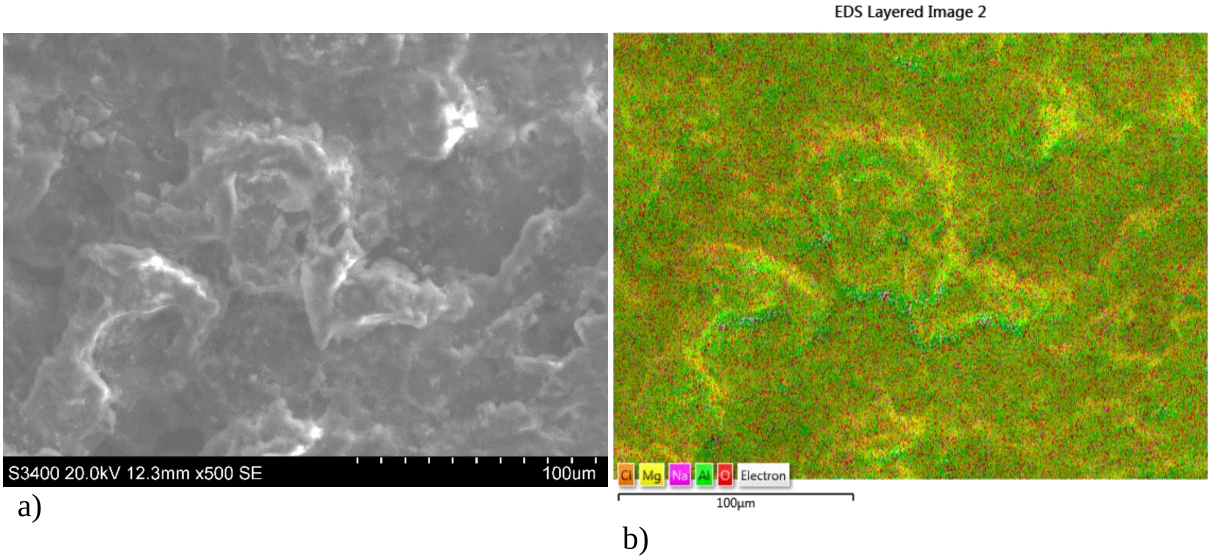
EDS Layered Image 2
S3400 20.0kV 12.3mm x500 SE
100um
a)
Cl
Mg
Na
Al
O
Electron
100µm
b)

Figure 73: EDS analysis of corrosion products on AA5083 polarized to −1500 mV vs Ag/AgCl at 32 °C. Image a) is a SEM image of an area on the surface, b) indicates the composition of the same area.

AA6082 at 32 °C

The EDS analysis for the corrosion products on AA6082 polarized to −1500 mV vs Ag/AgCl at 32 °C is presented in Figure 74. The corrosion products consists of Al, O, Si and C, but also Na from the seawater.

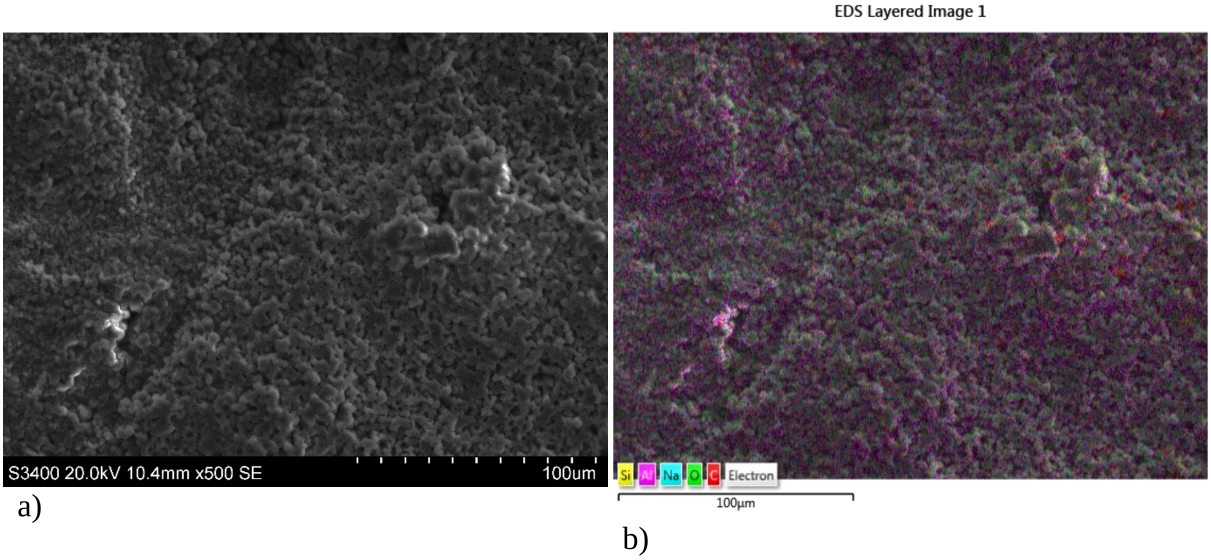
EDS Layered Image 1
S3400 20.0kV 10.4mm x500 SE
100um
a)
Si
Al
Na
O
C
Electron
100µm
b)

Figure 74: EDS analysis of corrosion products on AA6082 polarized to −1500 mV vs Ag/AgCl at 32 °C. Image a) is a SEM image of an area on the surface, b) indicates the composition of the same area.

Appendix G

OCP and current density for samples exposed in SSW with pH 8,2

In Figure 75 the development of OCP for freely exposed AA5083 and AA6082 in SSW with pH 8,2 (natural pH) at room temperature is shown.

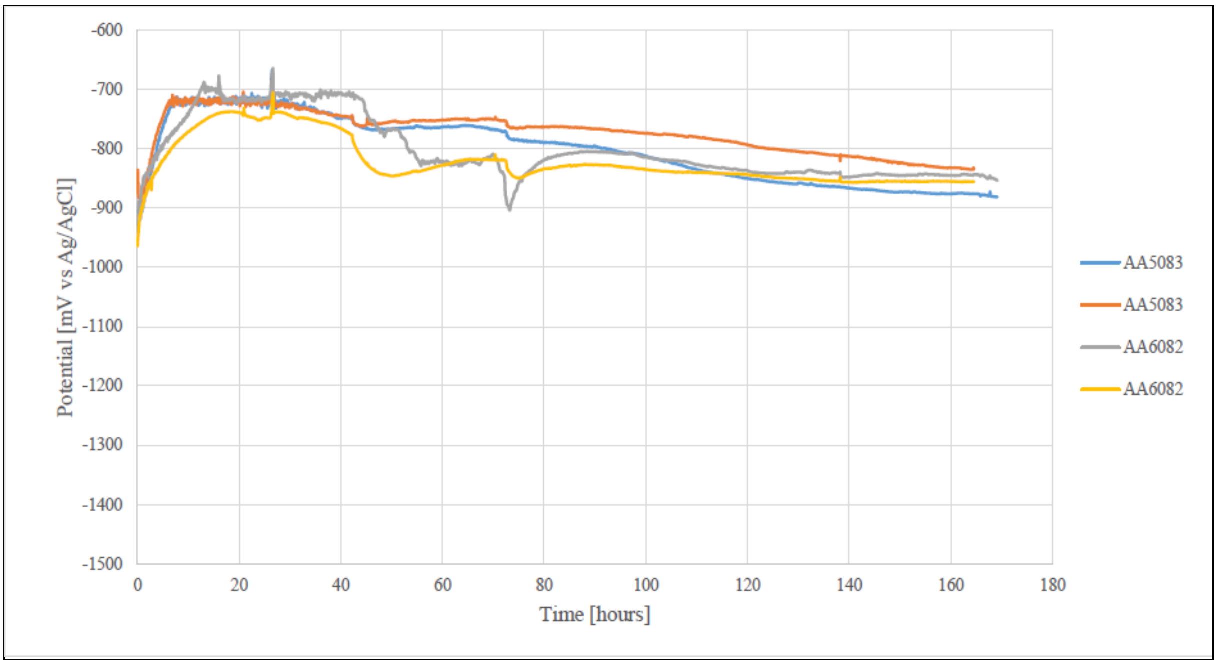

Figure 75: OCP for freely exposed AA5083 and AA6082 in SSW with pH 8,2 at room temperature.

Figure 76, Figure 77 and Figure 78 show the current density curves.

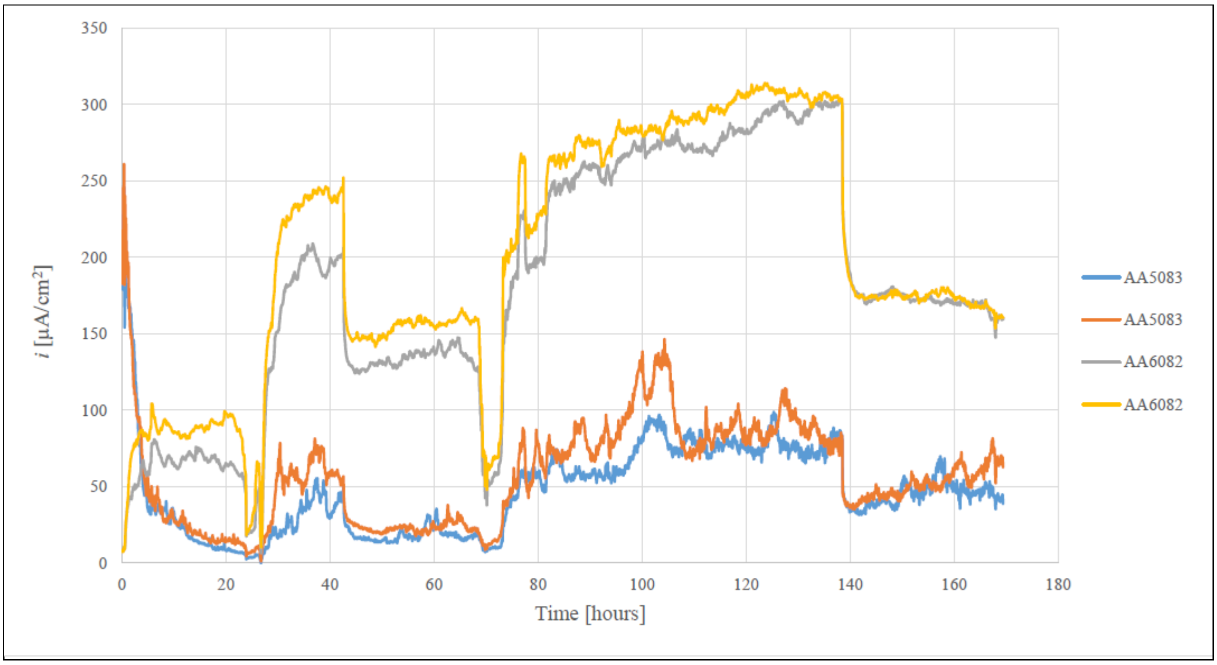

Figure 76: Current density for AA5083 and AA6082 polarized to −700 mV vs Ag/AgCl in SSW with pH 8,2.

OCP and current density for samples exposed in SSW with pH 8,2

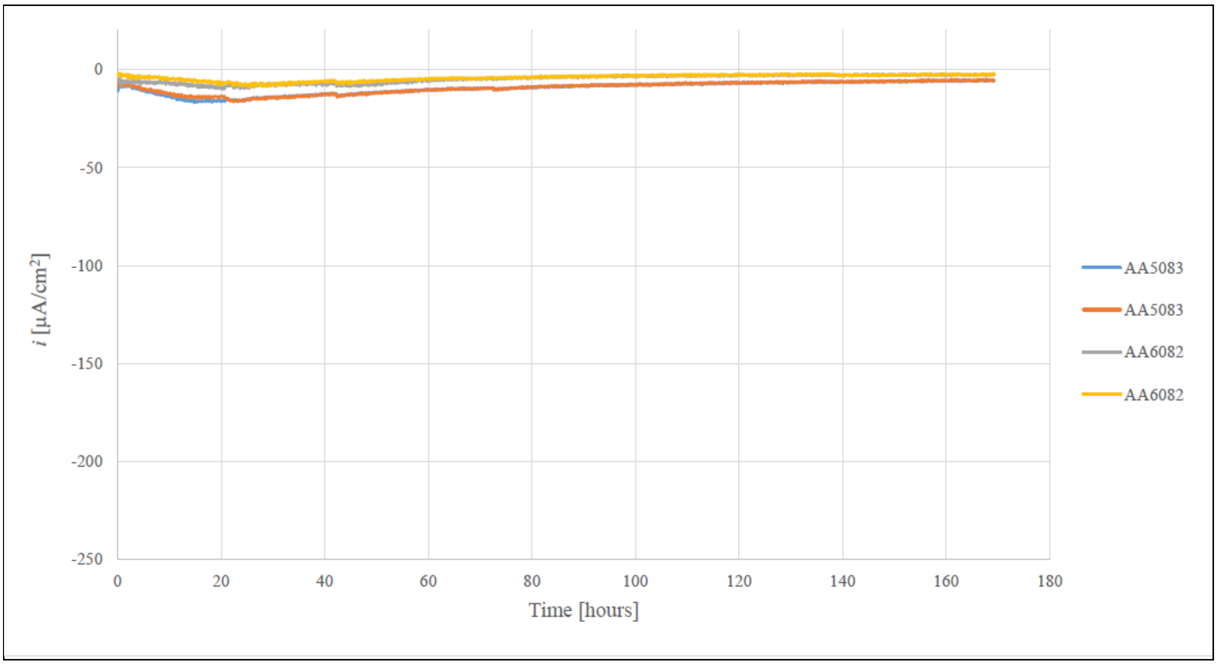

Figure 77: Current density for AA5083 and AA6082 coupled to a sacrificial anode (ca −1050 mV vs Ag/AgCl) in SSW with pH 8,2.

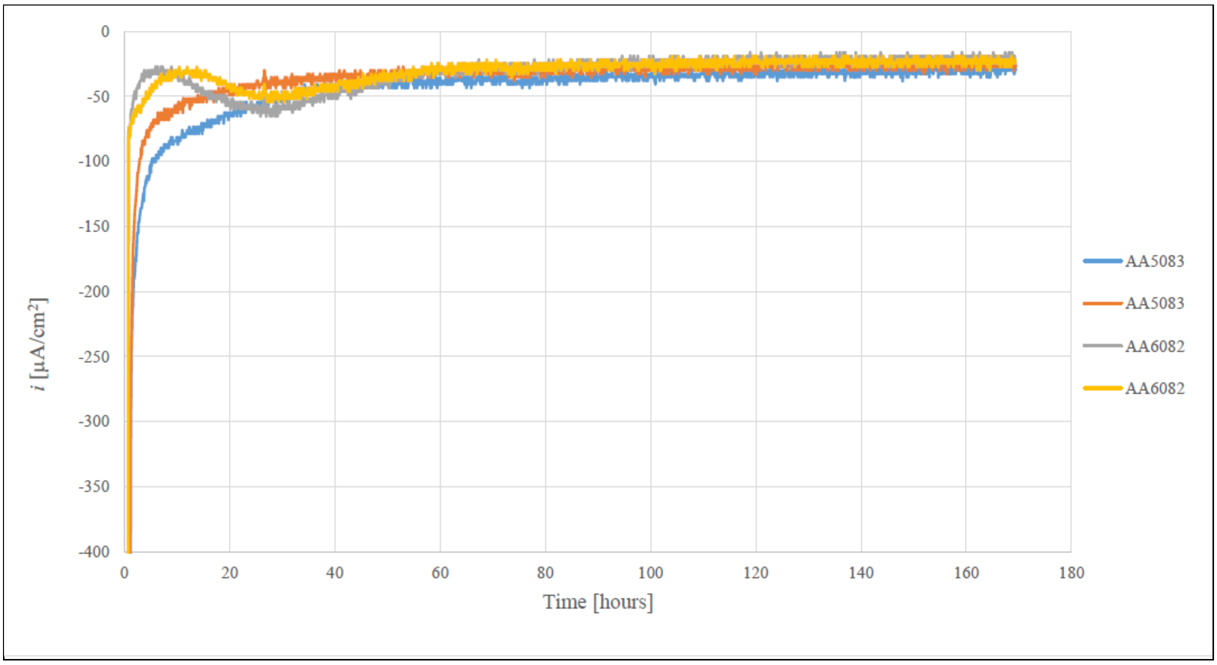

Figure 78: Current density for AA5083 and AA6082 polarized to −1500 mV vs Ag/AgCl in SSW with pH 8,2.

Appendix H

Potentiodynamic polarization curves for pH 3 and pH 10

It is interesting to the see the effect of exposure time for pH 3 and pH 10. This is because pH 3 may be relevant for aluminium placed in seawater mud. The pH-value 10 may occur on the surface of polarized aluminium samples.

AA5083 at pH 3

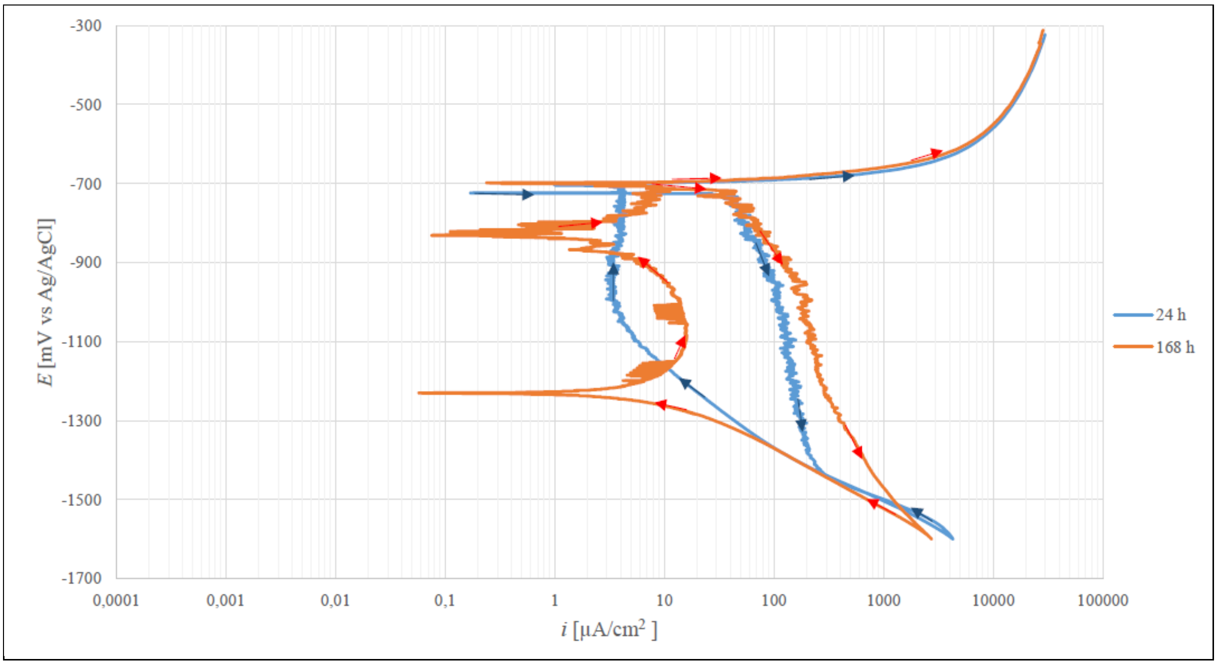

Figure 79: Potentiodynamic polarization curves for AA5083 in SSW with pH 3 after 24 hours and 168 hours of exposure.

From Figure 79 it can be seen that the OCP was slightly more positive after 168 hours. There was no difference in pitting potential. The passive current density was somewhat higher for the sample exposed for 168 hours than for the sample exposed for 24 hours.

AA6082 at pH 3

In Figure 80 it can be seen that the OCP for AA6082 in SSW with pH 3 was 20 mV more negative after 168 hours of exposure than after 24 hours. There was no difference in pitting potential. The passive current density was in a lower range for the sample exposed for 168 hours than for the sample exposed in 24 hours.

Potentiodynamic polarization curves for pH 3 and pH 10

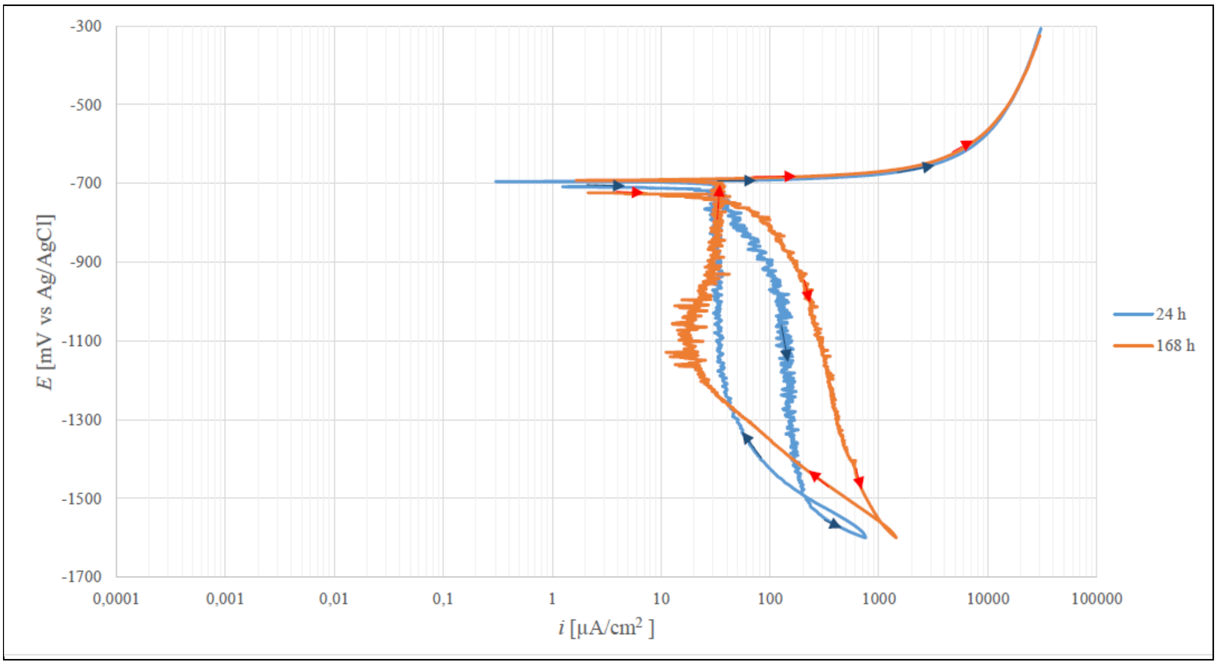

Figure 80: Potentiodynamic polarization curves for AA6082 in SSW with pH 3 after 24 hours and 168 hours of exposure.

AA5083 at pH 10

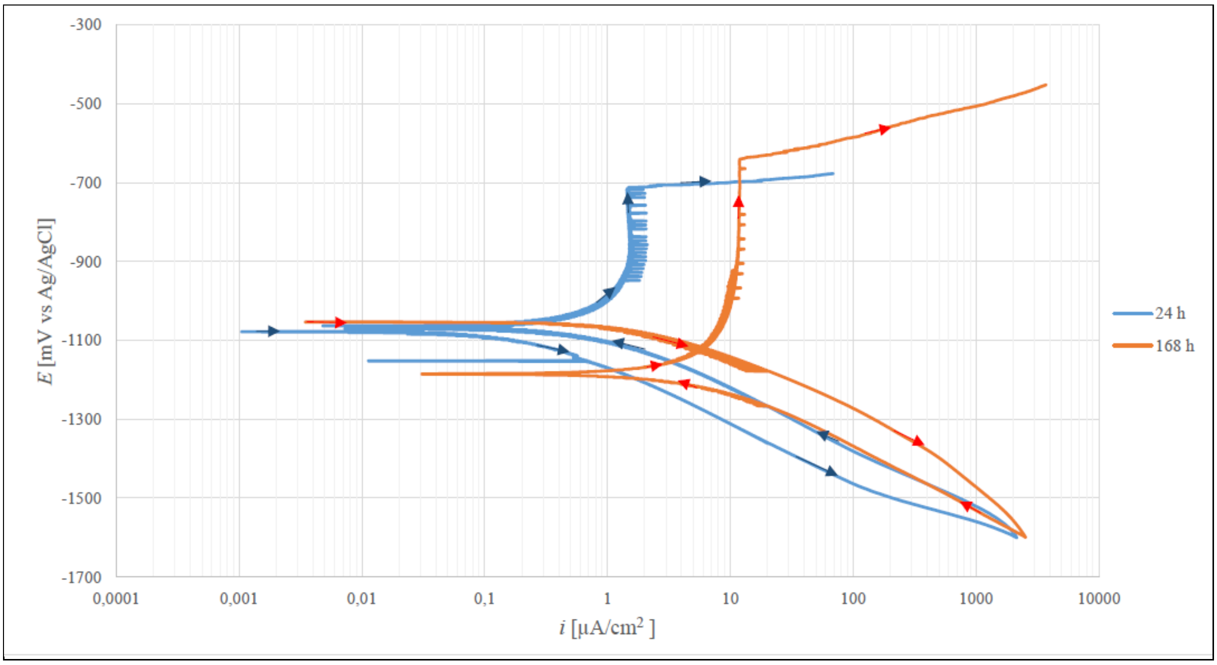

Figure 81: Potentiodynamic polarization curves for AA5083 in SSW with pH 10 after 24 hours and 168 hours of exposure.

Figure 81 shows that the OCP for AA5083 in SSW with pH 10 was about 20 mV more positive for the sample exposed for 168 hours than for the sample exposed for 24 hours. The difference in pitting potential was about 80 mV. The passive current density was significantly larger for the sample exposed in 168 hours.

AA6082 at pH 10

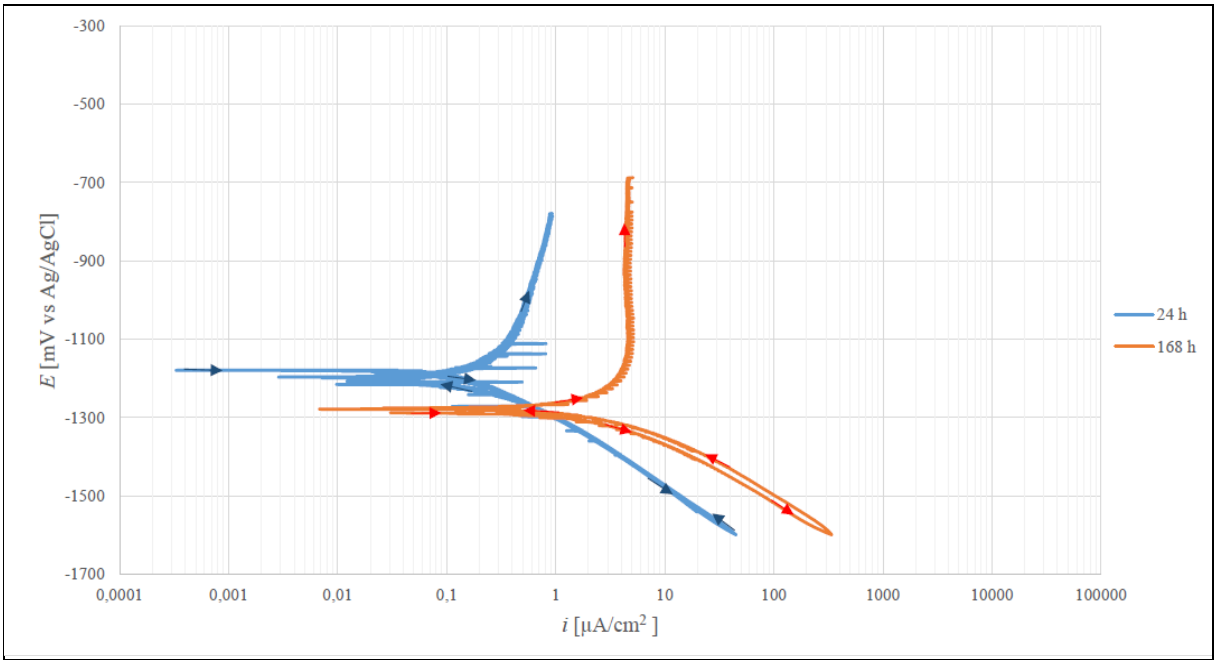

Figure 82: Potentiodynamic polarization curves for AA6082 in SSW with pH 10 after 24 hours and 168 hours of exposure.

Figure 82 shows that there was a significant difference in OCP, the OCP for the sample exposed for 168 hours was 110 mV more negative. No pitting potential can be seen, because the limits for the recording of the potentiodynamic polarization curves were not sufficient wide for these samples. The passive current density was significantly larger for the sample exposed for 168 hours.

Appendix I

Risk assessment

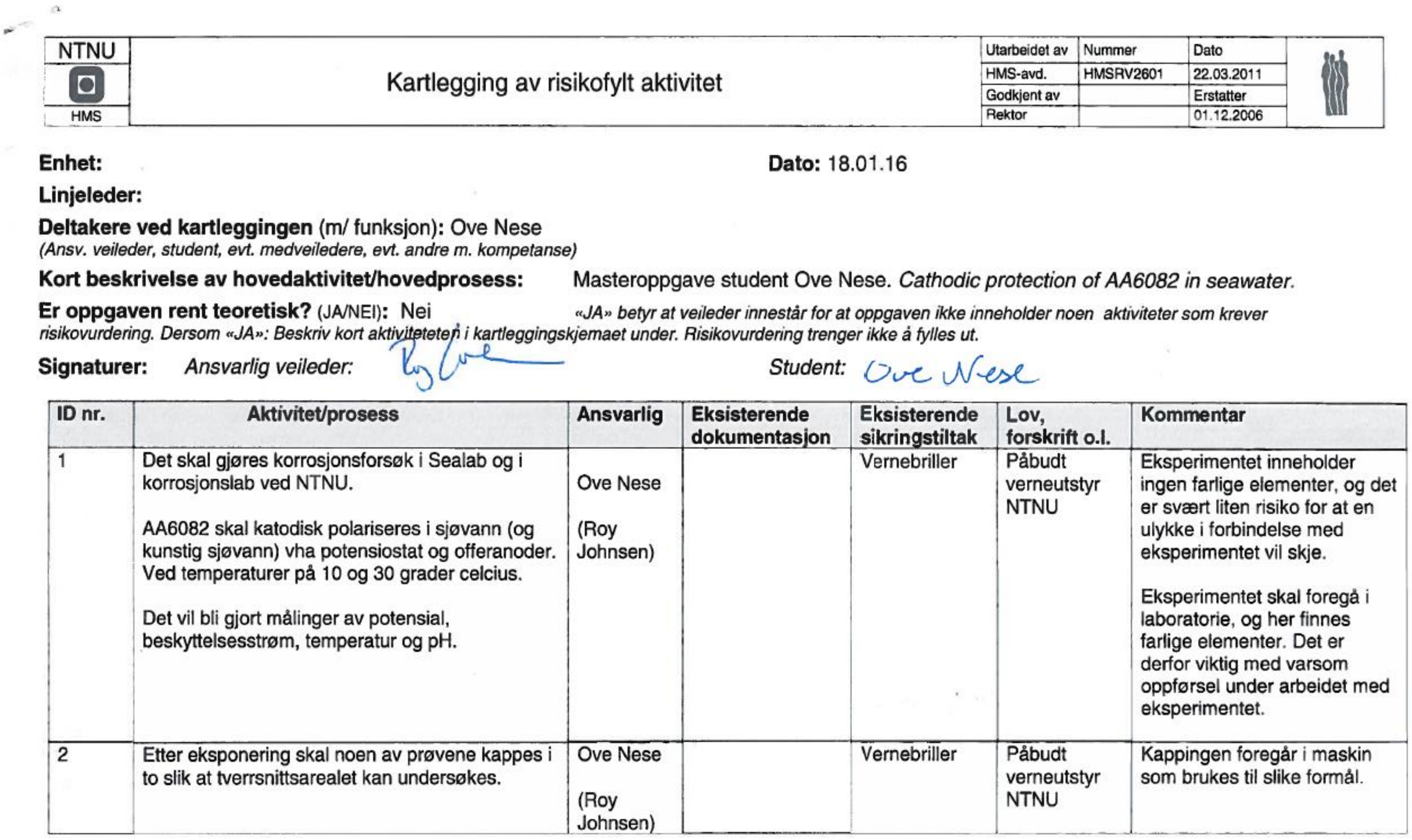

NTNU HMS	Kartlegging av risikofylt aktivitet	Utarbeidet av	Nummer	Dato
		HMS-avd.	HMSRV2601	22.03.2011
		Godkjent av		Erstatter
		Rektor		01.12.2006

Enhet: **Dato:** 18.01.16

Linjeleder:

Deltakere ved kartleggingen (m/ funksjon): Ove Nese
(Ansv. veileder, student, evt. medveiledere, evt. andre m. kompetanse)

Kort beskrivelse av hovedaktivitet/hovedprosess: Masteroppgave student Ove Nese. *Cathodic protection of AA6082 in seawater.*

Er oppgaven rent teoretisk? (JA/NEI): Nei *«JA» betyr at veileder innestår for at oppgaven ikke inneholder noen aktiviteter som krever risikovurdering. Dersom «JA»: Beskriv kort aktivitetene i kartleggingskjemaet under. Risikovurdering trenger ikke å fylles ut.*

Signaturer: *Ansvarlig veileder:* *Student:* Ove Nese

ID nr.	Aktivitet/prosess	Ansvarlig	Eksisterende dokumentasjon	Eksisterende sikringstiltak	Lov, forskrift o.l.	Kommentar
1	Det skal gjøres korrosjonsforsøk i Sealab og i korrosjonslab ved NTNU. AA6082 skal katodisk polariseres i sjøvann (og kunstig sjøvann) vha potensiostat og offeranoder. Ved temperaturer på 10 og 30 grader celcius. Det vil bli gjort målinger av potensial, beskyttelsesstrøm, temperatur og pH.	Ove Nese (Roy Johnsen)		Vernebriller	Påbudt verneutstyr NTNU	Eksperimentet inneholder ingen farlige elementer, og det er svært liten risiko for at en ulykke i forbindelse med eksperimentet vil skje. Eksperimentet skal foregå i laboratorie, og her finnes farlige elementer. Det er derfor viktig med varsom oppførsel under arbeidet med eksperimentet.
2	Etter eksponering skal noen av prøvene kappes i to slik at tverrsnittsarealet kan undersøkes.	Ove Nese (Roy Johnsen)		Vernebriller	Påbudt verneutstyr NTNU	Kappingen foregår i maskin som brukes til slike formål.

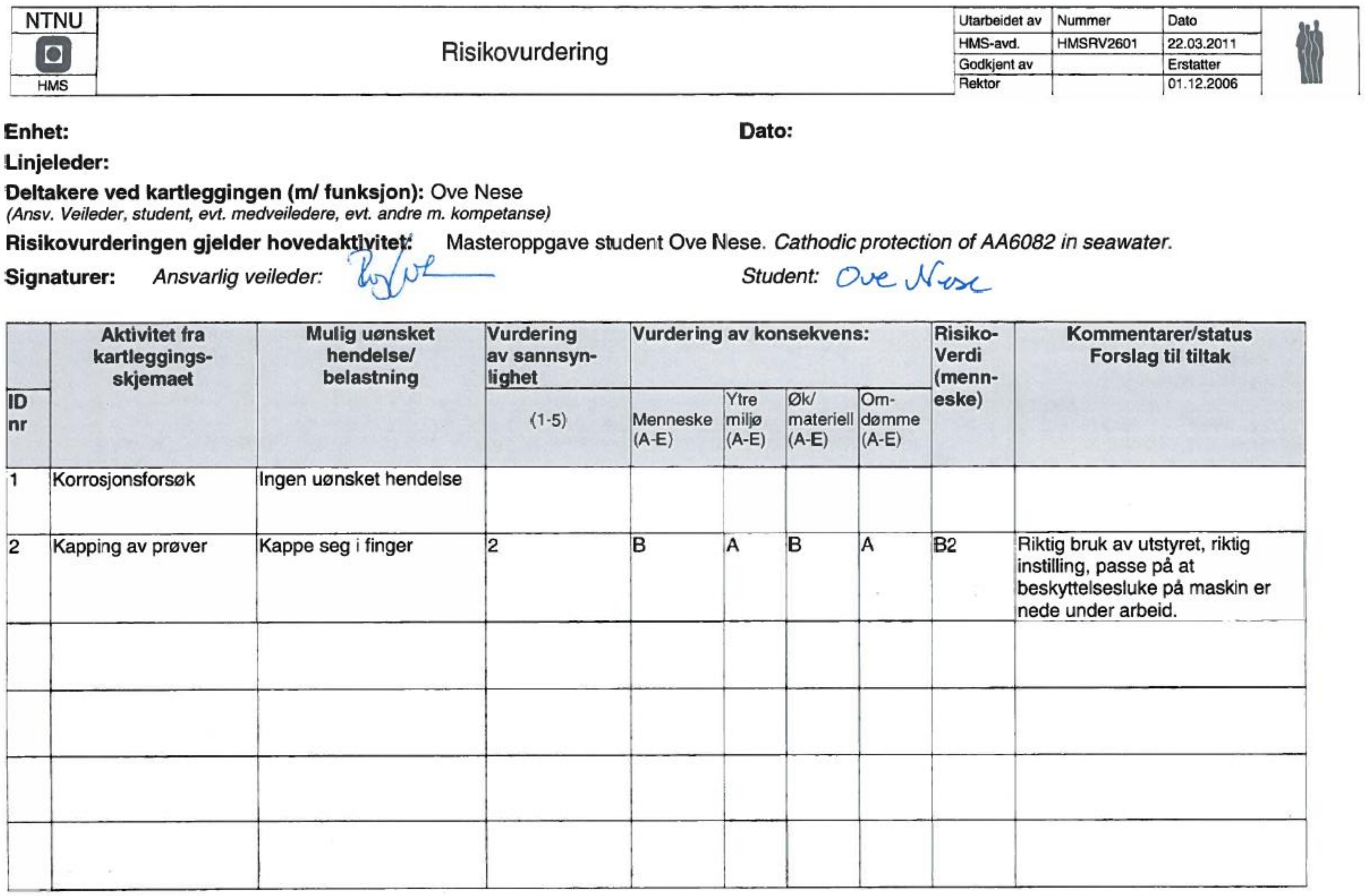

NTNU HMS	Risikovurdering	Utarbeidet av	Nummer	Dato
		HMS-avd.	HMSRV2601	22.03.2011
		Godkjent av		Erstatter
		Rektor		01.12.2006

Enhet: **Dato:**

Linjeleder:

Deltakere ved kartleggingen (m/ funksjon): Ove Nese
(Ansv. Veileder, student, evt. medveiledere, evt. andre m. kompetanse)

Risikovurderingen gjelder hovedaktivitet: Masteroppgave student Ove Nese. *Cathodic protection of AA6082 in seawater.*

Signaturer: *Ansvarlig veileder:* *Student:* Ove Nese

ID nr	**Aktivitet fra kartleggings-skjemaet**	**Mulig uønsket hendelse/ belastning**	**Vurdering av sannsyn-lighet**	**Vurdering av konsekvens:**				**Risiko-Verdi (menn-eske)**	**Kommentarer/status Forslag til tiltak**
			(1-5)	Menneske (A-E)	Ytre miljø (A-E)	Øk/ materiell (A-E)	Om-dømme (A-E)		
1	Korrosjonsforsøk	Ingen uønsket hendelse							
2	Kapping av prøver	Kappe seg i finger	2	B	A	B	A	B2	Riktig bruk av utstyret, riktig instilling, passe på at beskyttelsesluke på maskin er nede under arbeid.

NTNU HMS	Risikovurdering	Utarbeidet av	Nummer	Dato
		HMS-avd.	HMSRV2601	22.03.2011
		Godkjent av		Erstatter
		Rektor		01.12.2006

Sannsynlighet vurderes etter følgende kriterier:

Svært liten 1	Liten 2	Middels 3	Stor 4	Svært stor 5
1 gang pr 50 år eller sjeldnere	1 gang pr 10 år eller sjeldnere	1 gang pr år eller sjeldnere	1 gang pr måned eller sjeldnere	Skjer ukentlig

Konsekvens vurderes etter følgende kriterier:

Gradering	Menneske	Ytre miljø Vann, jord og luft	Øk/materiell	Omdømme
E **Svært Alvorlig**	Død	Svært langvarig og ikke reversibel skade	Drifts- eller aktivitetsstans >1 år.	Troverdighet og respekt betydelig og varig svekket
D **Alvorlig**	Alvorlig personskade. Mulig uførhet.	Langvarig skade. Lang restitusjonstid	Driftsstans > ½ år Aktivitetsstans i opp til 1 år	Troverdighet og respekt betydelig svekket
C **Moderat**	Alvorlig personskade.	Mindre skade og lang restitusjonstid	Drifts- eller aktivitetsstans < 1 mnd	Troverdighet og respekt svekket
B **Liten**	Skade som krever medisinsk behandling	Mindre skade og kort restitusjonstid	Drifts- eller aktivitetsstans < 1uke	Negativ påvirkning på troverdighet og respekt
A **Svært liten**	Skade som krever førstehjelp	Ubetydelig skade og kort restitusjonstid	Drifts- eller aktivitetsstans < 1dag	Liten påvirkning på troverdighet og respekt

Risikoverdi = Sannsynlighet x Konsekvens
Beregn risikoverdi for Menneske. Enheten vurderer selv om de i tillegg vil beregne risikoverdi for Ytre miljø, Økonomi/materiell og Omdømme. I så fall beregnes disse hver for seg.

Til kolonnen "Kommentarer/status, forslag til forebyggende og korrigerende tiltak":
Tiltak kan påvirke både sannsynlighet og konsekvens. Prioriter tiltak som kan forhindre at hendelsen inntreffer, dvs. sannsynlighetsreduserende tiltak foran skjerpet beredskap, dvs. konsekvensreduserende tiltak.

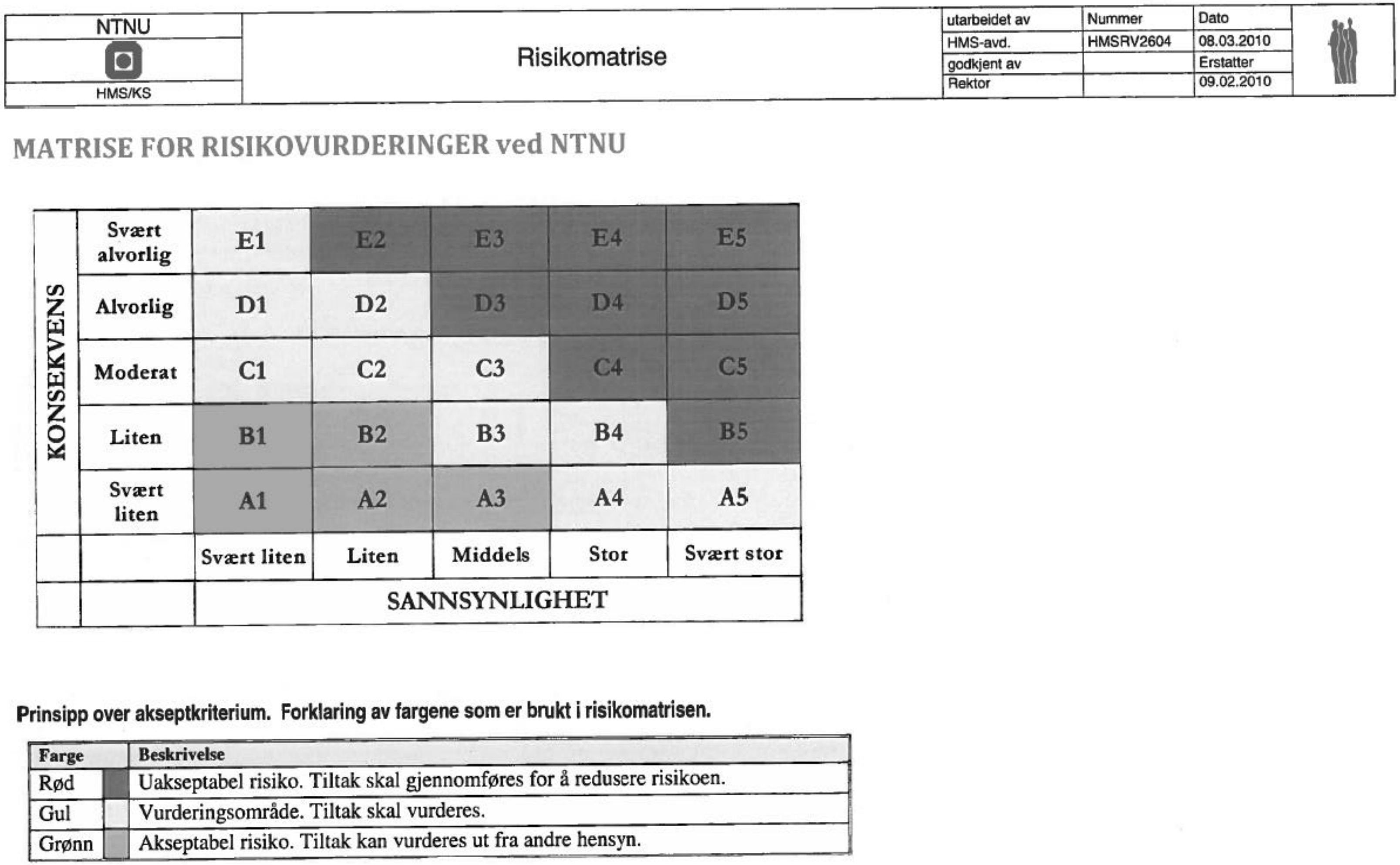

NTNU	Risikomatrise	utarbeidet av	Nummer	Dato
		HMS-avd.	HMSRV2604	08.03.2010
		godkjent av		Erstatter
HMS/KS		Rektor		09.02.2010

MATRISE FOR RISIKOVURDERINGER ved NTNU

KONSEKVENS	Svært alvorlig	E1	E2	E3	E4	E5
	Alvorlig	D1	D2	D3	D4	D5
	Moderat	C1	C2	C3	C4	C5
	Liten	B1	B2	B3	B4	B5
	Svært liten	A1	A2	A3	A4	A5
		Svært liten	Liten	Middels	Stor	Svært stor
		SANNSYNLIGHET				

Prinsipp over akseptkriterium. Forklaring av fargene som er brukt i risikomatrisen.

Farge		Beskrivelse
Rød	🟥	Uakseptabel risiko. Tiltak skal gjennomføres for å redusere risikoen.
Gul	🟨	Vurderingsområde. Tiltak skal vurderes.
Grønn	🟩	Akseptabel risiko. Tiltak kan vurderes ut fra andre hensyn.